THERMAL RUNAWAY REACTION HAZARD AND

DECOMPOSITION MECHANISM OF THE HYDROXYLAMINE

SYSTEM

A Dissertation

by

CHUNYANG WEI

Submitted to the Office of Graduate Studies of
Texas A&M University
in partial fulfillment of the requirements for the degree of

DOCTOR OF PHILOSOPHY

August 2005

Major Subject: Chemical Engineering

THERMAL RUNAWAY REACTION HAZARD AND

DECOMPOSITION MECHANISM OF THE HYDROXYLAMINE

SYSTEM

A Dissertation

by

CHUNYANG WEI

Submitted to the Office of Graduate Studies of
Texas A&M University
in partial fulfillment of the requirements for the degree of

DOCTOR OF PHILOSOPHY

Approved by:

Chair of Committee,	M. Sam Mannan
Committee Members,	Michael B. Hall
	David M. Ford
	Mahmoud El-Halwagi
Head of Department,	Kenneth R. Hall

August 2005

Major Subject: Chemical Engineering

ABSTRACT

Thermal Runaway Reaction Hazard and Decomposition Mechanism

of the Hydroxylamine System. (August 2005)

Chunyang Wei, B.E., Dalian University of Technology;

M.S., University of Tulsa

Chair of Advisory Committee: Dr. M. Sam Mannan

Chemical reactivity hazards have posed a significant challenge for industries that manufacture, store, and handle reactive chemicals. Without proper management and control of reactivity, numerous incidents have caused tremendous loss of property and human lives. The U.S. Chemical Safety and Hazard Investigation Board (CSB) reported 167 incidents involving reactive chemicals that occurred in the U.S. from 1980 to 2001. According to the report, 35 percent of the incidents were caused by thermal runaway reactions, such as incidents that involved hydroxylamine and hydroxylamine nitrate.

The thermal stability of hydroxylamine system under various industrial conditions was studied thoroughly to develop an understanding necessary to prevent recurrence of incidents. The macroscopic runaway reaction behavior of hydroxylamine system was analyzed using a RSST (Reactive System Screening Tool) and an APTAC (Automatic Pressure Tracking Calorimeter). Also, computational chemistry was employed as a powerful tool to evaluate and predict the measured reactivity. A method was proposed to develop a runaway reaction mechanism that provides atomic level of

information on elementary reaction steps, in terms of reaction thermochemistry, activation barriers, and reaction rates.

This work aims to bridge molecular and macroscopic scales for process safety regarding reactive chemicals and to understand macroscopic runaway reaction behaviors from a molecular point of view.

To my husband: Wei Chang

my daughter: Kaylee Chang

and

all my family members in China

ACKNOWLEDGEMENTS

I would like to express my gratitude to my advisor, Dr. Sam Mannan, for his support, guidance, and encouragement throughout my graduate study. His insights on chemical process safety always kept me motivated and inspired to pursue a career in this area. I feel grateful for Dr. William Rogers' contribution to this project. His technical and editorial advice was essential to the completion of this dissertation. My thank also goes to Dr. Michael Hall, Dr. David Ford, and Dr. Mahmoud El-Halwagi for serving on my committee and providing valuable comments on this work.

I am also grateful to my colleagues, Dr. Sanjeev Saraf, for his interesting discussions leading to this research, Dr. Marc Levin, for his humor and help that put me out of the misery of troubleshooting the APTAC, Dr. Lisa Pérez, for her help with theoretical calculations. I would like to thank the Laboratory for Molecular Simulation at Texas A&M University for software and support and the supercomputing facility at Texas A&M University for computer time.

Last, but not least, I would like to thank my husband Wei for his understanding and help during the past few years. He put his career on hold for our family, and this dissertation would not be possible without his support. We are lucky to have an adorable daughter Kaylee, and she knows exactly how to make me feel guilty when I leave her at home.

TABLE OF CONTENTS

LIST OF FIGURES

FIGURE   Page

LIST OF TABLES

TABLE   Page

CHAPTER I

INTRODUCTION

The U.S. Chemical Safety and Hazard Investigation Board (CSB) reported 167 incidents involving reactive chemicals that occurred in the U.S. from 1980 to 2001. According to the report, 35 percent of the incidents were caused by thermal runaway reactions [1]. To prevent the recurrence of similar incidents, it is important to identify and understand runaway reaction hazards. It is also essential to have knowledge of detailed chemical kinetics of energetic materials in order to optimize current systems, design new explosives, and control energy release for process safety. Traditionally, reactive chemicals have been tested by thermal analysis techniques. Temperature, pressure, and heat can be measured directly using different experimental techniques, and overall reaction kinetics can be derived from temperature or heat profile. The safe operating conditions and procedures can be defined by process risk analysis based on experimental data. However, the experimental tests are expensive and sometimes time-consuming. Besides, the underlying causes of runaway reactions have barely been understood at a fundamental level.

From the safety point of view, understanding the mechanisms of runaway reactions can help identify conditions that temper or control the reactions. A detailed kinetic model based on elementary reactions is reliable for scaling up laboratory

---

This dissertation follows the style and format of Thermochimica Acta.

experimental data to industrial conditions. This study will address this issue and study runaway reactions from both macroscopic and molecular points of view.

Runaway reactions are complex systems, and no detailed mechanism generation of runaway reactions has been conducted until now. Some groups have been working on generating complex mechanisms of combustion systems automatically using computers [2-4]. However, to the best of our knowledge, none of these automated mechanism generation programs has been commercialized or applicable to thermal runaway reactions of the hydroxylamine system. An approach is proposed in this study to predict runaway reaction mechanisms.

Hydroxylamine (HA) has been involved in two tragic incidents since 1999 [5, 6]. Thereafter, some efforts have been spent on the study of the thermal stability of 50 wt% HA/water solutions [7-9]. These studies show that HA decomposition is highly exothermic with a large pressure build-up in a contained environment [8]. The presence of air or oxygen is not necessary to initiate the decomposition because HA can undergo a redox reaction by itself [7]. The decomposition products under adiabatic conditions were also analyzed, and the overall equation is shown in Eqn. 1.1 [9]. The catalytic effect of metals and metal ions on the thermal decomposition of hydroxylamine was studied by Cisneros et al. [10] and Iwata et al. [11]. In this work, the effect of acid/base on the thermal decomposition of HA was analyzed, and the decomposition pathways of HA free base alone and in the presence of acid/base were proposed.
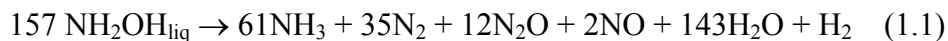
$$157\ NH_2OH_{liq} \rightarrow 61NH_3 + 35N_2 + 12N_2O + 2NO + 143H_2O + H_2 \quad (1.1)$$

Hydroxylamine nitrate (HAN) is an important member of the hydroxylamine family. High concentrations of HAN are used as liquid propellants and low concentrations of HAN are used primarily in the nuclear industry for decontamination of equipment. Due to its instability and autocatalytic decomposition behavior, HAN has been involved in several incidents [12]. Therefore, the thermal stability and decomposition pathway of HAN in water are of interest. Several groups have investigated the kinetics and mechanism of the HAN decomposition using various techniques and under different conditions [13-16]. However, due to its highly exothermic and rapid behavior of the reaction, these studies could not provide complete information about the decomposition process. In this work, the thermal decomposition hazard and mechanism of HAN is evaluated using both theoretical and experimental methods.

The commonly used experimental techniques to evaluate reactive hazards are reviewed in Chapter II. Some theoretical screening tools are applied to evaluate the 167 incidents from the CSB study in Chapter III. A method to predict runaway reaction mechanism is presented in Chapter IV. This method is applied to the thermal decomposition of hydroxylamine and hydroxylamine nitrate. The thermal runaway reaction hazards and decomposition mechanisms of HA in the presence of acid/base are presented in Chapter V, and the reactivity hazards of HAN are presented in Chapter VI. Chapter VII discusses the initial steps of hydroxylamine decomposition in the gas phase and the aqueous solutions. The decomposition network of HA is presented in Chapter VIII.

The objectives of this work are a) to analyze reactive hazards using calorimeters; b) to develop a methodology to predict and reduce runaway reaction mechanisms; c) to predict reactive hazards based on both thermodynamics and kinetics. Hydroxylamine and its salt hydroxylamine nitrate are used as the test systems to illustrate the approach.

CHAPTER II

EXPERIMENTAL METHODS

2.1. Introduction

A full assessment of the reactivity hazards of a chemical process should be based on specific test data for the desired reactions, undesired reactions, and process conditions [17, 18]. There are many hazard analysis methods, including the process hazards analysis (PHA) methodologies in the Occupational Safety and Health Administration (OSHA). No matter which hazard analysis methods are employed, it is essential to obtain accurate and reliable process safety data. Data for the reactants may be obtained from the literature, material safety data sheet (MSDS), and company records. However, due to the proprietary nature of the manufacturing processes, process hazards data is usually not available in the open literature. These data can only be obtained from appropriately designed experiments using appropriate testing techniques. The majority of reactivity hazard testing techniques are thermal analysis and calorimetric methods. The data obtained from the calorimetric tests can be transformed into relevant process safety information by expert interpretation [19].

2.2. Thermal Analysis Techniques

In order to study a sample of material, one of the easiest tests to perform is to heat it under controlled conditions. The behaviors of the samples and the changes upon heating can provide a great deal of information about the nature of the material. Thermal

analysis is a group of techniques in which the properties of a sample are studied while the sample is subjected to a controlled temperature program. The properties studied may include almost every physical or chemical property of the sample. The most frequently used thermal analysis techniques are shown in Table 2.1.

Table 2.1. The most frequently used thermal analysis techniques [20].

Technique	Abbreviation	Property to measure	Applications
Gravimetry or Thermogravimetric analysis	TG TGA	Mass	Decompositions, oxidations
Differential scanning calorimetry	DSC	Power difference or heat flow	Heat capacity, phase changes, reactions
Differential thermal analysis	DTA	Temperature difference	Phase changes, reactions
Evolved gas analysis Combined with Thermal and MS and FTIR	EGA	Gases produced or reacted	Decomposition
Thermomechanical analysis	TMA	Deformations	Mechanical changes

2.3. Calorimetric Techniques

For the chemical industries, it is important to identify reactive chemical hazards. We need to identify the conditions under which rapid exothermic reactions, explosions, or unwanted side reactions can occur, so that the processes may be carried out with the least risk and the most profitable production.

Calorimetry has been used to study reactive systems since 1780 by Lavoisier and Laplace. Calorimetry is the measurement of the heat changes that occur during a process,

and it encompasses a very large variety of techniques. These techniques can be used to evaluate both the desired and undesired reactions. These techniques can provide the basic data such as pressure, temperature, and power output as a function of time. These data can be transformed into specific parameters such as time to maximum rate, t_{MR}, onset temperature, T_{onset}, adiabatic temperature rise, ΔT_{ad}, approximate heats of decomposition, and global kinetics [19]. The safety information can be used to design cooling systems and adequate emergency response systems to manage runaway reactions. However, hazard evaluation is not merely performing calorimetric tests to determine the thermal parameters. The most important information we need to assess reactive chemical hazards is the pressure and pressure rise rates as functions of time and temperature. Unvented pressure rise due to a runaway reaction can lead to major vessel failures. It should be noted that the measurement of both temperature and pressure is a very important aspect of process safety.

2.4. Screening Level Tests

The DSC is a primary screening test apparatus. Measurement values obtained by the DSC can be used to determine heat capacity, heat of transition, purity, glass transition, and kinetic data [21]. For the application of safety, it can be used to indicate whether a material undergoes an exothermic or endothermic reaction and to identify a general temperature range in which significant reaction occurs. The DSC is often used to determine if further tests (adiabatic tests) are required.

A typical DSC test uses 1-5 mg of sample. The sample is heated from room temperature to an elevated temperature (150-400ºC) at a user defined ramp rate, usually 5-20ºC/min. Exotherms are usually detected by the DSC test at temperatures much higher than those that occur in plant equipment whose conditions are usually more adiabatic. The DSC cannot provide pressure information, which makes hazard evaluation from DSC data incomplete and possibly misleading.

In comparison with the DSC, the Thermal Screening Unit (TS^U) and the Reactive System Screening Tool (RSST) can provide both temperature and pressure information regarding the runaway characteristics of the chemicals under consideration. Both the TS^U and the RSST can produce important data, such as onset temperature of exotherm, rate of temperature rise, rate of pressure rise, maximum temperature and pressure, and time from exotherm initiation to maximum rate. They can be used to evaluate safe operating and storage temperatures, as well as the consequences of a runaway reaction.

The Thermal Screening Unit uses sample cells of up to 8ml in stainless steel, hastelloy, and other alloys as well as in glass. The TS^U can be operated at temperatures up to 400°C and pressures up to 2,900 psi. It can be used to evaluate long-term exposure at elevated temperatures (isothermal or "soak" test) [22].

The RSST, manufactured by Fauske & Associates, is a calorimeter for rapid measurements of reaction thermal behavior for temperatures up to 400 °C. It generates pressure rate and temperature rate data in an open system by comparison with an electronic standard. A 10 ml sample cell typically made of glass is placed inside and open to a pressure vessel (400 ml) that can withstand pressures up to 500 psia. The

RSST can be used not only for screening reactive chemicals, but also for designing emergency relief devices [23].

2.5. Adiabatic Calorimetry

Adiabatic calorimetry has proven to be an extremely useful tool to assess thermal hazards of reactive chemicals. The most frequently used adiabatic calorimeters are Accelerating Rate Calorimeter (ARC), Vent Sizing Package (VSP), the Advanced Reactive System Screening Tool (ARSST), and the Automatic Pressure Tracking Adiabatic Calorimeter (APTAC). This technique can minimize heat losses by keeping the temperature surrounding the sample as close as possible to the temperature of the sample. They can be used not only for screening but also for obtaining kinetic and thermodynamic data [24]. These thermokinetic and vapor pressure data can be used for constructing computer models that will predict the temperature and pressure as a result of a runaway reaction, and therefore the data can be used for sizing emergency relief devices for processes.

The ARC was developed by Dow Chemical in the 1970's [25], and it is commonly used to test thermal stability by chemical companies. A sample (usually 10 ml) is held in a sample cell that can be made of Hastelloy, titanium, tantalum, stainless steel, or inconel. The ARC proceeds with heat-wait-search mode. Initially, the sample is heated to a start temperature. Then during the wait mode, the temperatures of the sample and the containment stabilize. The ARC then goes to the search mode, in which the sample is constantly monitored for self-heating. If the sample doesn't exhibit self-

heating rate greater than a predetermined threshold (typically 0.02 °C/min), the ARC automatically heats the sample to the next 'heat step temperature' and repeats the sequence. These steps repeat until an exotherm is detected or an upper limit temperature is reached. The ARC can be operated at temperatures up to 500°C and pressures up to 1500 psig. The major drawback of the ARC is that a relatively heavy bomb must be used with the consequence that a significant fraction of the heat is absorbed by the bomb itself. In addition, the ARC is only capable of adiabatically following exotherms up to 20°C/min. The ARC cannot be used to study fast reactions unless the system is thermally diluted to lower the expected peak reaction rate.

In order to overcome the drawback of the ARC, the DIERS (the Design Institute for Emergency Relief Systems) program initiated the development of a bench scale low thermal inertia adiabatic calorimeter, which was first commercialized as the Vent Sizing Package (VSP) in 1985 and later improved to the VSP2 [26]. It consists of a 4L stainless steel vessel that can withstand pressures up to 1000 psig. The test cells are 120 ml in volume and can be made of 304SS, 316SS, Hastelloy C, Titanium, or glass-lined. The temperature operation range is −50 to 1000°C. It can be operated both in the open system and the closed system. The VSP uses the same operating mode (heat-wait-search) as the ARC. The advantage of the VSP over the ARC is that the VSP can produce low thermal inertia data because it utilizes the pressure compensating technique by the DIERS [27]. The VSP can test a large amount of materials in a thin wall sample cell because the pressure in the stainless steel vessel is automatically kept as close as possible to the pressure inside the sample cell.

The APTAC is also a low thermal inertia reaction calorimeter that uses the accelerating rate principle of the ARC and the pressure compensating principle of the VSP. It has improved data analysis software that makes it easier to process the data than the ARC. Another advantage of the APTAC is that it is possible to add reagents to the sample while the experiment is in progress. The pressure in APTAC's sample cell can be automatically released and the material collected into an external vessel. The APTAC can be operated in a variety of test modes, such as heat-wait-search, heat ramps, simulated fire exposure, and isothermal aging with temperatures up to 500°C and pressures ranging from vacuum to 2,000 psia. It can track exotherms at heat generation rates from 0.04 to 400 °C/min, a range 20 times wider than the ARC [24].

Following the introduction of the RSST that provides an easy, inexpensive approach to the DIERS testing method, recent enhancements led to the Advanced RSST (ARSST) in 1999. The ARSST retains the capabilities of the RSST, while incorporating the most recent advances in adiabatic calorimetry. Its new features include heat-wait-search methodology, isothermal hold tests, DSC mode of operation, injection of a sample (i.e. catalyst) against up to 750 psi backpressure during a test [28]. However, the open-cell feature of ARSST still limits its applications in accuracy.

The information about other adiabatic calorimeters such as PHI-TEC and Adiabatic High Pressure Dewar can be found from the website of HEL Group Ltd. (http://www.helgroup.co.uk/).

2.6. Comparison of the Calorimeters

At the screening level, the DSC, the TS^U, and the RSST are easy to operate and maintain. The test duration is usually 1-5 hours. The DSC is the most commonly used screening tool, but it cannot provide pressure rise information. The TS^U, and the RSST, on the other hand, can provide both temperature and pressure profiles during a runaway reaction.

The adiabatic calorimeters, especially the low thermal inertia calorimeters can simulate process equipment in the plants, they can provide accurate information about the reaction chemistry and process conditions to be avoided. However, they are usually time consuming and difficult to maintain. Comparisons of the adiabatic calorimeters are listed in Tables 2.2 and 2.3.

Table 2.2. Comparison of the different adiabatic calorimeters.

Apparatus	Adiabatic	Low ϕ factor	Pressure compensation	Heat Wait Search	Closed test cell	Easy to use	Stirring
ARC	X			X	X		X
VSP	X	X	X	X	X		X
APTAC	X	X	X	X	X		X
ARSST	X	X		X		X	X
PHI-TEC	X	X	X	X	X		X
Dewar Flask	X	X			X	X	X

Table 2.3. Comparison of the frequently used adiabatic calorimeters.

Parameter	ARC	VSP2	APTAC
Sample cell size (ml)	10	120	130
Sample container	SS, Ti, Tantalum, Hasteloy C	304SS, 316SS, Hastelloy C, Titanium, or glass-lined	Variety of metals, glasses, ceramics, and plastics(low temperature)
Typical phi factor	1.7+	1.05+	1.1+
Self-heat rate sensitivity(C/min)	0.02	0.05	0.04
Self-heat tracking(C/min)	Up to 15	100	400
Pressure tracking (psi/min)	none	Up to 3,000	Up to 10,000
Temperature range(°C)	Ambient -500	-50 to 1000	Ambient -500
Pressure range(psi)	Ambient - 1500	Ambient - 1000	Vacuum - 2000
Injection	none	yes	Metered and one-shot
Venting capability	none	Direct venting	Simple and controlled
Report generator	none	none	automatic
Software	Windows95	Windows98/NT	Windows95/NT
Stirring	Magnetic coupled	Magnetic coupled	Magnetic coupled/direct drive option

When safety information about a chemical process is not available in the open literature, a screening test is typically conducted. If the screening test indicates an exothermic activity or a high pressure generation, and it is not clear whether the process equipment can handle the condition, an adiabatic test is usually needed to obtain accurate information about the reaction chemistry and provide the basis for process improvement. In this work, the RSST was used for screening tests and the APTAC was

employed for advanced tests. The schematic figures of the two apparatus are shown in Figures 2.1 and 2.2.

Injection system

Heater connection

Thermocouple connection

Rupture disc

Containment vessel

Thermocouple

Sample cell

Insulation

Stirrer bar
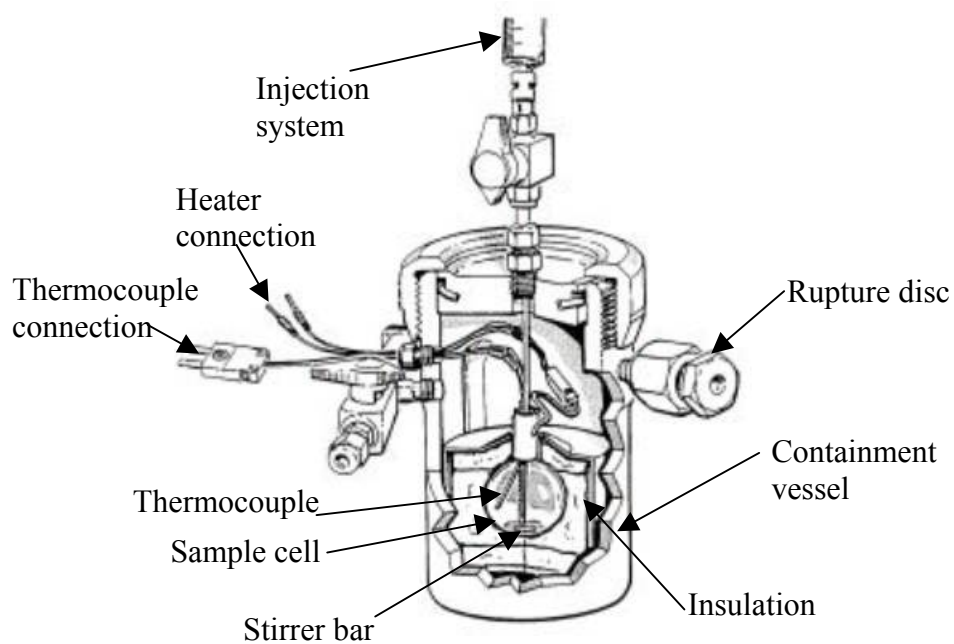
Figure 2.1.   Schematic of the RSST™ containment vessel, sample cell, and heating system.
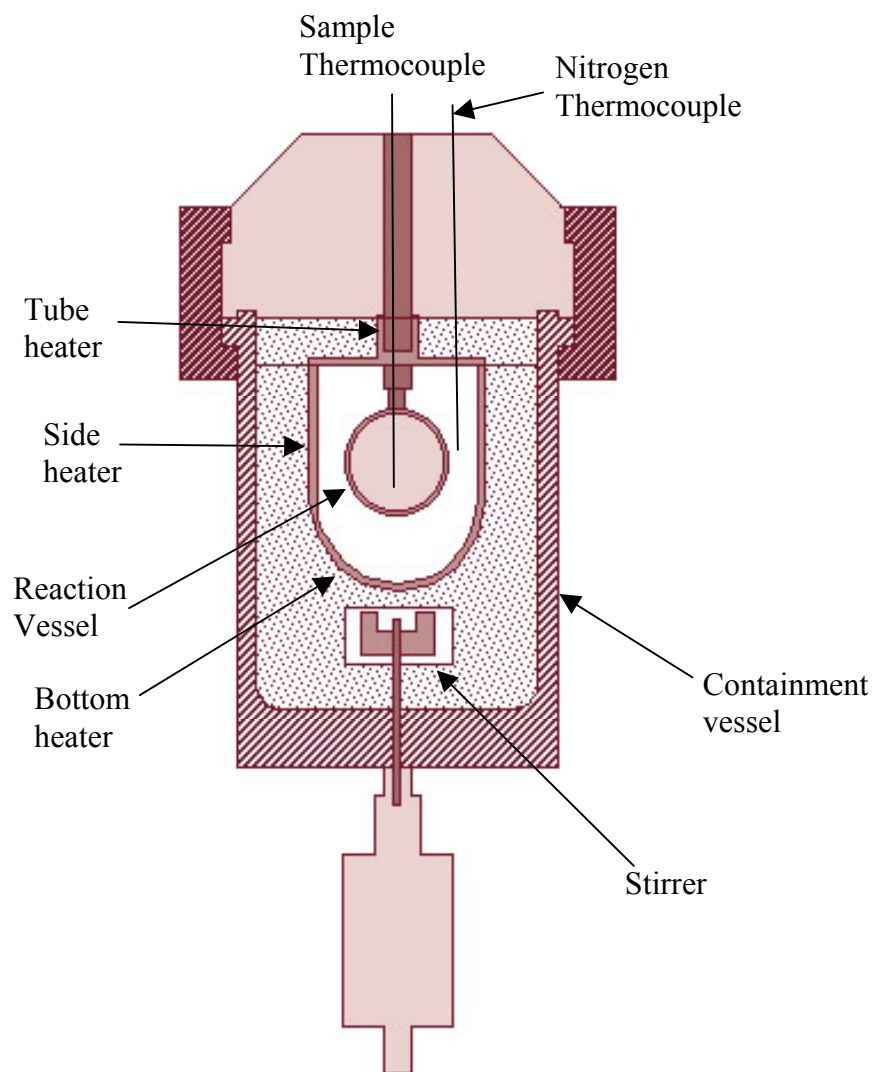
Figure 2.2. Schematic drawing of the APTAC™ containment vessel, reaction vessels, and heating system.

CHAPTER III

THEORETICAL SCREENING TOOLS[*]

3.1. Introduction

Reactive chemical hazards have been a significant concern for facilities that process, handle, transport, or store reactive chemicals [29]. The reactivity associated with chemicals is beneficial to produce a variety of stable products. However, chemical reactivity can lead to significant hazards under certain conditions, and uncontrolled reactions can develop into reactive chemical incidents. Without proper control of hazards and risks, reactive chemical incidents have caused catastrophic effects for human beings and the environment worldwide.

Previous efforts have analyzed reactive incidents data and provided information and lessons to help prevent similar incidents. An analysis of 142 thermal-runaway reaction incidents occurring in the UK during the period of 1962-1984 was presented by Nolan and Barton [30]. Ho et al. [31] provided case studies of 65 incidents involving runaway reactions and emergency relief in Taiwan. Trends in chemical hazards in Japan were reported by Wakakura and Iiduka [32]. Also, the U.S. Chemical Safety and Hazard Investigation Board (CSB) [1] released in 2002 a report on 167 reactive chemical incidents that occurred in the U.S. between 1980 and 2001 .

---

[*] This chapter contains material reprinted from Journal of Loss Prevention in the Process Industries, 17 (4), C. Wei, W.J. Rogers, M.S. Mannan, Application of screening tools in the prevention of reactive chemical incidents, 261-269, Copyright (2004) with permission from Elsevier Science.

The CSB report suggested that there are gaps in existing Occupational Safety and Health Administration (OSHA) and the Environmental Protection Agency (EPA) regulations, because over 50 percent of the 167 incidents involved chemicals not covered by OSHA or EPA regulations. The report also concluded that the National Fire Protection Association (NFPA) instability ratings used for determining coverage of reactive hazards in the OSHA PSM standard were designed for emergency response and have significant limitations with respect to identification of reactive hazards.

The failure of existing regulations in terms of coverage is that they are based on a limited list of individual chemicals that are inherently unstable. However, reactive hazards are not associated only with intrinsic properties of chemicals but also related to process-specific conditions. Almost any chemical can be reactive under certain conditions. It is extremely difficult to regulate reactive chemicals because both intrinsic properties and external process conditions must be considered.

3.2. Screening Tools

An effective screening tool must be easily applicable for hazard identification and risk elimination concerning reactive hazards. The limitations of each tool are stated, and recommendations are made to improve the efficiency and effectiveness of the hazard identification process.

3.2.1. Checklist for Reactive Hazard Management

In 1995, the Center for Chemical Process Safety (CCPS) published "Guidelines for Chemical Reactivity Evaluation and Application to Process Design" [33] and "Guidelines for Safe Storage and Handling of Reactive Materials" [34]. Because of recent incidents such as at Napp Technologies in 1995 and at Morton International in 1998, concerns about reactive hazards have been raised to a national level [35]. The effective management of reactive chemicals poses a major challenge that must be met urgently. Recently, CCPS published a new concept book "Essential Practices for Managing Chemical Reactivity Hazards" [36] which provides a simple screening methodology to identify the risk of reactive incidents and then guides the readers to resources on how to manage the risk. The essential practices include commitment, identification, risk assessment, control, and mitigation measures. Due to an agreement with several other organizations, this concept book is being provided free of cost via the Internet for a limited period.

The screening method discussed in detail in Chapter 3 of the CCPS concept book [36] classifies reactive hazards into general types. There are twelve questions in a checklist, which can also be used to document the general kinds of hazards. Because of the limited information in the CSB 167 incident database, not all of the questions can be answered. This paper concentrates on six general kinds of reactive hazards described in the CCPS concept book and listed below.

1. Pyrophorics or spontaneously combustible chemicals;

2. Peroxide forming chemicals;

3. Water reactive chemicals;

4. Oxidizers;

5. Self reactive chemicals including decomposition, polymerization, and rearrangement;

6. Incompatible materials.

3.2.2. Material Safety Data Sheet (MSDS)

MSDSs are provided by suppliers and also can be found through the Internet (http://www.ilpi.com/msds/). In this work, MSDS and safety card information from the search engine provided by Texas A&M University (available on-line at http://finance.tamu.edu/ehsd/resources/msds.htm) was used. The Stability and Reactivity section in a MSDS provides information about chemical stability, possible self-decomposition products, hazardous polymerization, and incompatibility with other materials.

3.2.3. NOAA Reactivity Worksheet

The U.S. National Oceanic and Atmospheric Administration (NOAA) Chemical Reactivity Worksheet [37] was employed to determine the reactive hazards of individual chemicals and incompatibility of mixtures. The worksheet is straightforward to use and easy to interpret with a database of over 6,000 chemicals, and it is available free of charge from the NOAA website. The worksheet can be used to check the intrinsic reactive properties of individual chemicals, such as peroxidability, polymerizability, and

water or air reactivity. In addition, the worksheet is a powerful tool to predict the reactivity of a mixture of chemicals based on the reactive groups to which the chemicals belong.

3.3.4. ChemOffice

ChemOffice Ultra 2004 suite of programs [38] includes ChemDraw Ultra 8.0, Chem3D Ultra 8.0 and ChemFinder Ultra 8.0. ChemDraw has a convenient new function as "Name = Struct" [39] which converts a systematic chemical name into a structure. The structure in ChemDraw can be transformed into 3-D model and linked into Chem3D, which provides an easy graphic interface for MOPAC to calculate heat of formation directly using AM1 [40], MNDO [41], MINDO/3 [42], and PM3 [43]. These semiempirical methods can be treated as a 'black box' and do not require much knowledge of chemistry to carry out calculations.

Semi-empirical molecular orbital methods have wide applications because of low computer costs and can calculate heat of formation directly. For these calculations, many electron interaction terms are neglected or replaced by empirical parameters. The quality of thermodynamic predictions using MNDO, AM1, and PM3 was reviewed by Thiel [44].

3.2.5. CHETAH

CHETAH computer program which was developed by the ASTM Subcommittee E27.07 can predict reactivity hazard potential from chemical structure using Benson's

second order group contribution method [45]. It is also a useful tool for the estimation of gas phase thermodynamic data, such as heat of formation, specific heat capacity, and entropy. The maximum energy available in a compound or mixture can be calculated, and the potential energy release is evaluated using a rating scheme based on experimental shock sensitivity data [46]. It has found its applications in many areas [46-50] because of its accuracy and easy accessibility and is therefore ideal for preliminary hazard evaluation. Some reviews and critical comments are available [51, 52].

To evaluate the potential of violent decomposition, CHETAH calculates the value of six hazard evaluation criteria, as follows:

1. maximum heat of decomposition;

2. fuel value minus heat of decomposition;

3. oxygen balance;

4. CHETAH ERE criterion;

5. overall energy release potential;

6. net plosive density.

These criteria are discussed in details in CHETAH User's Manual and review papers [51, 52].

3.2.6. CART

The other important hazard indication criteria are based on heat of reaction and adiabatic reaction temperature of the equilibrium mixture (CART). Some commercial software such as SuperChems can calculate heat of reaction and CART, and also the

Melhem index hazard rating. An analysis [53] of CSB incident data shows that the Melhem index is effective in hazard identification when the thermo-physical data of the mixtures are available. When the data are missing, CHETAH and ChemOffice can be used to estimate them to input into SuperChems.

3.3. Screening Results

3.3.1. MSDS and Reactivity Worksheet Results

MSDS and the Reactivity Worksheet were used to analyze the CSB 167 incident data using the checklist discussed in section 2.1. The screening results are shown in Figure 3.1. One hundred and forty four incidents involved chemicals that satisfy at least one of the hazard criteria. Twenty three incidents could not be analyzed because the CSB data did not include enough information about the chemicals involved in 19 incidents. The other four incidents involved chemicals that are not available in either the MSDS or the Reactivity Worksheet. These results show that the significant majority of the incidents involved chemicals for which hazard information was readily available in the literature. Additionally, this conclusion underscores the fact that MSDSs and Reactivity Worksheet are good resources for the required technical information. Figure 3.2 shows overall reactive hazard distribution for the 167 incidents. About 66 percent of the incidents involved chemicals that can self-decompose or polymerize at certain temperatures. Over 50 percent of the incidents can also be attributed to incompatible materials.
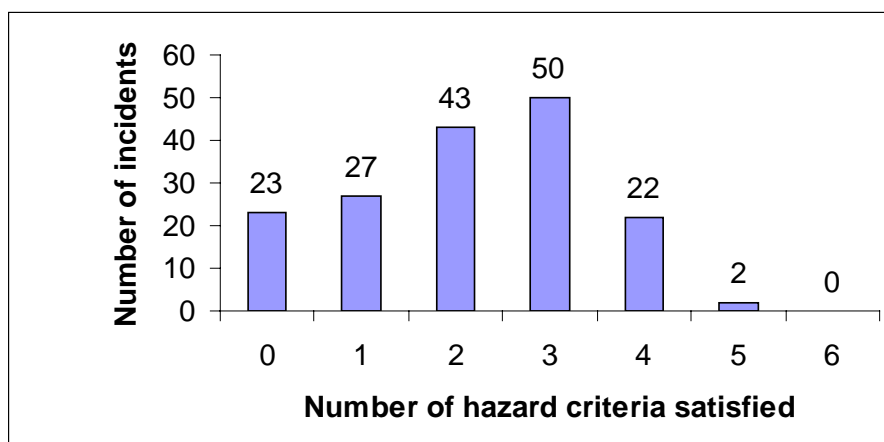
Figure 3.1. Screening results using MSDSs and Reactivity Worksheet.
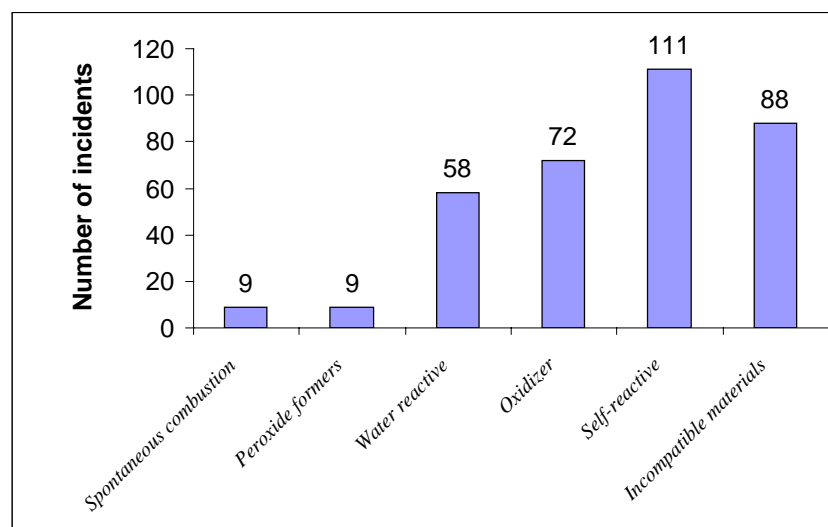
Figure 3.2. Distribution of reactive hazard criteria.
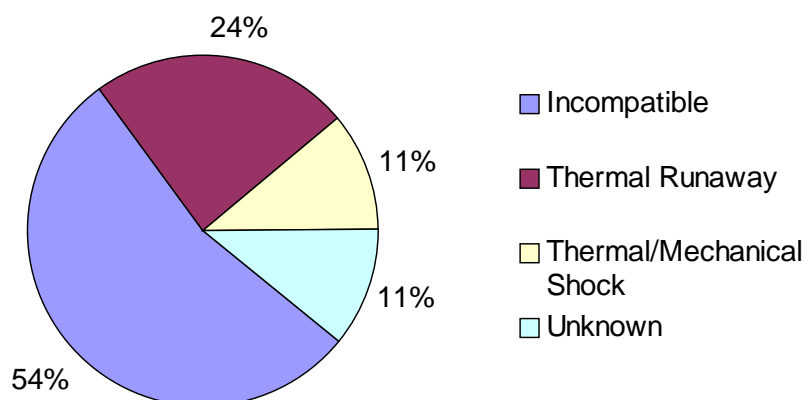
Figure 3.3. CSB reactive hazards distribution for incidents that occurred in storage equipment.

CSB data analysis classified reactive hazards as chemical incompatibility, runaway reaction, and impact or thermally sensitive materials. Figure 3.3 shows reactive hazard distribution based on the CSB analysis for incidents that occurred in storage equipment. Of the 37 incidents, 54 percent are attributed to incompatible materials, 24 percent to runaway reactions, 11 percent to impact or thermally sensitive materials, and 11 percent to unknown information. Analysis based on CCPS reactive hazard classification is shown in Figure 3.4. Both strong oxidizers and self-reactive chemicals contributed to about 50 percent of the incidents. Special precautions are needed to deal

with oxidizers and unstable compounds in storage facilities. Table 3.1 shows the frequency of some chemicals involved in the incidents that occurred in storage equipment. It is of particular interest to note that sodium hypochlorite was involved in 9 of the 37 incidents. These findings underscore the importance of learning and sharing lessons from previous incidents.
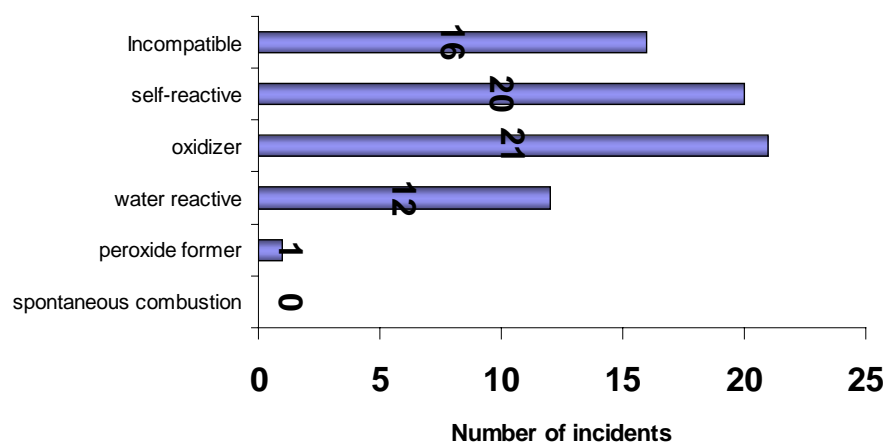
Figure 3.4. Distribution of reactive hazards for incidents that occurred in storage equipment.

Table 3.1. Frequency of the chemicals involved in the incidents that occurred in storage equipment.

Chemicals	Number of incidents involved
Sodium hypochlorite	9
Ferric chloride	4
Sulfuric acid	3
Nitric acid	3
Hydrochloric acid	3
Organic peroxides	3
Sodium azide	2
Sodium hydrosulfide	2
Others	1

3.3.2 CHETAH Results

In the previous section, self-reactivity was used as a criterion to identify reactive hazards. MSDSs and the Reactivity Worksheet can only give qualitative results concerning decomposition or explosive properties. The explosive hazard assessment of energetic materials is needed for reactive chemical management. CHETAH can provide measures of the likelihood that a chemical or mixture can undergo rapid self-decomposition when subjected to mechanical shock. This computerized tool is convenient for obtaining semi-quantitative results of potential explosive hazards. Compared with experimental analysis, time, and budget requirements for CHETAH calculations are relatively nominal.

In this work, a set of chemicals involved in incidents that occurred in reactors are analyzed using CHETAH. If the chemicals are available in the CHETAH database, gas molecules are used to calculate the hazard evaluation criteria. When they are not

available as gas molecules, Benson Groups are used to build the chemicals. In some cases, some functional groups are missing in the database, so the enthalpies of missing functional groups are estimated using a combination of selected Benson Groups in the database, as discussed in Appendix A of CHETAH User's Manual.

Table 3.2 shows the results of maximum heat of decomposition, the decomposition products yielding the maximum heat of decomposition, and overall energy release potential. Both values and hazard classification are shown for maximum heat of decomposition and overall energy release potential. Of the 33 incidents analyzed, 24 incidents involved at least one chemical with HIGH overall energy release potential. Among the remaining 9 incidents, 7 were caused by either polymerization or incompatibility with other process chemicals. Unfortunately, at present, CHETAH cannot assess the hazards associated with polymerization. Although CHETAH can calculate the heat of reaction and evaluate chemical reaction hazards involving more than one chemical, it is beyond the scope of this paper.

There are only two incidents with undetermined reactive hazards. As shown in the CSB data, incident 90 involved only one chemical called chlorakyl phosphite and incident 99 involved only nitrosylsulfuric acid. The authors believe there may be a typo in chlorakyl phosphite from either the CSB database or the original source. The correct name could be chloralyl phosphite. Both incidents showed unknown reaction types in the CSB data. Further information is needed to draw a conclusion about these two incidents. CHETAH results show MEDIUM hazard of maximum heat of decomposition and LOW hazard of overall energy release potential for the two incidents. Therefore, special

precautions should also be observed for chemicals with MEDIUM hazard of maximum heat of decomposition even though the overall energy release potential is low.

The CHETAH screening results show that the overall energy release potential is a suitable indicator of potential explosive self-reaction. The maximum heat of decomposition also provides significant guidance regarding self-reactivity hazard. A more negative value usually indicates a higher self-reactivity hazard. A zero value means the chemical will not decompose. The maximum heat of decomposition can also be used for the design of cooling systems and relief devices.

3.3.3. Heat of Formation

Heat of formation is an important thermodynamic parameter. Heat of reaction can be calculated only when heats of formation of all the reactants and products are known. The heats evolved from both desired and secondary reactions are crucial for reactive hazard evaluation. With present methods, heat of formation can be determined accurately using either calorimetric methods or computational methods. For many molecules, experimental heats of formation data are available, and they can be used to develop parameters of empirical and semi-empirical predictive methods. Sometimes, especially for unusual functional groups, reactive intermediates, and transition states, a calculation method is a convenient way to predict heat of formation when the experimental values are not available. High-level quantum chemical calculations can be time consuming and expensive. As screening tools, empirical and semi-empirical methods are available with fair accuracy at low cost.

Table 3.2. CHETAH screening results of the chemicals involved in the incidents occurred in reactors.

Incident no	Chemical name	Maximum heat of decomposition		Decomposition products	Overall energy release potential	
		Value(kcal/g)	Hazard class		Value	Hazard class
2	Hydrogen cyanide	-1.32	HIGH	$0.75C(s)+0.5\ N_2\ (g)+0.25\ CH_4\ (g)$	-1.158	**HIGH**
2,40,70,94	Formaldehyde	-1.061	HIGH	$C(s)+H_2O\ (g)$	-0.384	**HIGH**
2	HCN+CH2O	-1.183	HIGH	$1.75C(s)+0.5\ N_2\ (g)+0.25\ CH_4\ (g)+H_2O\ (g)$	-1.232	**HIGH**
7,163,167	Ethylene oxide	-1.229	HIGH	$1.5C(s)+0.5\ CH_4\ (g)+H_2O\ (g)$	-0.234	**HIGH**
9	Glycidol	-0.541	MEDIUM	$2.5C(s)+0.5\ CH_4\ (g)+2\ H_2O\ (g)$	0.406	**LOW**
9,132	Methanol	-0.582	MEDIUM	$0.5C(s)+0.5\ CH_4\ (g)+H_2O\ (g)$	0.418	**LOW**
9	Glycidol+Methanol	-0.553	MEDIUM	$4\ CO_2\ (g)+H_2O\ (g)$	0.41	**LOW**
25,74	Butadiene	-0.982	HIGH	$2.5C(s)+1.5\ CH_4\ (g)$	-0.141	**HIGH**
7	Aluminum chloride	-0.112	LOW	$0.5AL+2CH6(g)$	0.1	**LOW**
33	Dicyclopentadiene	-0.758	HIGH	$7C(s)+CH_4\ (g)$	-0.231	**HIGH**
33	Ethylene glycol	-0.507	MEDIUM	$1.5C(s)+0.5\ CH_4\ (g)+2\ H_2O\ (g)$	0.367	**LOW**
33,62	Maleic anhydride	-0.328	MEDIUM	$3C(s)+CO_2\ (g)+H_2O\ (g)$	0.268	**LOW**
33, 163	Diethylene glycol	-0.564	MEDIUM	$3C(s)+CH_4\ (g)+3\ H_2O\ (g)$	0.414	**LOW**
36	2-ethylhexylamine	-0.319	MEDIUM	$3.25C(s)+0.5\ N_2\ (g)+4.75\ CH_4\ (g)$	0.532	**LOW**
36,132	O-nitrochlorobenzene	-0.754	HIGH	$4.75C(s)+0.5\ N_2\ (g)+0.25CCl_4(g)+CO_2(g)$	-0.491	**HIGH**
39	n-butyl acrylate	-0.439	MEDIUM	$5C(s)+2\ CH_4\ (g)+2\ H_2O\ (g)$	0.462	**LOW**
39	di-tert butyl peroxide	-0.652	MEDIUM	$4.5C(s)+3.5\ CH_4\ (g)+2\ H_2O\ (g)$	-0.292	**HIGH**
40,70,94	Phenol	-0.559	MEDIUM	$5C(s)+CH_4\ (g)+H_2O\ (g)$	0.521	**LOW**
52	Ethylene	-1.084	HIGH	$C(s)+CH_4\ (g)$	-0.086	**HIGH**
63,161	2-ethylhexanol	-0.318	MEDIUM	$4C(s)+4\ CH_4\ (g)+H_2O\ (g)$	0.506	**LOW**
63	Hydrogen peroxide	-0.743	HIGH	$0.5O2(g)+H_2O\ (g)$	-1.375	**HIGH**
66, 106	Methyl chloride	-0.207	LOW	$0.5C(s)+0.5\ CH_4\ (g)+HCl\ (g)$	0.221	**LOW**

Table 3.2 Continued.

Incident no	Chemical name	Maximum heat of decomposition		Decomposition products	Overall energy release potential	
		Value(kcal/g)	Hazard class		Value	Hazard class
68	Ammonium nitrate	-0.582	MEDIUM	$0.8 N_2 (g)+0.4HNO_3(g)+1.8 H_2O (g)$	-0.634	**HIGH**
68,161	Nitric acid	0	LOW	$HNO_3(g)$	0.185	**LOW**
82	Dichloro-nitrosoethane	-0.598	MEDIUM	$1.75C(s)+0.5 N_2 (g)+0.25CO_2(g)+2HCl(g)+0.5H_2O (g)$	-0.621	**HIGH**
90	Chloralylphosphite	-0.133	LOW	$0.5C(s)+1.5CO_2(g)+Cl_3OP(g)$	0.104	**LOW**
91	Dimethyl sulfate	-0.502	MEDIUM	$1.5C(s)+S(s)+0.5CO_2(g)+3 H_2O (g)$	0.291	**LOW**
91	Dimethylhydroxylamine	-1.041	HIGH	$0.75C(s)+0.5 N_2 (g)+1.25CH_4(g)+ H_2O (g)$	-0.314	**HIGH**
92	Cyanopyridine	-0.804	HIGH	$5C(s)+N_2(g)+CH_4(g)$	-0.337	**HIGH**
99	Nitrosylsulfuric acid	-0.014	LOW	$0.5 N_2 (g)+0.75O_2(g)+0.5H_2O_4S(g)+0.5SO_3(g)$	0.123	**LOW**
106	Alcohol	-0.424	MEDIUM	$C(s)+ CH_4 (g)+ H_2O (g)$	0.436	**LOW**
106	Cumene hydroperoxide	-0.867	HIGH	$7C(s)+2 CH_4 (g)+2 H_2O (g)$	-0.296	**HIGH**
129	Sulfur dichloride	0	LOW	$Cl_2S(g)$	0.082	**LOW**
129	Toluene	-0.517	MEDIUM	$5C(s)+2 CH_4 (g)$	0.598	**LOW**
137,139,161	Sulfuric acid	0	LOW	$H_2SO_4 (g)$	0.09	**LOW**
137	Isopropyl alcohol	-0.323	MEDIUM	$1.5C(s)+1.5CH_4(g)+ H_2O (g)$	0.44	**LOW**
137,157	Acrylonitrile	-0.664	MEDIUM	$2.25C(s)+0.5 N_2 (g)+0.75 CH_4 (g)$	-0.372	**HIGH**
139	Glycerin	-0.492	MEDIUM	$2.5C(s)+0.5 CH_4 (g)+3 H_2O (g)$	0.353	**LOW**
139	Anisol	-0.622	MEDIUM	$5.5C(s)+1.5CH_4(g)+ H_2O (g)$	0.559	**LOW**
142	Nitro ethane	-1.277	HIGH	$1.75C(s)+0.5 N_2 (g)+0.25 CH_4 (g)+2 H_2O (g)$	-1.237	**HIGH**
163	Phosphorous oxychloride	0	LOW	$Cl_3OP(g)$	0.058	**LOW**
164	Terephthaloyl-dichloride	-0.32	MEDIUM	$7.5C(s)+0.5CO_2(g)+2HCl(g)+ H_2O (g)$	0.29	**LOW**

In this work, the chemicals involved in reactor incidents were analyzed. Experimental heats of formation values were obtained from the NIST Webbook (http://webbook.nist.gov). ASTM CHETAH computer program was used to estimate the gas phase heat of formation. MOPAC 2000 integrated in ChemOffice Ultra 2004 suite of programs [38] was used for semiempirical calculations. The optimized structures of the chemicals are shown in Appendix A.

Both ASTM CHETAH and ChemOffice are desktop software and are easy to use. Appendix B compares the calculation results using CHETAH and MOPAC with experimental values. The values without notations of specific phase are heats of formation of gas phase molecules. CHETAH results fall in the range of MOPAC calculation results when experimental data are missing. Compared with experimental data, CHETAH results are very close even when Benson Groups and estimated missing groups are used to calculate heats of formation, because the maximum error from available experimental values is 29.71 kJ/mol for dimethyl sulfate. The results indicate a reasonable accuracy of the bond additive method.

Semiempirical molecular orbital methods have wide applications because of low computer costs and can produce heat of formation directly. Many electron interaction terms are neglected or replaced by empirical parameters. The quality of thermodynamic predictions using MNDO, AM1 and PM3 was reviewed by Thiel [44]. Some theoretical values are not available as shown in Appendix B, because parameters are missing in a specific method. Generally speaking, AM1 and PM3 can provide better results than MNDO and MINDO/3 because more optimized parameters per element are included in

the AM1 and PM3 methods. The maximum deviations of AM1 from experimental values are 129.70 kJ/mol for di-tert butyl peroxide and −92.05 kJ/mol for sulfur dichloride, but PM3 improves the errors to 83.68 kJ/mol and −28.03 kJ/mol, respectively. Considering the fact that only a minute on a PC is required for one molecule, AM1 and PM3 can provide good accuracy to predict thermodynamic properties of many chemicals with low cost.

3.4. Proposed Methods for Screening Reactivity Hazards

Existing screening methods and hazard criteria like CHETAH and CART only consider thermodynamic effects. In most cases, pressure generation is responsible for equipment damage and personal injury. An endothermic reaction can also cause gas generation and pressure buildup. Another drawback of the theoretical screening tools is the lack of kinetic information. The rates of heat release and pressure generation are important indicators of the reaction rates. Thermal runaway reactions will occur when the heat generation rate is higher than the heat removal rate. At present, experimental testing has to be conducted in order to obtain the needed pressure and kinetic information.

Experimental testing is time and resource consuming. Most of the time, only small quantity of chemicals can be tested, and the experimental results depend on the testing conditions. It is ideal to simulate industrial conditions without experimental testing. Therefore, a theoretical tool is still needed to predict reactivity hazard and provide both kinetic and thermodynamic information. A detailed kinetic modeling

approach is proposed as shown in Figure 3.5. This approach incorporates reaction network generation, rate constants estimation, and simulation of industrial conditions. This hazard evaluation based on elementary reactions can offer best accuracy and reliability. In addition, a specific elementary reaction can be re-used for completely different operating conditions and in different species mixtures. With development of computer resources and kinetic databases, this theoretical approach will become applicable and practical in the future. In this work, efforts were focused on mechanism generation for runaway reactions, and the hydroxylamine system was used as examples.
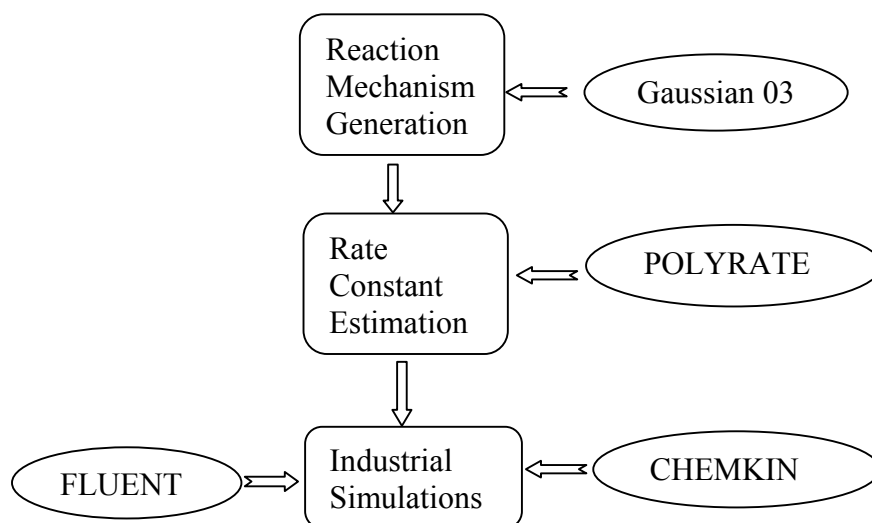
Figure 3.5. Proposed theoretical reactivity evaluation approach and some available commercial software.

3.5. Conclusions

Applying the CCPS screening method, qualitative reactive hazards can be easily assessed by MSDS and the NOAA Reactivity Worksheet. Of the 167 incidents reported in the CSB study, only four involved chemicals that are not available in MSDS or the Reactivity Worksheet.

The CHETAH screening results show that overall energy release potential and maximum heat of decomposition are suitable indicators of potential explosive self-reaction hazards. CHETAH can also be used to estimate heat of formation value when experimental data are not available. Accuracy of the results is comparable with that of semiempirical molecular orbital calculations.

MOPAC incorporated in the ChemOffice software is user friendly and the results are easy to interpret. AM1 and PM3 can provide accurate results of heats of formation data at low cost. These values are crucial for estimation of heat of reaction. Furthermore, adiabatic temperature rise can be estimated from heat of reaction, and the heat and temperature information are important for process hazard analysis and process design.

Based on the analysis of the 167 incidents reported in the CSB study, it can be concluded that the CCPS concept book is a good source for managing reactive chemicals. MSDS, Reactivity Worksheet, CHETAH, and MOPAC proved to be practical tools to screen reactive hazards. However, these tools have their limitations. A screening tool for kinetics was proposed to provide accurate simulation of industrial conditions. Reactive hazard evaluation should be followed by risk analysis for the facility. Based on

risk assessment, inherently safer equipment, and optimal operating conditions can be implemented to control reactive hazards.

CHAPTER IV

PREDICTION OF THE MECHANISMS OF RUNAWAY

REACTIONS

4.1. Introduction

In a chemical reaction, reactants undergo a change of composition, constitution, and/or configuration. A chemical equation is a way to describe what goes on in a reaction, with an arrow pointing to the right that indicates the action of the reaction. In the late nineteenth century, people started to realize that the kinetics of simple reactions were so different from what one would expect from the stoichiometry in a chemical equation because reactions followed complex mechanisms. It is common to measure mechanisms from kinetics information, instead of predicting mechanisms.

During last two decades, the idea of predicting mechanisms became practical because of powerful computer resources. Numerous detailed kinetic mechanisms have been manually constructed, especially in the area of combustion [54, 55]. These models consist of extensive amounts of elementary reactions based on kinetic parameters derived from a combination of experimental measurements, computational chemistry, and estimation of thermodynamic properties. The manually constructed mechanisms are time- and labor- intensive even for a simple reactant. Recently, there have been some efforts for automated kinetic mechanism generation [4, 56-59]. A mechanism consisting of thousands of elementary reactions can be generated using computer programs. The problems associated with large explicit mechanisms make it difficult to couple such

kinetic models with computational fluid dynamics (CFD) simulations. Large computational requirements prevent their application to practical industrial systems when non-homogeneous conditions may be dominant. Mechanism reduction has become a necessity to reduce computational size. By identifying the most important species and elementary reactions, the errors introduced by mechanism reduction should be minimized.

4.2. Prediction of Runaway Reaction Mechanisms

A runaway reaction is a complex system, and it may involve thousands of elementary reactions. In order to predict the reaction mechanism with a reasonable computational size, only kinetically important elementary steps should be included. A general approach is proposed that incorporates both empirical rules and quantum chemical calculations.

Gas phase reactions will be considered first because properties of gas phase species can be easily estimated using quantum chemical calculations. Most gas-phase reactions of neutral species follow initiation-propagation mechanisms [60]. The reactants break the weakest bond, forming reactive species, and the reactive species react with the reactants through a series of steps forming products. Most of the reactive species will often be radicals that have unpaired electrons. All of the reactive species and possible reactions must be predicted. Quantum chemical calculations are employed to estimate thermodynamic properties of the species, enthalpies of reactions, and activation barriers. However, it is time consuming to optimize the structures and calculate the energies of

the intermediates, especially transition states using quantum mechanical methods. Empirical rules can be used at a screening level to eliminate elementary reactions with high activation barriers.

4.3. Empirical Rules

To simplify the procedure of predicting the kinetics of elementary reactions, linear free energy relationship and the Evans-Polanyi empirical rule, as shown in Eqn. 4-1 [61], are used to estimate activation barriers from heats of reactions.

$$E_a = E_a^0 + \gamma_p \, \Delta H_r \qquad (4-1)$$

where E_a^0 is the intrinsic activation barrier, γ_p is the transfer coefficient, and ΔH_r is the heat of reaction. Empirical values of E_a^0 and γ_p can be found in reference [61].

The process of generating runaway reaction mechanism includes the following steps:

a. Initiation step: predict all of the radicals that are likely to form when breaking the bonds of the reactants and $E_a \leq 0.15T$ (kcal/mol/K) [21], where T (K) is the reaction temperature.

b. Propagation step: radicals must react with reactants or intermediates via a catalytic cycle. All reactions with $E_a \leq 0.07T$ (kcal/mol/K) [21] should be included. There should be a cycle satisfying $E_a \leq 0.05T$ (kcal/mol/K) [21]. For most explosions, there should be a branching reaction step in which the net numbers of reactive intermediates increase.

c. Termination step: radicals recombine into stable species.

4.4. Reaction Classes

To build a reaction mechanism, we need to start from reactants. Based on the structure of reactants, a series of elementary reactions can be postulated using the knowledge of reaction classes. In this work, the reaction types were classified as follows:

a. Simple bond scission includes unimolecular decomposition, radical decomposition, and hydrogen abstraction. It can be expressed as AB → A + B. A and B can be either atoms or functional groups. E_a^0 and γ_p are assumed to be 1 kcal/mol and 1.0, respectively, when predicting mechanisms.

b. An atom transfer reaction represents an atom transferring from one reactant to another. It can be expressed as $R_1x + R_2 \rightarrow R_1 + R_2x$, where x is an atom. The hydrogen transfer reaction is the most common type of reaction. The values of E_a^0 and γ_p depend on heats of reaction. When ΔH_r is between 0 and –40 kcal/mol, E_a^0 and γ_p are assumed to be 12 kcal/mol and 0.3, respectively. If ΔH_r is more exothermic than –40 kcal/mol, E_a^0 and γ_p are assumed to be 0. When ΔH_r is between 0 and 40 kcal/mol, E_a^0 and γ_p are assumed to be 12 kcal/mol and 0.7, respectively. If ΔH_r is more endothermic than 40 kcal/mol, E_a^0 and γ_p are assumed to be 2 kcal/mol and 1.0, respectively.

c. A ligand transfer reaction involves a functional group transferring from one reactant to another. This type of reaction usually has a high activation barrier. γ_p is assumed to be 0.5. E_a^0 is assumed to be 45 kcal/mol if the ligand is transferring to a hydrogen atom, and 50 kcal/mol for other ligand transfer reactions.

d. A recombination reaction can terminate two reactive intermediates and form a stable compound. The activation barrier is assumed to be 1 kcal/mol.

e. Other types of reactions such as isomerization require quantum mechanical calculations to estimate the activation barriers.

When the reactant follows Type a reaction, radicals will be produced. Therefore, Type a reaction serves as initiation reactions for reactants. Hydrogen abstraction reaction usually requires high activation energies. It is easier to break the weakest bond of the reactants. The produced radicals are unstable and react with reactant following Types b-d. The complete mechanism consists of many such steps. The products of each step can become the reactants of next steps. All the possible reactions will be studied, and the reactions with high activation barriers can be eliminated. However, some problems arise with this approach. A combinatorial increase of species and reactions may occur and many 'insignificant' molecules and reactions may arise. Some chemical intuition is required to select the most favorable reaction pathways. If final products and some key intermediates are known from experimental studies, the reaction network can be reduced by eliminating some reactions with non-relevant products.

4.5. Liquid Phase Reactions

Liquid phase reactions are more complex than the ones in the gas phase. In the gas phase, radicals are the most common species. In the liquid phase, ions are involved in the reactions. It is more challenging to simulate solvent effects because of the complex interaction between solvent and solute. In this research, water clusters were

used to simulate the effect of the water solvent. Continuum models describing solute-solvent interactions were also used to study the mechanisms. Single point energy calculations were conducted using the CPCM polarizable conductor calculation model with Klamt's radii and an iterative solution (COSMO) [62, 63] based on the optimized structures in the gas phase.

4.6. Summary

This work proposes an approach to predict runaway reaction mechanisms based on reaction classes. A linear free energy relationship was used to estimate activation barriers, and reduce the reaction network. Besides empirical rules, thermodynamic properties of reactants, products, intermediates, and some transition states were estimated using Gaussian 03 [64]. The rate constants of elementary reactions can be calculated using transition state theory or variational transition state theory (VTST) including the tunneling effect implemented in the software packages of GAUSSRATE [65] and POLYRATE [66]. Once the kinetics of elementary reactions is known, the concentrations of species can be expressed in differential equations. By numerically integrating the series of differential equations, the behavior of the reacting system can be predicted. This prediction approach incorporates both thermodynamic and kinetic information. One advantage of this approach is that the elementary reactions in the detailed kinetic model can also be applied to other systems with the same components. Therefore, a database of elementary reactions can simplify the procedure.

CHAPTER V

THERMAL DECOMPOSITION OF HYDROXYLAMINE IN THE

PRESENCE OF ACID/BASE[*]

5.1. Introduction

The effect of contamination is often considered as a cause of incidents in the chemical industry. The presence of trace impurities may reduce the thermal stability of a nominally pure chemical and cause unexpected runaway reactions under normal process conditions and they can explode and cause death and destruction of property [67]. Hydroxylamine (HA) has been involved in two tragic incidents since 1999 [5, 6]. Because of the industrial importance of hydroxylamine [68] and relatively limited information about its thermal stability in the open literature, it is important to study potential reactive hazards under process conditions and provide guidelines for safety and control measures. The catalytic effect of metals and metal ions on the thermal decomposition of hydroxylamine was studied by Cisneros et al. [10] and Iwata [11].

In this work, the effects of acid/base contamination on the thermal runaway reaction of HA were investigated using the RSST and the APTAC. The onset temperature (T_0), maximum temperature (T_{max}), adiabatic temperature rise ($\Delta T_{adabatic}$), maximum pressure (P_{max}), self-heat rate at onset temperature (dT/dt_0), maximum self-

heat rate (dT/dt$_{max}$), maximum pressure rate (dP/dt$_{max}$), and non-condensable gas pressure were determined for runaway hazard evaluation.

Understanding the mechanism behind the runaway reaction is important for process safety because conditions can be identified that may favor or temper the occurrence of the runaway reaction. It can also provide a good model for scale-up of the experimental information. The final products of the reaction can be analyzed by various experimental techniques. Most of the intermediates and transition states are short lived, and it is difficult to study them experimentally. Theoretical quantum mechanical calculation is a powerful tool to study the mechanism of runaway reactions. Based on the experimental runaway behavior, products, information from the literature, and chemical intuition, the most likely reaction pathway can be identified with the assistance of quantum mechanical calculations. In this work, frequency calculations were carried out on the optimized geometry of the reactants, the intermediates, and the products using hybrid density functional theory at the B3P86/cc-pVDZ [69-71] level of theory with the Gaussian 98 suite of programs [72]. The calculated enthalpies with zero-point energy corrections were used to estimate the heats of reaction for elementary steps in the proposed reaction networks.

5.2. Experimental

5.2.1. Materials

Standard hydrochloric acid solutions (Sigma, catalog numbers 35327 and 35328) and standard potassium hydroxide solutions (Aldrich, catalog numbers 31932 and

31937, Sigma, 17-8) were mixed with hydroxylamine solution (Aldrich, catalog number 45780, 99.999%, 50 mass % in water) to simulate acidic and basic contaminations, respectively. In order to maintain the same sample thermal inertia, the same amount of water (Aldrich, catalog number 32007, ACS reagent) was added to 50 wt% HA solution to prepare 43 wt% HA solutions to simulate thermal runaway conditions without contamination. Potassium chloride solution (Fluka, catalog number 60142, 1M in water) was also used to study the effects of potassium or chloride ions on the thermal runaway hazards. All of these chemicals were used without further purification and analysis.

5.2.2. Reactive System Screening Tool (RSST)

The RSST, manufactured by Fauske & Associates, is a calorimeter for rapid measurements of reaction thermal behavior for temperatures up to 400 °C and pressures up to 3,549 kPa. An open, 10 ml sample cell typically made of glass is placed inside a pressure vessel (400 ml), which can withstand pressures up to 3,549 kPa. The RSST can be used not only for screening the reactive chemicals, but also for designing emergency relief devices. Detailed descriptions of the RSST can be found in references [73, 74]. The RSST is a pseudo-adiabatic calorimeter, and it attempts to compensate heat losses by adding additional energy determined by calibration of the heater. The heating rate can be varied from 0.25 °C/min up to the rates required to simulate fire or explosion. In this work, glass thermocouples and polymer coated magnetic stirrer bars were used to provide a neutral environment for the reactions. A fixed heating rate of 1 °C/min was used for the temperatures up to 400 °C. The shut-down pressure limit was 3,204 kPa.

Initial nitrogen pressures of 1,480-1,825 kPa were used to minimize material loss from the sample cell.

5.2.3. Automatic Pressure Tracking Adiabatic Calorimeter (APTAC)

Adiabatic calorimeter has proven to be an extremely useful tool to assess thermal hazards of reactive chemicals. It can minimize heat losses by keeping the temperature of the sample surroundings as close as possible to the temperature of the sample. Following the RSST tests, measurements were made with an APTAC [12]. The APTAC calorimeter can be operated in a variety of test modes, such as heat-wait-search, heat ramps, and isothermal aging with temperatures up to 500°C and pressures ranging from vacuum to 13,790 kPa. It can track exotherms at heat generation rates from 0.04 to 400 °C/min. It can produce low thermal inertia data because it utilizes the DIERS pressure compensating technique in which the pressure outside the sample cell is controlled to match the pressure inside the sample cell. For the present work, the measurements were conducted in glass sample cells of nominal 100 ml, which can provide a neutral environment for the reactions. Teflon coated thermocouples were used to prevent the contact of hydroxylamine solution with metals.

APTAC heat-wait-search mode was used: the sample was heated at 2 °C/min to a starting temperature, and the temperature was allowed to stabilize for 20 minutes. Then the APTAC continued at that temperature and started searching for exothermic behavior. During the search period, the temperature of the containment vessel gas was adjusted to match that of the sample. If the self-heat rate of the sample was greater than a preset

threshold (0.1 °C/min), the apparatus tracked the reaction adiabatically until the reaction ended or one of the shut-down criteria was met. If no exotherm was detected, the apparatus would heat the sample to the next search temperature and the steps repeated until one of the shut-down criteria was met. The onset temperature is defined as the temperature when an exotherm is detected, and it is usually the lowest temperature when the sample self-heat rate surpasses the preset threshold in the 'search' or 'adiabatic' mode.

A summary of APTAC test setup conditions can be found in Table 5.1. Due to the high exothermic reactivity of hydroxylamine solution, only small sample sizes (about 4 grams) were used in these tests, so stirring was not necessary. To prevent undesired contaminations, the tubing lines between sample cell and transducers and also the tubing leading to valve 1 were flushed with acetone following every experiment. The tubing was allowed to dry by flushing with compressed nitrogen.

APTAC cannot measure heat of reaction directly, but the system of sample and sample cell was kept nearly adiabatic during runaway reaction. Therefore, part of the reaction heat was adsorbed by the sample cell, and the remainder was used to increase the temperature of the sample and vaporize the volatile materials. The fact that sample heat capacity changes with temperature, composition, and phase changes makes it even more difficult to estimate the heat of the reaction from the experiment. The liquid heat capacity of hydroxylamine is missing in the literature, but the heat capacities in gas and solid phases are very close to those of water. Because water was the solvent and a major product in this experiment, the liquid heat capacity of water (4.18 J/g/°C) was used to

estimate the thermal inertia [75] ($\phi = m_sC_{vs}/(m_sC_{vs}+m_bC_{vb})$, m_s and m_b are the mass of sample and sample cell, respectively, C_{vs} and C_{vb} are the heat capacity of sample and sample cell, respectively.).

Table 5.1. Summary of the APTAC experimental setup conditions.

Thermocouple	Teflon coated		
Heat mode	H-W-S		
Start Temperature (ºC)	50	Minimum Pressure (kPa)	138
Limit Temperature (ºC)	180	Over pressure (kPa)	7
Temperature Increment (ºC)	10	Lower Band (kPa)	-70
Cool Down Temperature (ºC)	50	Upper Band (kPa)	70
Exotherm Threshold (ºC)	0.1	Exotherm Limit (ºC)	300
Heat Rate (ºC/min)	2		
Stirring	NO		
Venting	NO		
Injection	NO		
Shut Down Criteria			
Temperature Level (ºC)	300	Pressure Level (kPa)	8,273
Heat Rate (ºC/min)	400	Pressure Rate (kPa/min)	13,790
Pressure Imbalance (kPa)	1034		

5.3. Results and Discussions

5.3.1. Potassium Hydroxide (KOH)

Potassium hydroxide is a strong base, alkaline in solution, highly corrosive, and incompatible with high concentration acids. The Chemical Reactivity Worksheet from the National Oceanic and Atmospheric Administration (NOAA) [37] shows no reaction between KOH and hydroxylamine if they are to be mixed. When a catastrophic hydroxylamine explosion occurred on February 19, 1999, at the Concept Sciences, Inc.

facility, potassium hydroxide was being used to react with hydroxylamine sulfate in the hydroxylamine production process. To the best of our knowledge, there is little information on the thermal stability of hydroxylamine with alkaline contaminants in the literature.

Various concentrations of KOH solutions were used to mix with 50 wt% hydroxylamine solution. The experimental conditions and results of the RSST and the APTAC tests are listed in Tables 5.2 and 5.3, respectively. Each sample was tested three times to establish reproducibility and develop an estimate of the uncertainty. The apparent activation energies were calculated using SuperChems Software [76], assuming first order reaction. As seen from Table 5.2 and Figure 5.1, the onset temperature decreases significantly with increasing concentrations of KOH. Compared to HA decomposition in water, additional heat was detected by the RSST for mixtures of HA with KOH. High concentration KOH can also decrease the apparent activation energies of the thermal decomposition. Onset temperature was below 50 °C for sample 7 with the highest concentration of KOH demonstrating that it is extremely hazardous to mix high concentration KOH with HA solutions. From a comparison of samples 4 with 7, the onset temperature is more sensitive to the concentration of KOH than the concentration of HA. However, this cannot be applied to low concentration KOH conditions (samples 2, 3, 5, and 6).

Table 5.2. Experimental results of the RSST tests.

Samples	Mass Concentration		Onset Temperature °C	Maximum Temperature °C	Ea kJ/mol
	HA	KOH			
No.1 6ml 50 wt% HA/H$_2$O	50%	0	139±4	218±2	160.7±14.6
No.2 6ml 50 wt% HA/H2O + 1ml 0.1N KOH	43%	0.15%	134±4	212±2	122.6±2.1
No.3 6ml 50 wt% HA/H2O + 1ml 1N KOH	43%	1.5%	114±4	214±2	114.6±19.2
No.4 6ml 50 wt% HA/H2O + 1ml 8N KOH	43%	12%	86±2	246±6	92.5±7.9
No.5 6ml 50 wt% HA/H2O + 2ml 0.1N KOH	39%	0.17%	125±5	209±1	123.8±7.1
No.6 6ml 50 wt% HA/H2O + 2ml 1N KOH	39%	1.7%	112±4	215±2	100.8±5.4
No.7 6ml 50 wt% HA/H2O + 2ml 8N KOH	39%	13.6%	46±2	246±8	74.1±0.4

Table 5.3. APTAC experimental results of the KOH effect on the thermal decomposition of hydroxylamine.

Samples	HA 3ml	KOH 0.5ml	T$_0$ °C	T$_{max}$ °C	P$_{max}$ kPa	dT/dt$_0$ °C/min	dT/dt$_{max}$ °C/min	dP/dt$_{max}$ kPa/min	Non-condensable kPa (50°C)	ΔH$_{rxn}$ kJ/mol
HA + Water	43 wt%	0	123.4±0.6	236.7±3	4157±214	0.14±0.04	38±3	1910±148	414±7	113.8±2.5
HA +0.1N KOH	43 wt%	0.15 wt%	122.6±0.3	234±1	3992±148	0.11±0.01	24±3	1262±152	414±14	114.2±0. 8
HA +1N KOH	43 wt%	1.5 wt%	112.7±0.8	244.7±2	4909±207	0.17±0.07	34±4	1510±110	579±34	134.3±2.9

Note: Phi factor=3.25, assuming constant sample Cp = 4.18 J/g/K
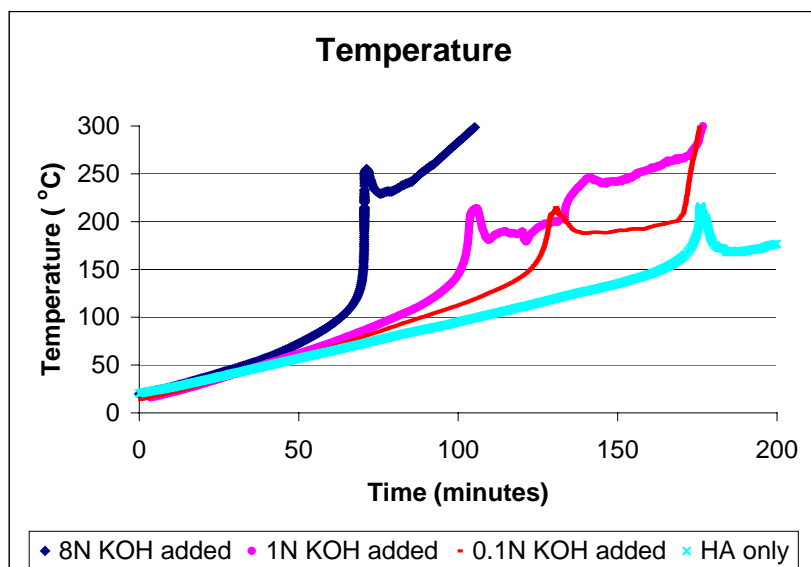
Figure 5.1. RSST results of thermal decomposition of 6ml 50 wt% HA/H$_2$O with 1ml various concentrations of KOH.
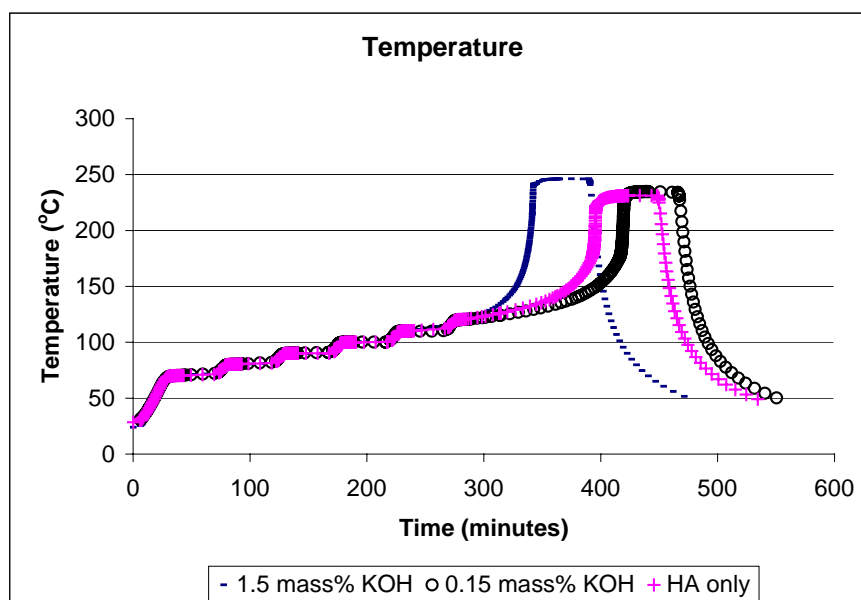

Figure 5.2. APTAC results of temperature for thermal decomposition of HA with KOH.

Figure 5.3. APTAC results of self-heat rate for thermal decomposition of HA with KOH.

Figure 5.4. APTAC results of pressure for thermal decomposition of HA with KOH.

Low concentration KOH conditions were tested in the closed cells of the APTAC. It is not uncommon to encounter contaminant concentrations from 0.1 to 2 wt% in process and storage conditions. Another reason is the corrosive nature of KOH. White residues were observed in the glass sample cells because SiO2 was dissolved in the basic media at high temperatures. The APTAC results are presented in Table 5.3 and Figures 5.2-5.5. In all of these tests, the liquid products were colorless and weighed about 3 grams. 0.1N and 1N KOH solutions were added to 50 wt% HA/water. The concentration of HA in all the resulting HA/KOH mixtures is 43 wt%. The resulting concentrations of KOH are 0.15 wt% and 1.5 wt%, respectively. The decomposition behavior of the 0.15 wt% KOH mixture is very close to that of HA without KOH. The maximum heat and pressure rates are very close for the three samples, as shown in Figures 5.3 and 5.5. For the mixture of 1.5 wt% KOH, the onset temperature decreased by approximately 11 °C, and 18% more heat was released compared to those of hydroxylamine without KOH. Additionally, the maximum pressure was increased and also increased was the non-condensable gas pressure at 50 °C. The findings reveal that the decomposition pathway initiated by KOH or the ratio of the decomposition products is different from the hydroxylamine decomposition without impurities. Further investigation is needed to resolve this issue and determine the reaction mechanism.
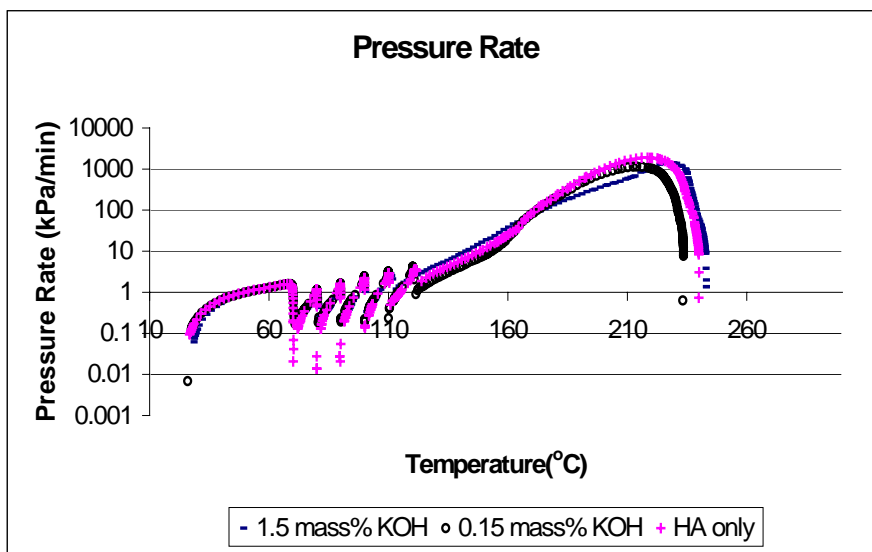
Figure 5.5. APTAC results of pressure rate for thermal decomposition of HA with KOH.
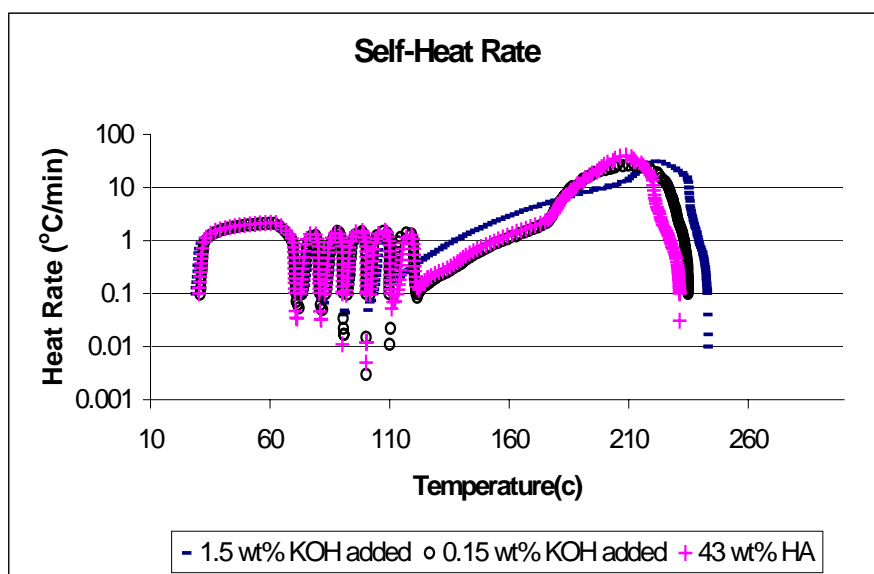

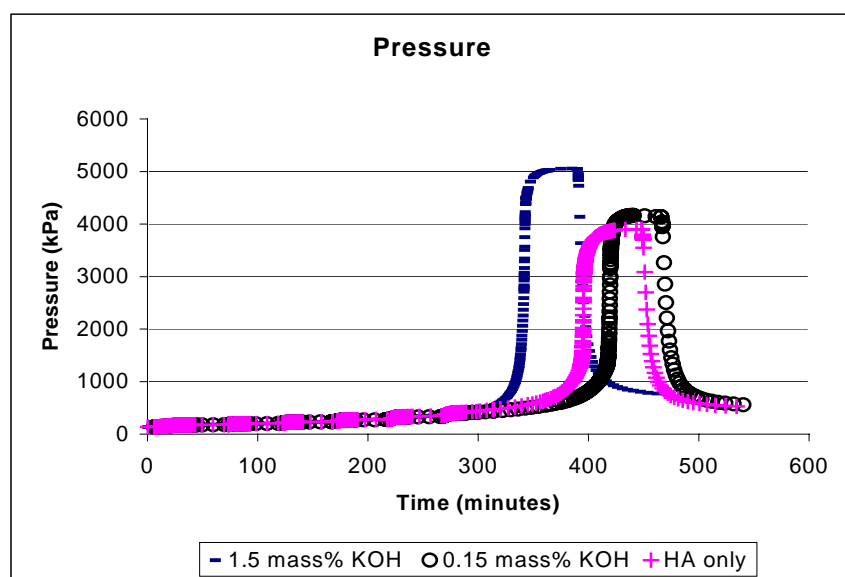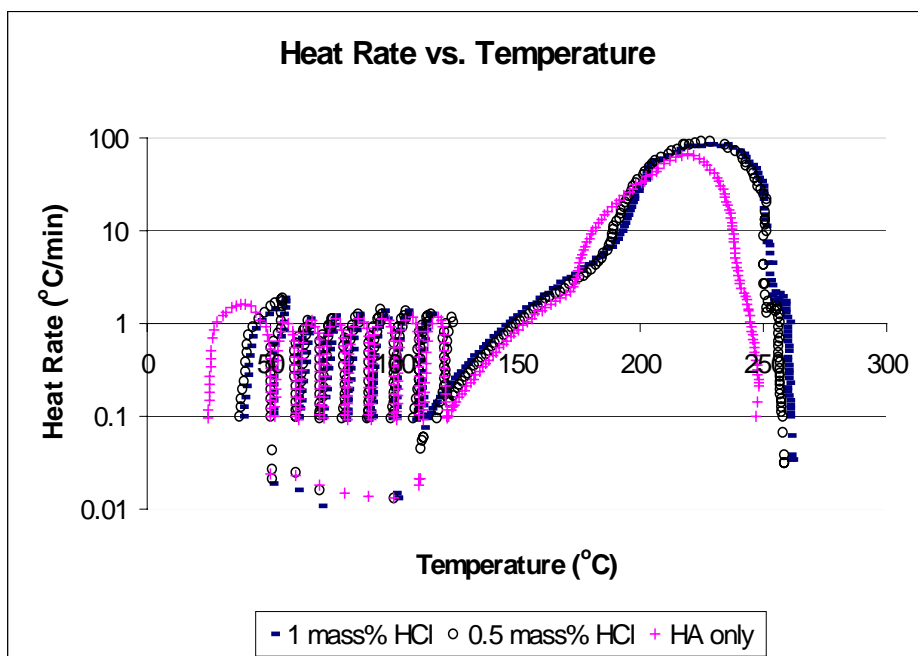Figure 5.6. APTAC results of self-heat rate for thermal decomposition of HA with HCl.
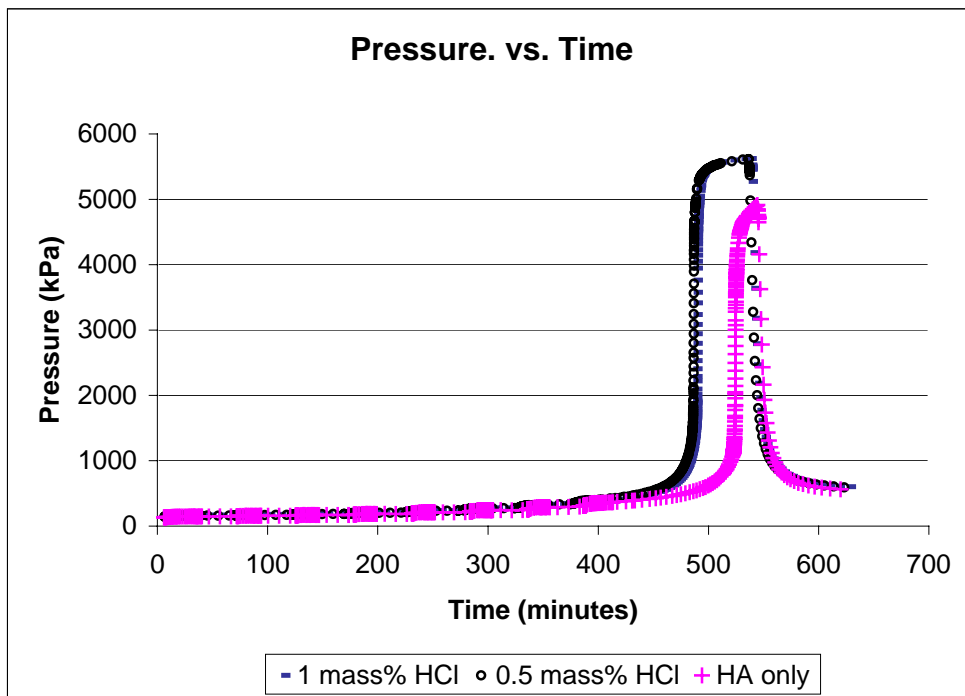
Figure 5.7. APTAC results of pressure for thermal decomposition of HA with HCl.
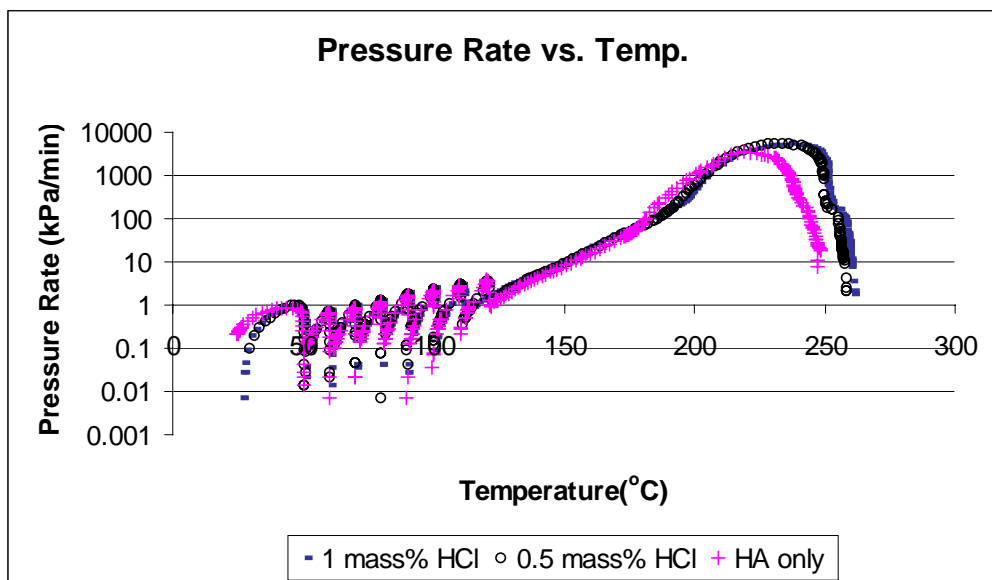
Figure 5.8. APTAC results of pressure rate for thermal decomposition of HA with HCl.

5.3.2. Hydrochloric Acid (HCl)

As shown in the previous section, the thermal decomposition of HA is accelerated by KOH. In order to test the effect of acidic impurity on the thermal decomposition of HA, 1N and 2N hydrochloric acid solutions were added to 50 wt% HA/H_2O solution, and the concentrations of the acid impurity in the resulting mixtures were about 0.5 wt% and 1 wt%, respectively. The concentration of HA in the resulting mixtures was 43 wt%. The experimental results from the APTAC are presented in Table 5.4 and Figures 5.6-5.8. At the low concentration of 0.5 wt% HCl, the maximum pressure increases by 689 kPa and maximum temperature by 10 °C. The maximum self-heat rate and pressure rate also increase significantly. The decomposition behavior of the mixtures with 0.5 wt% and 1 wt% HCl are very close except that the onset temperature of the 1 wt% HCl mixture is about 10 °C lower. The liquid products of these tests were clear, and there was odor of ammonia. In addition, the non-condensable gas pressures for mixtures with acidic impurities are a little higher than those of HA without HCl. The addition of 1 wt% HCl solutions resulted in 16% more heat release from the mixtures. From these results, we conclude that hydrochloric acid also can accelerate the thermal decomposition of HA at elevated temperatures, and mixing of HCl with HA should be avoided during process and storage conditions.

Table 5.4. APTAC experimental results of the HCl effect on the thermal decomposition of hydroxylamine.

	HA	HCl	T_0	T_{max}	P_{max}	dT/dt_0	dT/dt_{max}	dP/dt_{max}	Non-condensable	ΔH_{rxn}
Samples	3ml	0.5ml	°C	°C	kPa	°C/min	°C/min	kPa/min	kPa (50°C)	kJ/mol
HA+water	43 wt%	0	122.8±0.7	246.5±2	4750±117	0.12±0.01	69±3	3585±207	414±7	116.7±2.9
HA+1N HCl	43 wt%	0.5 wt%	123.2±0.6	257.2±1	5530±110	0.17±0.04	95±8	5695±275	441±14	123.0±3.8
HA+2N HCl	43 wt%	1 wt%	113.4±0.5	257±4	5340±296	0.13±0.04	95±12	5667±345	434±7	136.0±5.9

Note: Phi factor=2.9, assuming constant sample Cp=4.18 J/g/K

Table 5.5. APTAC experimental results of KCl effect on the thermal decomposition of hydroxylamine.

Sample		Average T_0	Average T_{max}	Average $\Delta T_{adabatic}$	Average P_{max}	Average dT/dt_{max}	Average dP/dt_{max}	Average non-condensable
50 wt% HA/H_2O	KCl(1M)	°C	°C	°C	kPa	°C/min	kPa/min	kPa (50°C)
g	g							
2.3	0	124.7	216	92	2992	21	1006	296
2.3	0.34	125	230	105	3585	10	496	317

Note: Phi factor is about 5, assuming constant sample Cp= 4.18 J/g/K.

Table 5.6. Comparison of the decomposition of hydroxylamine with the addition of HCl, KCl, and H_2O.

Sample		Average T_0	Average T_{max}	Average $\Delta T_{adabatic}$	Average P_{max}	Average dT/dt_{max}	Average dP/dt_{max}	Average non-condensable	Average ΔH_{rxn}
3ml	0.5ml	°C	°C	°C	kPa	°C/min	kPa/min	kPa (50°C)	kJ/mol
50 wt% HA/ H_2O	1M HCl	123.2	257.2	129	5530	95	5695	441	123.0
50 wt% HA/ H_2O	1M KCl	121.8	253	128	5171	44	2344	434	122.6
50 wt% HA/ H_2O	H_2O	122.8	246.5	122	4750	69	3585	420	116.7

Note: Phi factor is about 2.9, assuming sample Cp=4.18 J/g/K and glass Cp=0.84 J/g/K

5.3.3. Potassium Chloride (KCl)

As discussed above, both KOH and HCl can accelerate the thermal decomposition of hydroxylamine. The addition of 1N KOH solution decreases the onset temperature by 10 ºC and the addition of 1N HCl solution increases the maximum self-heat rate and pressure rate. In order to verify if these changes in the HA decomposition behavior were caused by hydroxide and hydrogen ions, mixtures of 1M KCl solution and HA were tested with the APTAC. The summary of the results is listed in Tables 5.5 and 5.6. As shown in Table 5.5, the onset temperature did not decrease after the addition of KCl solution, the maximum self-heat and pressure rates became lower, but the maximum temperature, maximum pressure, and non-condensable gas pressure increased. As shown in Table 5.6 and Figures 5.9 and 5.10, the decomposition characteristics following the addition of KCl were very close to that of HCl except for the maximum self-heat rate and maximum pressure rate, which were considerably large for the HCl. It is most likely that potassium ion does not catalyze the decomposition of hydroxylamine. Chloride ion may participate in the decomposition and it may be oxidized by hydroxylamine, which caused more heat release. Based on the comparison, we can conclude that hydroxide ion caused a decrease in the onset temperature and hydrogen ion caused an increase in the maximum self-heat and pressure rates.
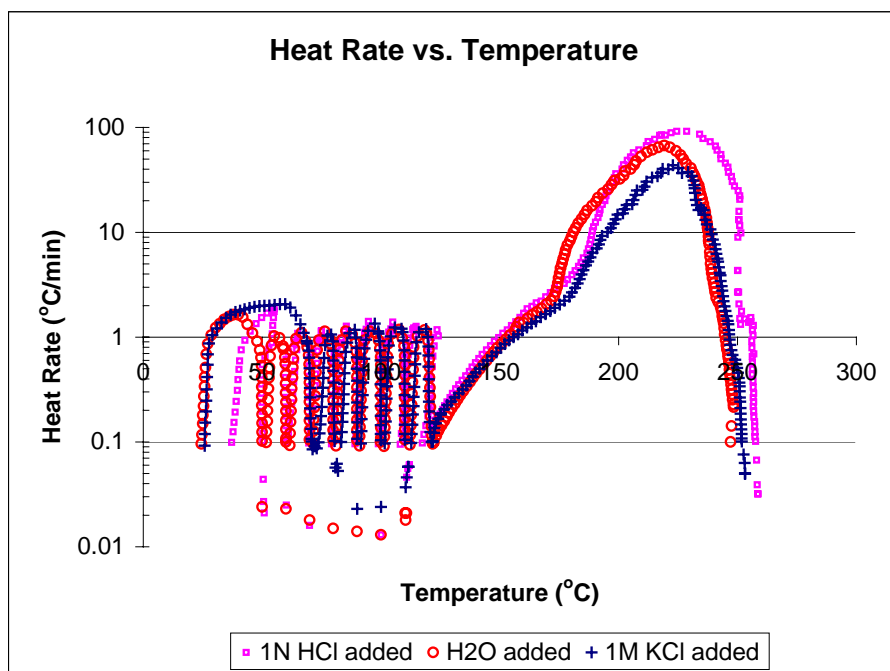
Figure 5.9. Comparison of HCl and KCl on the self-heat rate of HA decomposition.
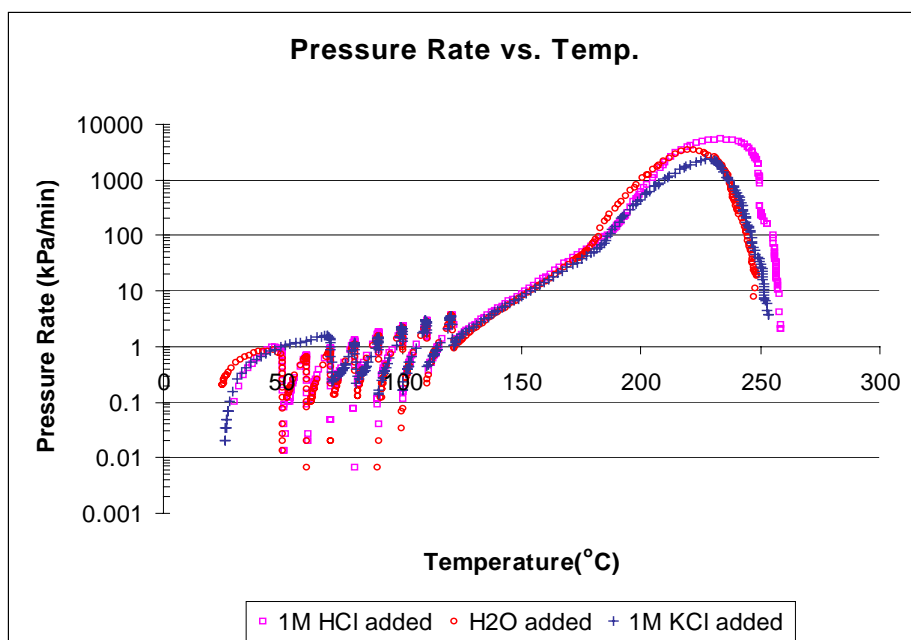
Figure 5.10. Comparison of HCl and KCl on the pressure rate of HA decomposition.

5.4. Proposed Decomposition Mechanisms

5.4.1. Decomposition Products under Acidic and Alkaline Conditions

In the literature, the decomposition of HA has been described by a few mechanisms. Most of the proposed mechanisms are controversial, and especially the intermediates of the decomposition are still in debate [77]. The decomposition of hydroxylamine is known to depend on the pH of the solution [68]. The pH of 50 wt% hydroxylamine/water solution is 10.6. HA decomposes at high temperatures according to Equations (5.1) and (5.2) with the ratio of 5/7 and 2/7, respectively [78]. The addition of base suppresses Reaction (5.2) in favor of Reaction (5.1), but the addition of acid causes the reverse effect and Reaction (5.2) becomes dominant [78].

$$3NH_2OH \rightarrow N_2 + NH_3 + 3H_2O \qquad (5.1)$$

$$4NH_2OH \rightarrow N_2O + 2NH_3 + 3H_2O \quad (5.2)$$
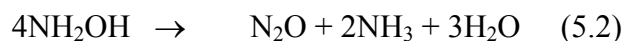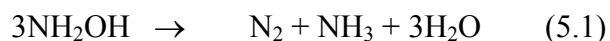
The initiation reaction in both cases was proposed to be the formation of hydroxyhydrazine (HONNH$_2$), as in following reaction:

$$2NH_2OH \rightarrow HONNH_2 + H_2O + H\bullet \quad (5.3)$$

Because this reaction is catalyzed by alkaline conditions and inhibited by acidic conditions, it was believed that hydroxylamine was more stable in acidic than in alkaline solutions [68].

Our results show that HA is not stable in acid solution, and the maximum self-heat and pressure rates are higher than those in alkaline solution. Therefore, the initiation reactions and the decomposition mechanism must be different under the two conditions.

Under runaway conditions, the products of the thermal decomposition of 50 wt% hydroxylamine were reported as NH_3, H_2O, N_2, N_2O, and a small amount of NO and H_2 by Cisneros et al [9]. The ratio of N_2 to N_2O was 2.9 in ref. [9] which was close to 2.5 in ref. [78]. A small amount of NO and H_2 was also detected because a wide spectrum of reactions can be initiated at high temperatures and in closed containment. In addition, the products and the intermediates may react with each other at high temperatures. As expected, the final products depend on the process conditions and contaminants. It is a challenging task to propose a complete mechanism and simulate the runaway process. It is also impractical because a thermal explosion will occur before the maximum temperature can be reached in most process conditions. Therefore, Equations (5.1) and (5.2) were considered as the basis for the proposed mechanisms.

5.4.2. Decomposition Mechanism in Alkaline Medium

Hughes and Nicklin [79] studied the autoxidation of hydroxylamine in alkaline solutions and concluded that NH_2O^- was involved in the rate-limiting step. The reaction scheme is given in Equations (5.4) and (5.5).

$$NH_2OH + OH^- \leftrightarrow NH_2O^- + H_2O \qquad (5.4)$$

$$NH_2O^- + O_2 \rightarrow HNO + HO_2^- \qquad (5.5)$$

However, the recent study by Cisneros et al. [7] showed that air had no significant effect on the thermal decomposition of HA solutions, and concluded that the oxygen atoms in the products came from the HA molecule.

In this work, the following simplified mechanism in Table 5.7 was proposed for HA decomposition in alkaline solutions. The species in bold are the final products. Quantum chemical calculations were performed at the B3P86/cc-pVDZ level of theory using Gaussian 98. The enthalpies of reaction (ΔH_{rxn}) were calculated according to ΔH_{rxn} = $\Delta H_{products}$ - $\Delta H_{reactants}$, where $\Delta H_{products}$ is the total enthalpies of products, and $\Delta H_{reactants}$ is the total enthalpies of reactants.

Table 5.7. The reaction scheme of HA decomposition in alkaline conditions.

Reaction Scheme	ΔH_{rxn} (kJ/mol)	
$NH_2OH + OH^- \rightarrow NH_2O^- + H_2O$	-109.6	(5.6)
$NH_2O^- + NH_2OH \rightarrow NH_2NHOH + OH^-$	-14.6	(5.7)
$NH_2NHOH \rightarrow HNO + NH_3$	29.7	(5.8)
$HNO + NH_2OH \rightarrow NH_2O\bullet + NH_2O\bullet$	-3.8	(5.9)
$2NH_2O\bullet \rightarrow N_2 + 2H_2O$	-477.8	(5.10)
The overall equation is		
$3NH_2OH \rightarrow N_2 + NH_3 + 3H_2O$	- 192.0	(5.1)

The reaction involves intermediates of NH_2O^-, NH_2NHOH, HNO, and radical NH_2O. The radical NH_2O is produced from the branching reaction, as shown in Equation (5.9). The branching reaction is responsible for the explosive behavior of HA decomposition because more intermediates are produced and the reaction rate is increased significantly. Adding both sides of Equations (5.6) to (5.10) and canceling the intermediates, the overall reaction is Equation (5.1). Equation (5.6) is exothermic and related to the initiation of the decomposition. With the increasing concentration of hydroxide ions, the reaction rate of Equation (5.6) will increase and more heat will be released, which explains why the measured onset temperature decreases with the increasing pH. Applying steady-state assumption on all the intermediates, the concentration of HNO is proportional to that of hydroxide ions. So, the ratio of the branching reaction will also increase with increased pH, more NH_2O radicals will be produced, the reaction rate of Equation (5.10) will be increased even more significantly because it is a second-order reaction, and therefore, more heat will be generated, and more nitrogen will be produced with the increased concentration of hydroxide ions.

5.4.3. Decomposition Mechanism in Acid Solutions

According to the study by Ebler and Schott [80], hydroxylamine exists as NH_2OH in alkaline and weakly acid solutions and normally acts as a reducing agent. In strongly acid solutions, it exists as H_3NO and acts as an oxidizing agent. In acid solutions, hydroxylamine is more likely to combine with the proton (H^+) than water (from Equation 5.13). The proton affinity of hydroxylamine was determined to be higher

for protonation on nitrogen than on oxygen by experimental evaluation and theoretical calculation [81].

$$NH_2OH + H^+ \Leftrightarrow NH_3OH^+ \qquad (5.11)$$

Equation (5.11) is most likely when strong acid is mixed with hydroxylamine, although the heat of solvation was not detected by the APTAC because of the small amount of H^+. Hydroxylamine and protonated hydroxylamine are in equilibrium under acidic conditions. When the concentration of the acid is much less than that of hydroxylamine, most of the hydroxylamine molecules exist as NH_2OH because it is more stable than H_3NO. From our experimental results, we conclude that the onset temperature decreases and maximum self-heat and pressure rates increase with the addition of acid. NH_3OH^+ must be responsible for the initiation reaction and can easily initiate decomposition as compared to NH_2OH, but further experimental analysis and quantum mechanical calculations are needed to verify it. The reaction scheme in Table 5.8 including Equations (5.12) to (5.19) is proposed based on information from the literature, Equation (5.2), quantum chemical calculations, and chemical intuition.

Table 5.8. The reaction scheme of HA decomposition in acidic conditions.

Reaction Scheme	ΔH_{rxn} (kJ/mol)	
$NH_3OH^+ \rightarrow NH(triplet) + H_3O^+$	301.7	(5.12)
$H_3O^+ + NH_2OH \rightarrow NH_3OH^+ + H_2O$	-134.3	(5.13)
$NH(triplet) + NH_2OH \rightarrow \bullet NH_2 + NH_2O\bullet$	-107.1	(5.14)
$NH_2O\bullet + NH_2OH \rightarrow NH_2NHOH + \bullet OH$	73.2	(5.15)
$\bullet OH + NH_2OH \rightarrow H_2O + NH_2O\bullet$	-197.5	(5.16)
$NH_2NHOH \rightarrow HNO + NH_3$	29.7	(5.17)
$NH_2O\bullet + \bullet NH_2 \rightarrow HNO + NH_3$	-154.8	(5.18)
$HNO + HNO \rightarrow N_2O + H_2O$	-366.9	(5.19)
The overall equation		
$4NH_2OH \rightarrow N_2O + 2NH_3 + 3H_2O$	-138.9	(5.2)

This decomposition pathway is more complicated than the one in alkaline medium. Besides the same intermediates of NH_2NHOH, HNO, $NH_2O\bullet$ as in alkaline solutions, NH(triplet), H_3O^+, $\bullet NH_2$, and $\bullet OH$ are also involved in the reactions. Equation (5.12) was studied in detail by Øiestad and Uggerud [81]. NH(triplet) was detected as the dominant product in the unimolecular decomposition of protonated hydroxylamine. NH(triplet) is more reactive than HNO with hydroxylamine and it plays an important role in the branching reaction. The difference of the branching reactions in the two cases may explain why the maximum self-heat rate and pressure rate were higher in acid

solutions than in alkaline solutions. Once the decomposition is initiated in acid solutions, NH(triplet) is produced and the branching reaction begins with heat-release, while in alkaline solutions, the branching reaction is less exothermic. The major gas product, N_2O is produced by the dimerization of HNO as shown in Equation (5.19), which was studied thoroughly by Lin et al. [82] and Ruud et al. [83]. The calculated heat of reaction of -366.9 kJ/mol for Equation (5.19) is in agreement with the experimental value of -360.2 kJ/mol [84].

The heats of reaction were calculated at the B3P86/cc-pVDZ level of theory using Gaussian 98 [72]. All species were treated in the gas phase. The calculated overall heat of reaction of -138.9 kJ/mol is close to our experimental results (about -125.5 kJ/mol) even though the runaway reaction starts in the condensed phase.

5.5. Conclusions

The thermal decomposition of hydroxylamine with acid/base impurity was studied based on experimental results from the RSST and APTAC calorimeters and quantum mechanical calculations. Our studies have shown that thermal decomposition behavior of hydroxylamine is affected by the presence of acid or base. Two different decomposition reaction pathways can be initiated when acid or base is mixed with hydroxylamine. Hydrogen ion can increase the maximum self-heat and pressure rates while hydroxide ion can decrease the onset temperature and generate more gas products. Hydroxylamine must be handled and stored with caution because accidental mixing with

impurities can pose an energy release hazard at lower temperatures. The mechanisms proposed in this paper provide a better understanding of hydroxylamine chemistry.

CHAPTER VI

THERMAL DECOMPOSITION STUDY OF HYDROXYLAMINE

NITRATE[*]

6.1. Introduction

Hydroxylamine nitrate (HAN) is an important member of the hydroxylamine family. High concentrations of HAN are used as liquid propellants, and low concentrations of HAN are used primarily in the nuclear industry for decontamination of equipment. Due to its instability and autocatalytic decomposition behavior, HAN has been involved in several incidents [12]. Therefore, the thermal stability and decomposition pathway of HAN in water are of interest for safe industrial applications. Several groups have investigated the kinetics and mechanism of the HAN decomposition using various techniques and under different conditions [13-16]. However, due to its highly exothermic and rapid behavior of the reaction, these studies could not provide complete information about the decomposition process. In this work, the thermal decomposition hazard of HAN is evaluated using both theoretical and experimental methods.

An autocatalytic reaction is a chemical reaction in which a product (or a reaction intermediate) acts as a catalyst [85], and the observed reaction rate is found to increase with time. This property poses a challenge for the prolonged storage of chemicals that

---

[*] This chapter contains material reprinted from Journal of Thermal Analysis and Calorimetry, C. Wei, W.J. Rogers, and M.S. Mannan, Detection of autocatalytic decomposition behavior of energetic materials using the APTAC, in press.

can undergo autocatalytic decomposition. Chervin and Bodman [86] studied the autocatalytic decomposition phenomenon and kinetic models using isothermal DSC data. A screening method based on dynamic DSC measurement was developed to identify autocatalytic decomposition by Bou-Diab and Fierz [87]. According to this method, the decomposition is autocatalytic if the apparent activation energy calculated by a first order kinetic model is higher than 220 kJ/mol. Under adiabatic conditions, the temperature versus time curves for nth order reactions and autocatalytic reactions are different. For nth order reactions, the temperature increase starts immediately after the onset temperature, while for autocatalytic reactions, the temperature increase is relatively small during the induction period and then suddenly grows rapidly. This work presents the study of autocatalytic decomposition using APTAC heat-wait-search and heat-soak-search modes. The objective of this study is to explore the potential of adiabatic calorimeters to identify autocatalytic decomposition of energetic materials.

6.2. Theoretical Screening Methods and Results

On May 14, 1997, an incident occurred in the Chemical Preparation Room of the Plutonium Reclamation Facility at DOE Hanford's Plutonium Finishing Plant. The explosion destroyed the HAN storage tank and the room, and residual plutonium leaked from the building mixed with wastewater [88]. After the investigation, it was determined that the root causes of the incident were inadequate hazard evaluation, inadequate auditing of safety management systems, and inadequate training for personnel on reactive hazards [1].

A systematic approach was proposed to evaluate reactive chemical hazards [89]. The first step of hazard evaluation is to apply simple screening tools. MOPAC (Molecular Orbital Package) and CHETAH (ASTM Chemical Engineering Thermodynamics and Hazard Evaluation) have proven to be reliable and practical screening tools based on the analysis of the 167 incidents reported by the CSB (Chemical Safety and Hazard Investigation Board) [90].

In this study, the semi-empirical quantum mechanical method MOPAC was employed to calculate heat of formation of HAN at the AM1 [40] and PM3 [43] levels of theory. The optimized structure of gas phase HAN is shown in Figure 6.1. The estimated gas phase heats of formation at 298 K are -64.8 and -57.8 kcal/mol using AM1 and PM3, respectively. In order to validate the results, the high level quantum mechanical method G2MP2 [91] was also used to calculate the heat of formation of HAN with the Gaussian 03 suite of programs [64]. The detailed method of calculating heat of formation is described in a Gaussian Whitepaper [92]. The obtained heat of formation of –61 kcal/mol is about the average of the results using the AM1 and PM3 methods.
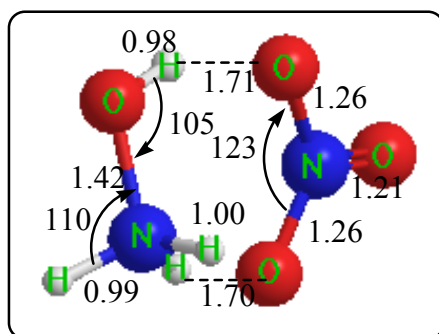

Figure 6.1. The optimized gas phase structure of hydroxylamine nitrate at the PM3 level.

The energy release potential of HAN decomposition was evaluated by the ASTM CHETAH program, for which the gas phase heat of formation of −61 kcal/mol was used as an input to CHETAH. The maximum heat of decomposition of HAN was estimated to be −0.595 kcal/g with a hazard classification of MEDIUM, but the overall energy release potential is HIGH. Therefore, further experimental study is necessary for a reliable hazard evaluation of HAN decomposition.

6.3. Experimental

6.3.1. Sample

Hydroxylamine nitrate (24 wt% in water solution, Aldrich catalog number 438235) was used without further purification and analysis.

6.3.2. RSST^{TM} (Reactive System Screening Tool)

The RSST, manufactured by Fauske & Associates, is a calorimeter designed for rapid measurements of reaction thermal behavior for temperatures up to 400 °C and pressures up to 500 psig. An open, 10 ml sample cell typically made of glass is placed inside a pressure vessel (400 ml) that can withstand pressures up to 500 psig. The RSST can be used not only for screening reactive chemicals, but also for designing emergency relief devices. In this work, glass thermocouples and polymer coated magnetic stirrer bars were used to provide a neutral environment for the reactions. A fixed heating rate of 1 °C/min was used for temperatures up to 400 °C. The shut-down pressure limit was 450

psig. Initial nitrogen pressures of 250 psig were used to minimize material loss from the sample cell.

6.3.3. APTAC^{TM} (Automatic Pressure Tracking Adiabatic Calorimeter)

Adiabatic calorimetry has proven to be an extremely useful tool to assess thermal hazards of reactive chemicals. It can minimize heat losses by maintaining the temperature of the sample surroundings as close as possible to the temperature of the sample. The APTAC calorimeter can be operated in a variety of test modes, such as heat-wait-search, heat ramps, and isothermal aging with temperatures up to 500°C and pressures ranging from vacuum to 2,000 psia. It can track exotherms at heat generation rates from 0.04 to 400 °C/min. It can produce low thermal inertia data because it utilizes the DIERS pressure compensating technique in which the pressure outside the sample cell is controlled to match the pressure inside the sample cell. For the present work, the measurements were conducted in glass sample cells of nominal 100 ml, which can provide a neutral environment for the reactions, and also in titanium and stainless steel sample cells of nominal 130 ml and 50 ml, respectively, to test the effects of metals on the thermal decomposition of HAN. Teflon coated thermocouples were used to prevent the contact of hydroxylamine solution with thermocouple sheath metals.

6.3.4. Experimental Methods

The APTAC heat-wait-search mode was used: the sample was heated at 2°C/min to a starting temperature, and the temperature was allowed to stabilize for 25 minutes,

following which the APTAC searched for exothermic behavior. During the search period, the temperature of the containment vessel gas was adjusted to match that of the sample. If the self-heat rate of the sample was greater than a preset threshold (0.05 °C/min), the apparatus tracked the reaction adiabatically until the reaction ended or one of the shutdown criteria was met. If no exotherm was detected, the apparatus heated the sample to the next search temperature and the steps repeated until one of the shutdown criteria was met. The onset temperature is defined as the temperature at which an exotherm is detected, and it is usually the lowest temperature that the sample self-heat rate surpasses the preset detection threshold (0.05 °C/min) in the 'search' or 'adiabatic' mode.

The APTAC heat-soak-search mode was also used: the sample was heated to a certain soak temperature and held adiabatically. Every sixty minutes, or if the sample temperature rose 1 °C above the soak temperature, the self-heating rate would be polled and compared with a pre-defined sensitivity threshold. If the self-heating rate exceeded the threshold, a runaway reaction was detected and the sample was kept adiabatically. If the self-heating rate was less than the threshold, the sample would be cooled back to the soak temperature. The steps continued for a defined period. If it failed to detect self-heat at the end of the soak period, the system would proceed with a standard Heat-Wait-Search mode. The HSS method is generally used to test the effectiveness of inhibitors added to the reactants. In this study, the HSS method was employed to study the effect of autocatalysis on the decomposition of the HAN reactive system. The autocatalysis would be generated during the soak period and thus allowed the reactants to eventually

runaway in an adiabatic system when its concentration reached a certain level. Appropriate soak time and temperature should be chosen based on the knowledge of the reactive system.

For the glass sample cell, the maximum allowable pressure imbalance is 150 psi. Due to the extremely rapid exothermic reactivity of hydroxylamine nitrate solution, it is difficult for the APTAC to track the pressure rise fast enough. The pressure imbalance was above 100 psi even when small samples (about 4 grams) were used in these tests. Stirring was not necessary because only small amount of sample was used. To prevent undesired contaminations, the tubing lines between sample cell and transducers and also the tubing leading to the on/off valve that can close the sample cell during tests were flushed with acetone following every experiment. The tubing was allowed to dry by flushing with compressed nitrogen.

6.4. Results and Discussions

6.4.1. RSST Experimental Results

The RSST experimental results for HAN are shown in Figure 6.2. At the temperature of 180°C, pressure increases dramatically but the temperature profile does not show increase like a typical exothermic runaway reaction. From the results, it appears that the decomposition starts around 180°C. No temperature increase can be attributed either to an endothermic reaction or to the displacement of the thermocouple. The reaction starts very rapidly, and the generated vapor and gas products can blow the thermocouple out of the sample cell into the pressure containment vessel. The

temperature of the containment vessel is much lower than that of sample cell because only the sample cell is surrounded by a bottom heater. In addition, the glass sample cells were broken into pieces after the experiments probably because of the rapidly generated pressure. In order to obtain a complete temperature profile, a closed cell experiment is necessary and the APTAC is an ideal apparatus for this task.
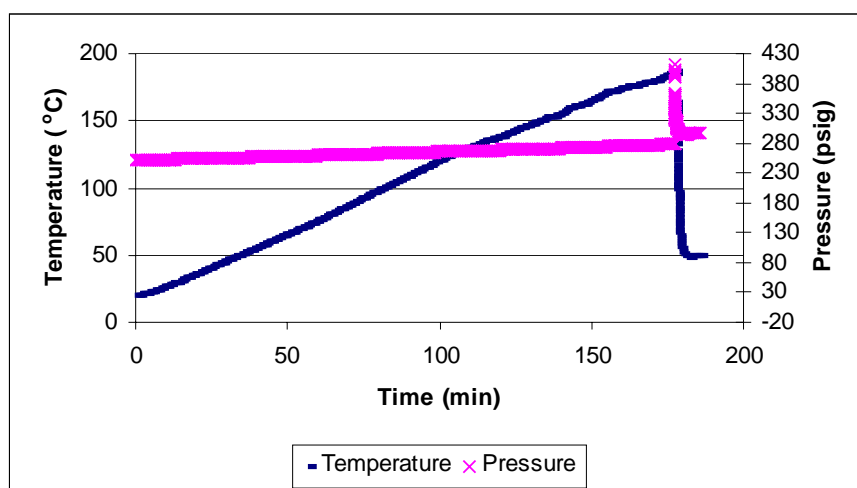
Figure 6.2. RSST experimental results of the thermal decomposition of HAN.

Table 6.1. APTAC Heat-Wait-Search results (the averages of three runs under each conditions) of HAN thermal decomposition.

HAN	T_0	T_{max}	P_{max}	dT/dt_0	dT/dt_{max}	dP/dt_{max}	Non-condensable	Phi factor	ΔH_{rxn}
4.2g	°C	°C	psia	°C/min	°C/min	psi/min	psia (50°C)	ϕ	kcal/mol
Glass cell	171	196	296	0.07	416	174	41	3.3	33
Ti cell	150	179	194	0.06	279	28	26	2.0	23
SS cell	139	169	227	0.06	179	294	55	3.6	43

6.4.2. Effect of Materials of Construction

The APTAC HWS mode was employed to determine the overall decomposition behavior of hydroxylamine nitrate, such as onset temperature, T_0, maximum temperature, T_{max}, and maximum pressure, P_{max}. The experimental results using glass, titanium, and stainless steel sample cells are presented in Table 6.1 and Figures 6.3-6.4. The experiments reveal that the reaction is exothermic and the RSST temperature profile is caused by the displacement of the thermocouple due to the rapid pressure increase.
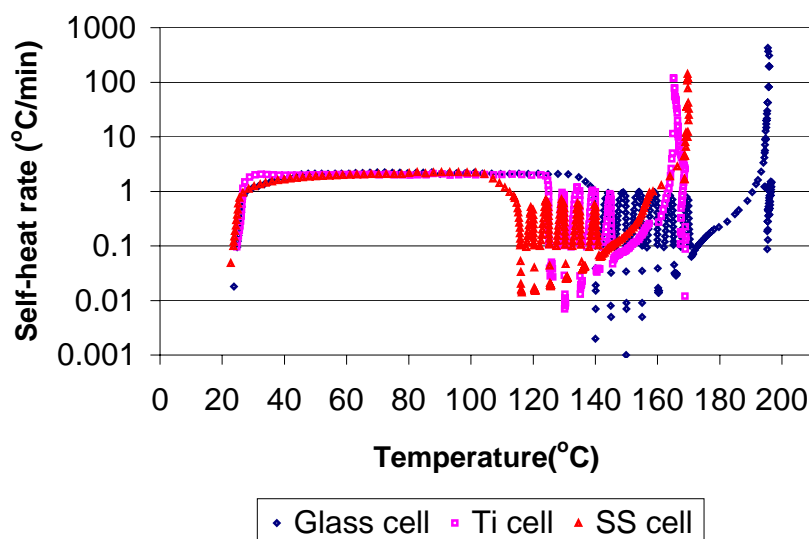

Figure 6.3. Effect of materials of construction of sample cells on the self-heat rate vs. temperature profiles of HAN decomposition.
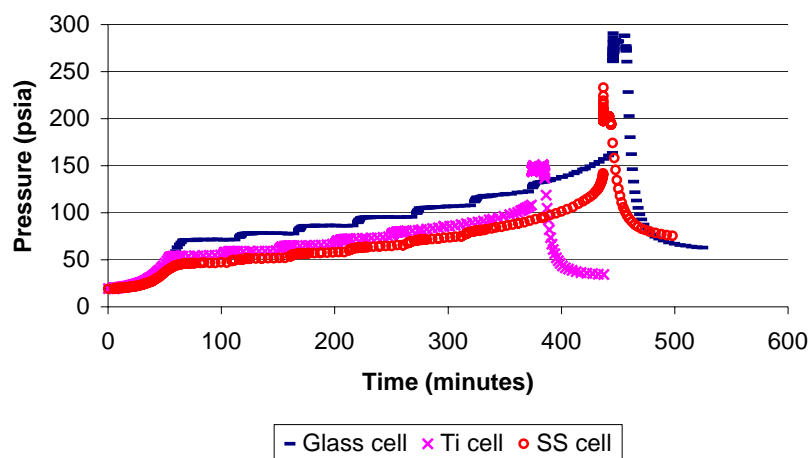
Figure 6.4. Effect of materials of construction of sample cells on the pressure profiles of HAN decomposition.

The effect of sample cell material on onset temperatures shows that a glass cell can provide a neutral environment, and metals such as titanium and stainless steel can catalyze the decomposition of hydroxylamine nitrate. Compared with glass, titanium initiates the decomposition at a lower temperature, but less heat is evolved from the reaction, while stainless steel can cause 30% more heat release from the decomposition.

6.4.3. Comparison of Gas Phase and Liquid PhaseTemperatures

The Teflon coated thermocouple was located as close to the bottom of the sample cell as possible to measure liquid temperature. A stainless steel sheath thermocouple with a diameter of 0.02 inch was positioned around the neck of the sample cell to detect gas phase temperature. The gas and liquid temperatures of the HAN decomposition in a

stainless steel cell are compared in Figure 6.5. The temperatures are very close until the

fast explosion occurs. The gas phase jumps to the maximum temperature of 185°C, and

then cools down. The gap of 25°C (from 160 to 185°C) in the gas phase may be due to

slow sampling of data points by the APTAC. Meanwhile, the liquid temperature keeps

increasing to the maximum temperature of 170°C, which is much lower than the gas

phase maximum temperature. It is most likely that the explosion starts in the gas phase,

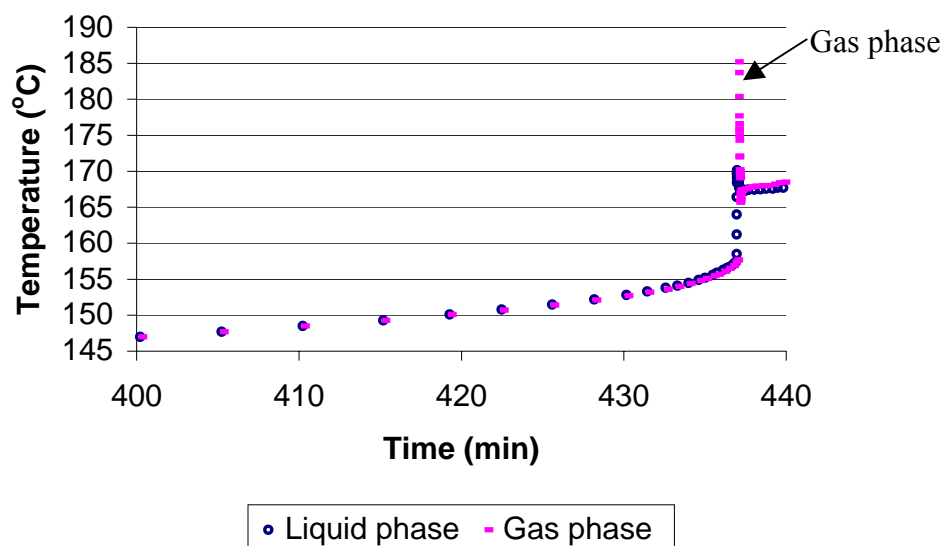and then released heat transfers to the liquid phase.

Figure 6.5. Comparison of the gas phase and liquid phase APTAC temperature profiles
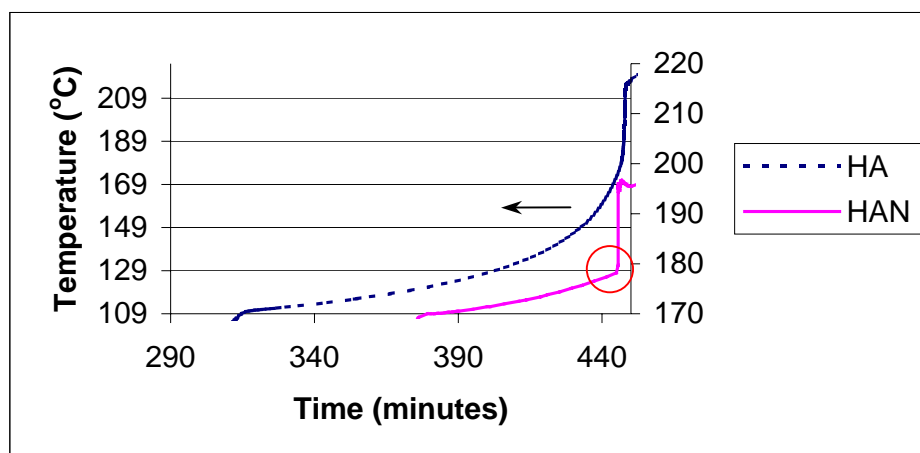for HAN decomposition in a stainless steel cell.

Figure 6.6. Comparison of decomposition curve of hydroxylamine nitrate with hydroxylamine.

6.4.4. Autocatalytic Decomposition

Previous studies have showed that hydroxylamine decomposition is an overall 1st order reaction with apparent activation energy of 29 kcal/mol [7]. The decomposition curve of hydroxylamine nitrate is compared with that of 50 wt% HA/water in Figure 6.6. Hydroxylamine nitrate decomposition starts at 170°C and the temperature increases slowly until 180°C at which point the temperature suddenly increases very rapidly to a maximum temperature of 196°C. The temperature curve of hydroxylamine nitrate appears to be two stages: a slow initiation stage followed by a fast explosion stage. These two stages form a sharp corner as emphasized by the circle in Figure 6.6. On the contrary, for the decomposition of HA, the temperature increase starts immediately after the onset temperature and smoothly curves up to the maximum temperature. From

comparison of the decomposition temperature curves, it can be concluded that HAN decomposition is an autocatalytic reaction. Initially the decomposition shows only little heat release and therefore the temperature increase is slow. After an induction period, the concentration of the autocatalyst reaches a certain level and the reaction rate becomes very rapid.

Table 6.2. APTAC Heat-Soak-Search results of HAN thermal decomposition.

HAN 4.2g	Soak temperature °C	T_0 °C	T_{max} °C	P_{max} psia	dT/dt_0 °C/min	dT/dt_{max} °C/min	dP/dt_{max} psi/min	Non-condensable psia (50°C)	Phi factor ϕ	ΔH_{rxn} kcal/mol
Glass cell	150	165	184	233	0.07	344	111	41	3.3	25
Ti cell	130	131	143	103	0.05	128	12	24	2.0	10
SS cell*	120	127	140	137	0.07	139	6	53	3.6	18

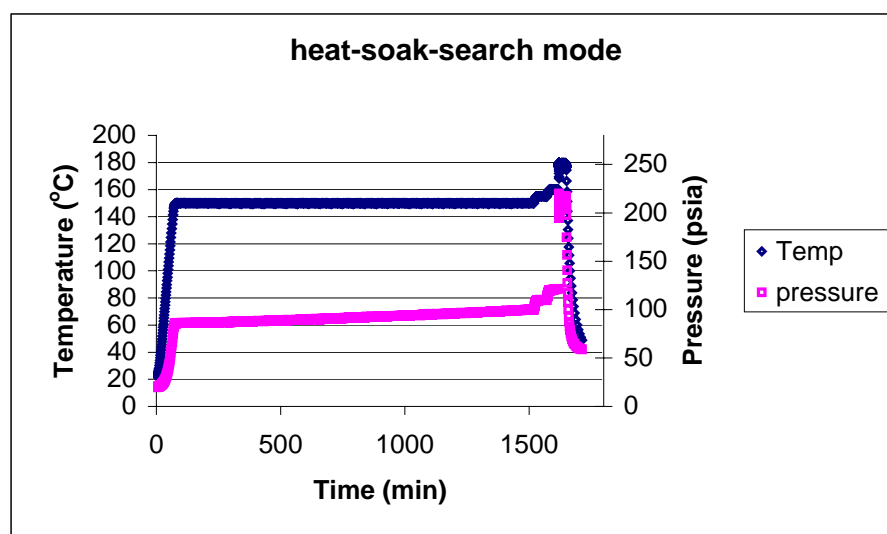* Results for the second exothermic peak were shown.

Figure 6.7. HSS experimental results of HAN in a glass sample cell.

In order to test the aging effect on the thermal decomposition of hydroxylamine nitrate, the HSS method was employed. The experimental results using glass, titanium, and stainless steel sample cells are presented in Table 6.2 and Figures 6.7-6.9. The soak temperatures were chosen as 20 degree lower than the onset temperatures of the HWS results, and the soak period was 24 hours. During the soak and search periods, although temperature was almost constant, the pressure increase was detected because the decomposition is undergoing with a low self-heat rate.
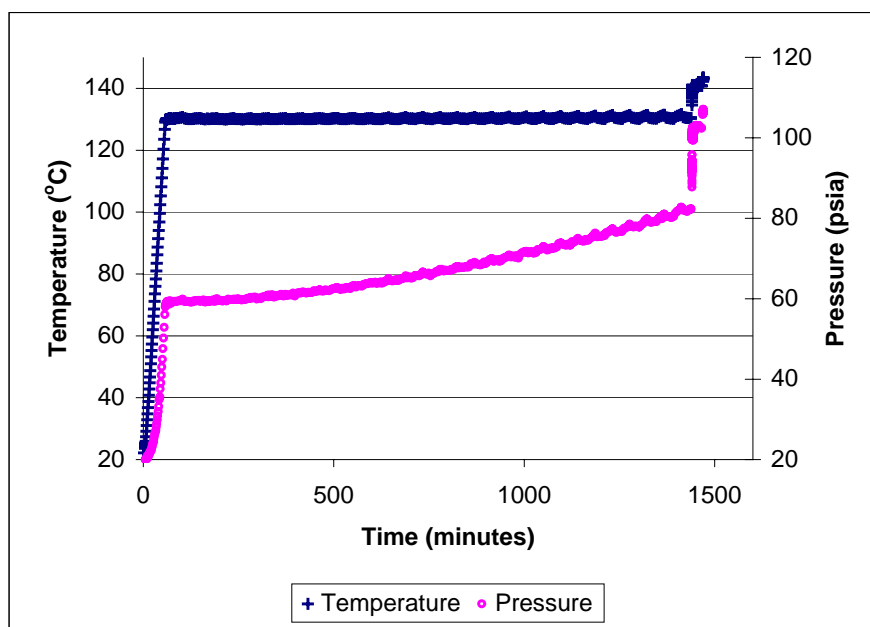

Figure 6.8. HSS experimental results of hydroxylamine nitrate in a titanium sample cell.
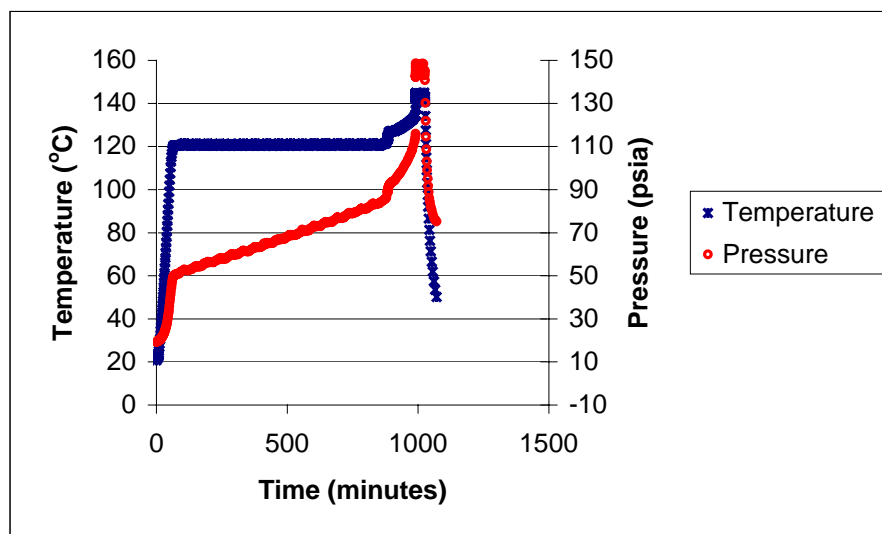
Figure 6.9. HSS experimental results of hydroxylamine nitrate in a stainless steel sample cell.

In the titanium cell, a fast explosion occurred at the end of soak period of 24 hours. In the glass and stainless steel cells, significant self-heat rates were not detected during the soak period, so the apparatus proceeded with the HWS mode. The detected onset temperatures were lower than those of the HWS mode alone. Besides the onset temperatures, the maximum HSS self-heat rates and maximum pressure rates were also lower in Table 6.2 than the HWS ones in Table 6.1. During the soak and search periods, the initiation reaction starts and the autocatalyst is generated. If the self-heat rate is not sufficient, the temperature will be cooled down to the soak temperature. Therefore, some heat loss occurred during the isothermal soak period, and the estimated heats of reaction were therefore significantly reduced in the HSS mode.
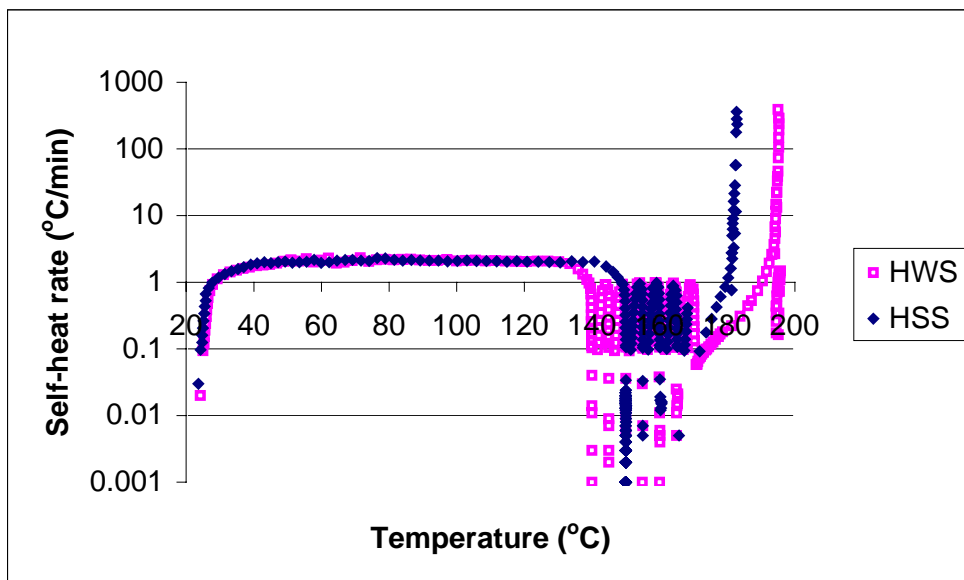
Figure 6.10. Comparison of HWS and HSS experimental results of hydroxylamine nitrate in a glass cell.

The self-heat rates of the HWS and HSS modes in a glass cell are compared in Figure 6.10. The peaks correspond to the fast explosion, and the corresponding self-heat rate points seem like straight lines because the reaction is very fast. The temperature corresponding to the maximum self-heat rate was 15 degree lower in the HSS mode than that in the HWS mode. The fast explosion can occur at a significantly lower temperature because a significant amount of autocatalyst is accumulated during the soaking period of 24 hours. This autocatalytic decomposition property poses a challenge for stable long-term storage of reactive chemicals.

6.5. Proposed Mechanism

Thermal decomposition products of hydroxylamine nitrate were analyzed to be nitric acid, water, and gas products (83% nitrous oxide, 17% nitrogen), and two overall equations (1-2) of equal importance were proposed [16], as shown in Equations 6.1 and 6.2. The decomposition pathway was also studied by a few groups [15, 16]. Based on information from the literature and quantum mechanical calculations using Gaussian 03 [13], a detailed decomposition mechanism is represented by a digraph in Figure 6.11. Hydroxylamine nitrate is in equilibrium with nitric acid and hydroxylamine. The dissociated hydroxylamine will react with nitric acid, producing nitrous acid, nitroxyl (HNO), and water most likely via an intermediate N-hydroxyl hydroxylamine (H_3NO_2). The intermediate nitrous acid is scavenged by hydroxylamine also via the intermediate H_3NO_2, producing nitroxyl and water. Nitroxyl can be either dimerized into nitrous oxide or scavenged by nitric acid to form nitrous acid, the autocatalyst, an important intermediate that causes the autocatalytic decomposition of hydroxylamine nitrate. A small amount of nitrogen is most likely due to interaction between nitroxyl and hydroxylamine.

$$3\ HONH_3^+\ NO_3^- \Rightarrow N_2O + N_2 + 2\ HNO_3 + 5\ H_2O \tag{6.1}$$

$$4\ HONH_3^+\ NO_3^- \Rightarrow 3\ N_2O + 2\ HNO_3 + 7\ H_2O \tag{6.2}$$

Figure 6.11. Detailed mechanism of hydroxylamine nitrate decomposition. Note: underlined **species** are final products; Species in red is autocatalyst; HAN represents hydroxylamine nitrate; HA represents hydroxylamine; Solid lines represent dominant steps; Dashed lines represent less dominant steps.

6.6. Conclusions

The thermal decomposition hazard of 24 wt% HAN/water was evaluated using both theoretical and calorimetric methods. Screening tools predict the hazard of potentail heat release and pressure generation. The temperature curve of the APTAC results shows two stages: a slow initiation stage and a fast explosion stage. The explosion stage occurs very suddenly and quickly. By comparing the HWS and HSS experimental results, the decomposition shows strong autocatalytic behavior, and the explosion stage can start at a much lower temperature after an aging period.

A plausible decomposition mechanism for hydroxylamine nitrate was proposed. Nitrous acid was found to be the intermediate that caused the autocatalytic behavior and another intermediate N-hydroxyl hydroxylamine was identified in this study. In order to temper the autocatalytic reaction, the concentration of nitrous acid should be reduced.

CHAPTER VII

THERMAL DECOMPOSITION PATHWAYS OF

HYDROXYLAMINE: A THEORETICAL STUDY OF INITIAL

STEPS

7.1. Introduction

Hydroxylamine free base (HA) plays an important role in the semiconductor, chemical, and pharmaceutical industries. It is used as a solvent in microchip production for removing organic and inorganic impurities from the wafers, and also as an important feedstock for dyes and rust inhibitors, and for the products such as painkillers, antibiotics, and tranquillizers [68]. However, hydroxylamine free base is challenging to handle, and pure hydroxylamine is known to decompose rapidly at room temperature [93]. Because of its chemical instability, HA has been involved in two tragic incidents [5, 6]. Since then, thermal decomposition hazards of hydroxylamine/water solutions have been investigated using calorimeters [7-11, 94]. Hydroxylamine decomposition is sensitive to metals [8], metal ions [10, 11], and pH of the solutions [94]. The final decomposition products [9] were analyzed as NH_3, H_2O, N_2, and N_2O, and small amount of NO and H_2, and the proportion of the products depends on experimental conditions [9, 78].

Previous experimental tests have provided only the overall decomposition behavior of hydroxylamine. The mechanism of hydroxylamine decomposition is barely understood, and the proposed mechanisms in the literature are controversial. Nitroxyl

(HNO) was proposed to be an intermediate for the decomposition of hydroxylamine by Nast [95], and a reaction scheme was developed in which the decomposition is controlled by disproportionation of hydroxylamine to ammonia and nitroxyl, according to Equation 7.1. The presence of nitroxyl as an intermediate was verified by the appearance of the violet tricyanonitrosonickelate(II) on the addition of tetracyanonickelate(II) [95], but Lunak [96] disagreed with the conclusion and demonstrated that the formation of tricyanonitrosonickelate was not due to nitroxyl, but a tricyanohydroxylammonickelous complex, resulting from replacement of a cyanide group in tetracyanonickelate by a molecule of hydroxylamine. Holzapfel [97] studied the kinetics of hydroxylamine decomposition in strong alkaline solutions, and it was assumed that OH-NH-OH and OH-NH-NH-OH were formed during the decomposition. In Chapter V and a previous study [94], it was found that acid or base can initiate different decomposition pathways of hydroxylamine. Hughes [79, 98] reported the oxidation of hydroxylamine by molecular oxygen in alkaline solutions, and nitrite, peroxonitrite, and hydrogen peroxide were detected as intermediates in significant quantities together with some nitrate. Also, the mechanisms of catalytic effects of metal ions on the decomposition of hydroxylamine were studied under different conditions [79, 96, 99, 100].

$$2NH_2OH \rightarrow H_2O + NH_3 + HNO \quad (7.1)$$
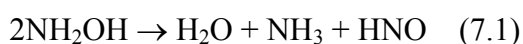
Hydroxylamine isomers and decomposition intermediates play an important role in N/O/H chemistry. In this chapter, hydroxylamine decomposition pathways were studied in the gas phase and in aqueous solution without adventitious ions. The objective

of this study was to elucidate the initiation steps of hydroxylamine decomposition using quantum mechanical calculations. Several possible decomposition pathways were investigated, and the most favorable decomposition pathway was proposed. Density functional and *ab initio* calculations were performed on all the species involved in the proposed pathways to give a quantitative description of the reaction mechanism involving the thermal decomposition of hydroxylamine. The findings from this study will provide a better understanding of the stability of hydroxylamine and some guidance on the design of effective inhibitors to control the hydroxylamine decomposition.

7.2. Theoretical Calculations

Density functional and *ab initio* calculations were carried out using the GAUSSIAN 03 suite of programs [64]. The geometries of reactants, products, various intermediates, and transition states were fully optimized using density functional methods, Becke3-Lee-Yang-Parr (B3LYP) [101, 102] and modified Perdew-Wang 1-parameter model for kinetics (MPW1K) [103], with Dunning's correlation consistent polarized valence double zeta basis set (cc-pVDZ) [71] and Pople-style basis set 6-31+G(d,p) [104] including diffuse [105] and polarization [106] functions, respectively. Previous theoretical work [107, 108] shows that MPW1K can provide more accurate energy barriers than B3LYP and excellent low cost performance. Becke88-Becke95 1-parameter model for kinetics (BB1K) is a new hybrid Hartree-Fock-density functional model developed by the Truhlar group, and a previous theoretical study [109] shows that BB1K can give excellent saddle point geometries and barrier heights. To compare the

methods and achieve accurate energetics, single-point energies were calculated with coupled cluster singles and doubles with triples correction CCSD(T) [110] using a 6-311+G(3df,2p) basis set, based on respective optimized geometries obtained with Møller-Plesset second-order perturbation theory (MP2) [111] using the same basis set, and the composite complete basis set (CBS-Q) [112] method was also employed to calculate the reaction paths of unimolecular reactions. Because the standard abbreviations for basis sets are lengthy, we used shorthands in the rest of the paper, as follows:

$$cc\text{-}pVDZ \rightarrow BSI$$

$$6\text{-}31+G(d,p) \rightarrow BSII$$

$$6\text{-}311+G(3df,2p) \rightarrow BSIII$$

Frequency calculations at B3LYP, MPW1K, and MP2 levels of theory were performed to obtain zero-point energies and frequencies for all species in the reaction pathways. The calculated structures were characterized as either a local minimum with no imaginary frequency or transition states with only one imaginary frequency. Some intrinsic reaction path (IRC) calculations [113, 114] were conducted to follow the reaction paths and validate that the transition states connect two minima of interest on the potential energy surface.

Solvent effects on the decomposition pathway were studied using both cluster methods and Polarizable Continuum models (PCM) [63]. Cluster methods were fully optimized. Single point energy calculations using the optimized gas phase geometry were conducted with PCM model due to geometry optimization convergence problems.
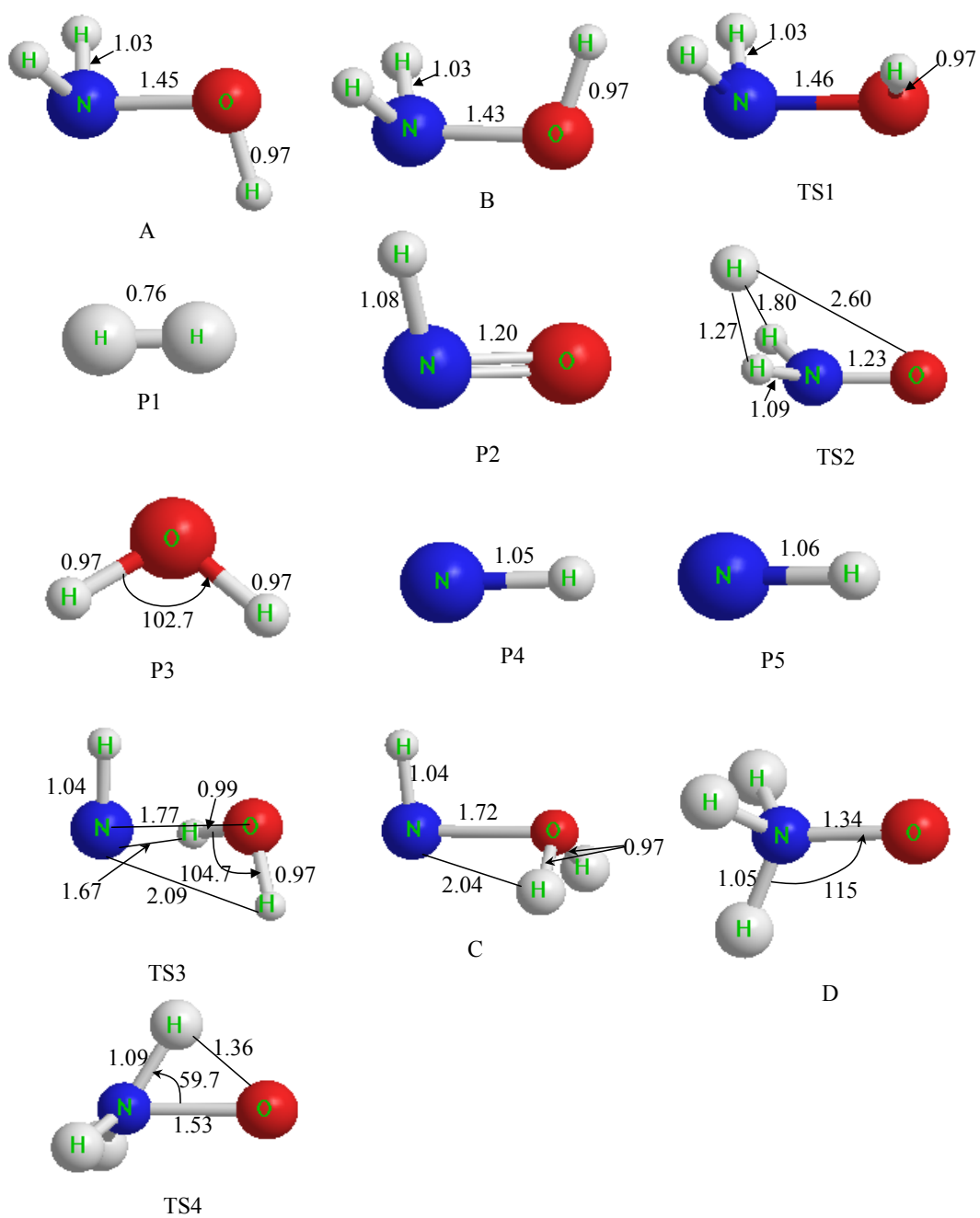
Figure 7.1. Molecular structures of hydroxylamine, transition states, and products involved in unimolecular decomposition pathways at the B3LYP/BSI level.

7.3. Results and Discussions

7.3.1. Molecular Geometries of Hydroxylamine

Experimental data on the molecular geometry for hydroxylamine are available [115], and some theoretical calculations [116, 117] on equilibrium geometries, rotational barriers, and vibrational analysis have also been conducted. HA possesses C_s symmetry and two conformations ("*trans*" and "*cis*"), as shown structures A and B in Figure 7.1. The optimized geometries of A and B at the density functional and CCSD levels of theory are compared with experimental and theoretical results in Table 7.1. B3LYP/BSI provides relatively accurate bond lengths within 0.01 Å of the experimental values, but a poor H-N-H bond angle (103.9º), compared with the experimental value (107.1º). MPW1K and BB1K results are very similar to each other, but the calculated N-O bond lengths are both 0.04 Å shorter than the experimental value, and the calculated H-N-H bond angles (106.8º and 106.6º, respectively) are closer to the experimental value (107.1º). From the deviations in Table 7.1, CCSD/BSII provides slightly better results than MP2/BSIII, as compared with experimental values, especially the bond lengths (zero deviation for CCSD/BSII). In order to obtain accurate results on the geometry of HA, the CCSD level of theory with relatively large basis set is necessary to carry out the calculations.

Table 7.1. Comparison of optimized geometries of NH_2OH at different levels of theory with experimental data (Bond lengths are in Å and angles in degree, and the deviations from experimental values are shown in parenthesis).

Parameter	Experimental[a]	B3LYP /BSI	MPW1K /BSII	BB1K /BSII	CCSD /BSII	MP2 /BSIII[b]
trans- NH_2OH						
R_{N-H}	1.02	1.03 (0.01)	1.01 (-0.01)	1.01 (-0.01)	1.02 (0.00)	1.01 (-0.01)
R_{N-O}	1.45	1.45 (0.00)	1.41 (-0.04)	1.41 (-0.04)	1.45 (0.00)	1.43 (-0.02)
R_{O-H}	0.96	0.97 (0.01)	0.95 (-0.01)	0.96 (0.00)	0.96 (0.00)	0.96 (0.00)
∠HNH	107.1	103.9 (-3.2)	106.8 (-0.3)	106.6 (-0.5)	106.1 (-1.0)	106.0 (-1.0)
∠HNO	103.2	103.3 (0.1)	105.0 (1.8)	104.8 (1.6)	103.5 (0.3)	104.2 (1.0)
∠HON	101.4	101.7 (0.3)	103.7 (2.3)	103.6 (2.2)	102.5 (1.1)	102.4 (1.0)
cis- NH_2OH						MP2/6-311++G(d,p)[c]
R_{N-H}		1.03	1.01	1.01	1.02	1.02
R_{N-O}		1.43	1.40	1.40	1.44	1.42
R_{O-H}		0.97	0.96	0.96	0.97	0.96
∠HNH		105.8	109.3	109.1	108.1	107.9
∠HNO		107.3	108.7	108.5	107.1	107.9
∠HON		107.9	109.2	109.1	108.1	107.5

a. S. Tsunekawa, J. Phys. Soc. Jpn. **1972**, *33*, 167.
b. A. Chung-Phillips and K.A. Jebber, J. Chem. Phys. **1995**, *102(18)*, 7080.
c. P. Boulet et al., Chem. Phys., **1999**, *244*, 163.

Table 7.2. The calculated relative energies, barrier heights $\Delta E_0^{\ddagger}$ (in kcal/mol at 0K), and optimized geometry of transition state between the *trans* and *cis* conformation of hydroxylamine at different levels of theory (Bond lengths are in Å and angles in degree).

Molecule	B3LYP /BSI[a]	MPW1K /BSII[a]	BB1K /BSII[a]	CCSD /BSII[a]	MP2 /BSII[b]	CCSD(T)/BSIII //MP2/BSIII[a]
trans (A)	0.00	0.00	0.00	0.00	0.00	0.00
Transition state (TS1)	6.56	7.88	7.79	7.59	7.25(6.45[d])	6.28
cis (B)	4.43	5.32	5.31	5.55	4.34(4.15[d])	4.14
Geometry of TS1						
R_{N-H}	1.03	1.01	1.01	1.02	1.01	
$R_{N-H'}$	1.03	1.01	1.01	1.02	1.02	
R_{N-O}	1.46	1.42	1.42	1.46	1.44	
R_{O-H}	0.97	0.95	0.96	0.96	0.96	
∠HNH	102.7	105.6	105.5	105.1	104.4	
∠HNO	102.3	103.5	103.3	102.3	102.7	
∠H'NO	106.6	108.2	108.1	106.9	107.2	
∠HON	105.9	107.9	107.8	106.7	106.3	

a. Zero-point energy (ZPE) correction included.
b. A. Chung-Phillips and K. A. Jebber, J. Chem. Phys. **1995**, *102(18)*, 7080.
c. H and H′ are symmetry equivalent.
   Zero-point energy (ZPE) correction included.

The rotational barrier for the conversion from A to B is not available from experiment, but high-level theoretical calculations [117, 118] have been conducted. The transition state (TS1 in Fig. 1) geometry and the calculated rotational barrier heights at different levels of theory are presented in Table 7.2. In previous work [117], it has been shown that the calculated rotation barrier and relative energy decrease with the increase of the size of the basis sets and correlation corrections. In this work, the highest level of theory in calculation of energetics was obtained at the CCSD(T)/BSIII level of theory

with the inclusion of zero point energy corrections at the MP2/BSIII level. The *trans* conformation (A) is found to be 4.14 kcal/mol more stable than the *cis* conformation (B), and the A to B rotation barrier at the CCSD(T)/BSIII// MP2/BSIII level is 6.28 kcal/mol. Density functional theories with small basis sets provide higher barriers, especially MPW1K (7.88 Kcal/mol) and BB1K (7.79 kcal/mol). Since the results from MPW1K and BB1K calculations are so close, only MPW1K was employed for the pathway analysis. The rotation barrier and relative energy at the B3LYP/BSI level (6.56 kcal/mol and 4.43 kcal/mol, respectively) are close to the results at the CCSD(T)/BSIII//MP2/BSIII level (6.28 kcal/mol and 4.14 kcal/mol, respectively), but B3LYP/BSI provides poor geometry of the transition state, especially the H-N-H bond angle (102.7°) compared with CCSD/BSII (105.1°). CCSD/BSII provided a comparable result on the geometry of TS1 with MP2/BSIII. CCSD(T)/BSIII (6.28 kcal/mol) yielded a slightly lower energies than MP2/BSIII (6.45 kcal/mol) because of higher correlation corrections at the CCSD(T) level, and this finding agrees with previous work [117].

7.3.2. Bond Dissociation Enthalpies (BDE)

Bond strengths and bond dissociation energies are fundamental to chemical reactions, and they can provide insight into the stability of chemicals. Experimental data on the BDE of HA are not available, but O-H bond strengths of unhindered dialkylhydroxylamines were determined to be in the range of 72-74 kcal/mol using calorimetric measurements [119].

The calculated bond dissociation energies of HA are shown in Table 7.3. The N-O bond is the weakest bond of HA, and the BDE is estimated to be 59.56 kcal/mol at the CCSD(T)//MP2 level, 67.21 kcal/mol at the MP2 level, 54.74 kcal/mol at the MPW1K level, and 60.21 kcal/mol at the B3LYP level. Compared with high-level theoretical calculations (CCSD(T)), density functional theories tend to underestimate the BDEs, although MPW1K yielded good results on N-H BDE, while MP2 tends to overestimate the BDEs. Therefore, relatively high energy is required to break the N-O bond, and this reaction is not likely significant at room temperature. The simple bond breaking reaction cannot explain the highly reactive nature of hydroxylamine. Other reaction pathways will be explored to investigate the mechanism of hydroxylamine decomposition.

Table 7.3. The calculated bond dissociation enthalpies (BDE in kcal/mol) at various levels of theory. (E at 0K (E_0) = Σelectronic and zero point energies of products - Σelectronic and zero point energies of reactants. H at 298K (H_{298}) = Σelectronic and thermal correction to enthalpy of products - Σelectronic and thermal correction to enthalpy of reactants.)

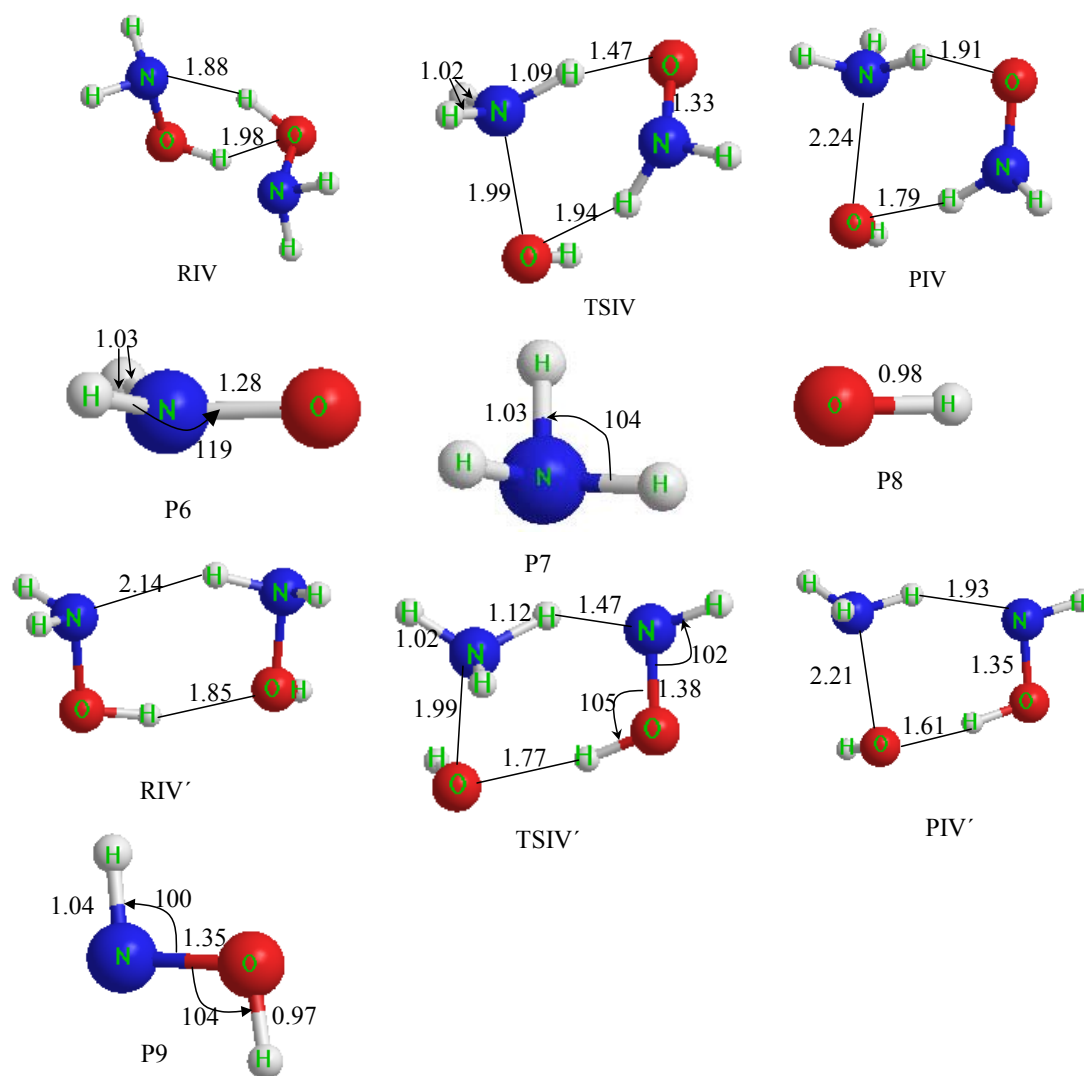| BDEs	B3LYP/BSI	MPW1K/BSII	MP2/BSIII	CCSD(T)/BSIII //MP2/BSIII
$E_0(H_{298})_{N-O}$	60.21(62.03)	54.74(56.60)	67.21(69.06)	59.56(61.40)
$E_0(H_{298})_{N-H}$	76.61(77.91)	86.12(87.55)	88.46(89.84)	86.35(87.73)
$E_0(H_{298})_{O-H}$	67.90(69.30)	69.80(71.37)	75.44(77.00)	74.06(75.61)

Figure 7.2. Molecular structures of hydroxylamine, transition states, and products involved in bimolecular decomposition pathways IV and IV´.
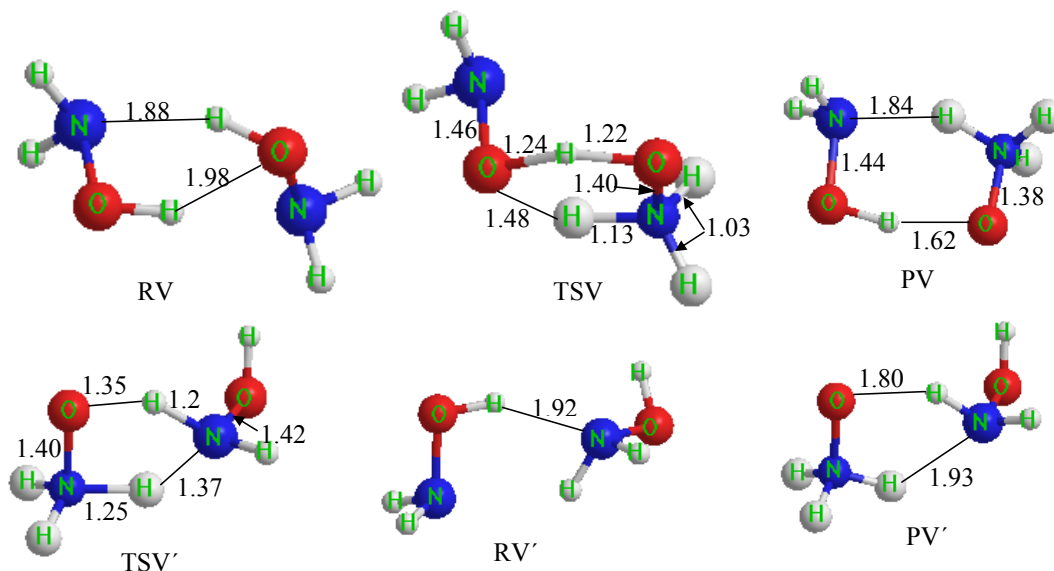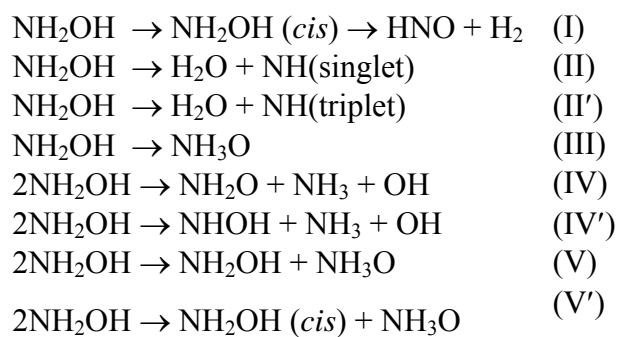
Figure 7.3. Molecular structures of hydroxylamine, transition states, and products involved in bimolecular decomposition pathways V and V′.

Scheme 7.1. Pathways of hydroxylamine decomposition.

$$NH_2OH \rightarrow NH_2OH \ (cis) \rightarrow HNO + H_2 \quad (I)$$
$$NH_2OH \rightarrow H_2O + NH(singlet) \quad\quad\quad (II)$$
$$NH_2OH \rightarrow H_2O + NH(triplet) \quad\quad\quad (II')$$
$$NH_2OH \rightarrow NH_3O \quad\quad\quad\quad\quad\quad\quad\quad (III)$$
$$2NH_2OH \rightarrow NH_2O + NH_3 + OH \quad\quad (IV)$$
$$2NH_2OH \rightarrow NHOH + NH_3 + OH \quad\quad (IV')$$
$$2NH_2OH \rightarrow NH_2OH + NH_3O \quad\quad\quad (V)$$
$$2NH_2OH \rightarrow NH_2OH \ (cis) + NH_3O \quad\quad (V')$$

Note: NH$_2$OH without specification is *trans*-hydroxylamine.

7.3.3. Decomposition Pathways

As represented in Scheme 7.1, five decomposition pathways were investigated including unimolecular and bimolecular reactions of hydroxylamine. The optimized structures of the species involved in the pathways at the B3LYP level of theory are shown in Figures 7.1- 7.3.

7.3.3.1. Pathway I

Pathway I involves two steps: (1) isomerization of *trans*-hydroxylamine into *cis*-hydroxylamine; (2) concerted hydrogen elimination to form molecular hydrogen. The hydrogen elimination step involves the simultaneous breaking of the N-H and O-H σ bonds, and the formation of a H-H σ bond and an O-N π bond. The optimized geometry of the transition state for the hydrogen elimination step (TS2) is represented in Figure 1. The O-H bond becomes very long (2.6 Å), and the H-H (1.27 Å) and N-O (1.23 Å) bonds become short. The rest of the molecule becomes more planar with the formation of the N-O double bond. This is a late transition state based on the N-O bond length (1.23 Å), which is closer to the product nitroxyl (1.20 Å) than the reactant *cis*-hydroxylamine N-O bond length (1.43 Å). A frequency calculation on TS2 had one imaginary frequency (1138i cm^{-1}) at the B3LYP/BSI level, whose normal mode is consistent with the forming H-H and breaking H-O bonds.

Table 7.4 lists the calculated activation barriers of the hydrogen elimination reaction. The energy barrier at MP2/BSIII is 72.33 kcal/mol, lower than the MPW1K result (79.58 kcal/mol). CCSD(T) single point energy calculations on the optimized MP2

geometry lowered the barrier by 2 kcal/mol. The activation barrier at CBS-Q level is

68.3 kcal/mol, which is close to the CCSD(T)/BSIII//MP2/BSIII result (69.78 kcal/mol).

Table 7.4. Energetics (in kcal/mol at 298 K) for species involved in the unimolecular decomposition pathways at various levels of theory.

Relative E(298K)	B3LYP/BSI[a]	MPW1K/BSII[b]	MP2/BSIII[c]	CCSD(T)/BSIII //MP2/BSIII[c]	CBS-Q
Pathway I					
B	0.00	0.00	0.00	0.00	0.00
TS2	63.01	79.58	72.33	69.78	68.30
P1+P2	23.74	37.74	30.78	28.66	29.34
Pathway II					
A	0.00	0.00	0.00	0.00	0.00
TS3	63.23	68.23	68.21	64.54	62.39
C	63.64	64.66	64.93	61.82	60.44
P3+P4	94.00	91.03	92.21	79.17	78.91
P3+P5	40.79	33.52	38.91	35.04	33.44
Pathway III					
A	0.00	0.00	0.00	0.00	0.00
TS4	50.26	51.06	49.81	50.03	48.53
D	28.23	24.72	24.95	25.16	20.23

a. B3LYP zero-point energy (ZPE) and thermal corrections included.
b. MPW1K zero-point energy (ZPE) and thermal corrections included.
c. MP2 zero-point energy (ZPE) and thermal corrections included.

7.3.3.2. Pathway II

Pathway II involves a hydrogen transfer from the nitrogen to the oxygen atom,

forming water and an NH radical that is either in its singlet excited state or triplet ground

state. In this study, both the singlet pathway (II) and triplet pathway (II′) are considered.

The optimized geometry for NH singlet (P4) and triplet states (P5) can be found in

Figure 7.1, and their corresponding energetics are given in Table 7.4. The NH triplet ground state is 35.5 kcal/mol more stable than the singlet state at the CBS-Q level. A singlet transition state (TS3) was located with a calculated barrier of 62.39 kcal/mol above *trans*-hydroxylamine. The singlet transition state (TS3) as shown in Figure 1 is a late transition state, because the N-O bond is very long (1.77 Å), and H_2O and NH are almost fully formed. A frequency calculation on TS3 had one imaginary frequency ($543i$ cm^{-1}) at the B3LYP/BSI level, whose normal mode is consistent with the hydrogen atom transferring from the N atom to O atom. The product of the singlet pathway is an imidogen-water complex (C in Figure 1), the energy of which is slightly lower than the singlet transition state.

7.3.3.3. Pathway III

Pathway III involves isomerization of hydroxylamine into ammonia oxide (NH_3O) via a 1,2-hydrogen shift from the oxygen to the nitrogen atom. The optimized structure of ammonia oxide (D) is shown in Figure 7.1. The N-O bond length of ammonia oxide (1.34 Å) is shorter than that of *trans*-hydroxylamine (1.45 Å), because ammonia oxide is a zwitterionic compound ($H_3N^+–O^-$). The electrostatic force between N and O in ammonia oxide brings the two atoms closer and shortens the N-O bond length, while in hydroxylamine, the repulsion of lone pairs push N and O atoms away. The energy of ammonia oxide is about 25 kcal/mol higher than *trans*-hydroxylamine at the CCSD(T)//MP2 level. The optimized transition state structure (TS4) for Pathway III is shown in Figure 7.1. This is a central transition state, as evidence by the O-N-H angle

of 60º that is about half of the corresponding angle of ammonia oxide (115º). The shifting hydrogen atom is between the N and O atoms with an N-H bond length of 1.09 Å and an O-H bond length of 1.36 Å. A frequency analysis at the B3LYP/BSI level reveals only one imaginary frequency ($1441i$ cm^{-1}), the normal mode of which corresponds to hydrogen shifting from the O to the N atom. The energetics of the species involved in this pathway are presented in Table 7.4, and the activation energy of this reaction is about 50 kcal/mol at CCSD(T) and MP2 levels.

All of the unimolecular decomposition pathways we have considered so far have high activation barriers. The lowest barrier on the potential energy surfaces is pathway III, and the calculated barrier for isomerization of hydroxylamine into ammonia oxide is 50 kcal/mol, as shown (TS4) in Figure 7.4. This finding is consistent with the experimental and theoretical results published by Brönstrup et al [120], although they reported some other hydrogen shift pathways with even higher activation energies.
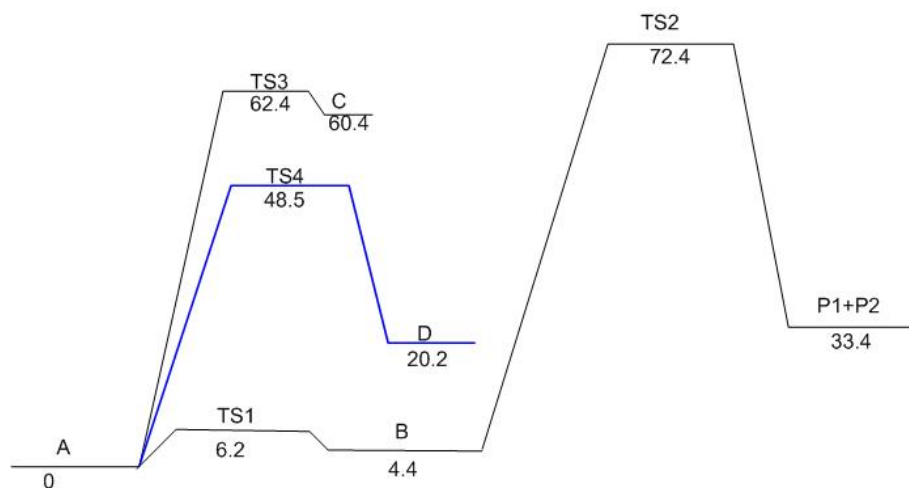
Figure 7.4. Unimolecular decomposition pathways of HA. Energetics were calculated at the CSB-Q level.

7.3.3.4. Pathways IV and IV´

Bimolecular decomposition pathways were explored in search of low barriers on the potential energy surface. A bimolecular path [95] as in Equation 7.1 was proposed to initiate the decomposition, but a transition state could not be located for this reaction, implying that it may not be an elementary reaction. Instead, it may involve two steps: (1) pathway IV or IV´; (2) NH_2O or NHOH reacts with OH to generate nitroxyl and water.

Pathway IV involves a hydrogen shift from the oxygen atom of one hydroxylamine molecule to the nitrogen atom of another hydroxylamine molecule. Pathway IV´ involves a hydrogen shift between the nitrogen atoms of two hydroxylamine molecules. When the transferring hydrogen atom is attacked by the nitrogen atom of another HA and forms ammonia, the N-O bond of the attacking HA molecule is broken (TSIV and TSIV´ in Figure 7.2). The optimized structures of the species involved in the Pathways IV and IV´ are shown in Figure 7.2, and the energetics of the species are presented in Table 7.5. Because the transition states in Pathways IV and IV´ are open shell systems with two unpaired electrons, unrestricted density functional and coupled-cluster UCCSD(T) methods were used to optimize the structure and to calculate the energetics, respectively. The geometry optimizations were carried out using either UB3LYP/BSI or UMPW1K/BSII levels of theory. Although the energetics differ significantly at the B3LYP/BSI and MPW1K/BSII levels (59.63 kcal/mol and 77.28 kcal/mol, respectively, in Pathway IV, and 63.43 kcal/mol and 87.36 kcal/mol, respectively, in Pathway IV´), the UCCSD(T) single point energy calculations provided very close results (57.33 kcal/mol and 46.47 kcal/mol, respectively, in Pathway

IV, and 46.85 kcal/mol and 45.31 kcal/mol, respectively, in Pathway IV´) based on the optimized structures and thermal corrections at the corresponding density functional theories. The activation barriers at the UCCSD(T) level are significantly lower than those using density functional theories, especially the MPW1K level of theory. Even though NH_2O (in Pathway IV) is more stable than NHOH (in Pathway IV´), the activation barrier above the reactant well of Pathway IV is higher than that of Pathway IV´ because of stronger hydrogen bonding in the reactant well of Pathway IV. Solvent effects on Pathways IV and IV´ will be addressed later in section 3.3.6.

7.3.3.5. Pathways V and V´

In Pathways V and V´, two hydrogen atoms shift between two HA molecules, forming ammonia oxide. Two transition states, TSV and TSV´, are shown in Figure 7.3. Analogy to transition state TSIV in Pathway IV, the H atom in the OH group transfers to the N atom of another HA molecule; meanwhile, the electron repulsion weakens the O-H bond in TSV, forming ammonia oxide, instead of the O-N bond in TSIV. The H atom in the weakened O-H bond transfers back to the other O atom, forming a HA molecule. The difference between Pathways V and V´ is the conformation of the formed HA molecule, and the H contributing groups in pathway V´ are NH_2 and OH, instead of two OH groups in Pathway V.

Table 7.5. Energetics (in kcal/mol at 298 K) for species involved in the bimolecular decomposition pathways at various levels of theory.

Relative E(298K)	B3LYP/BSI[a]	MPW1K/BSII[b]	CCSD(T)/BSII //B3LYP/BSI[a]	CCSD(T)/BSII //MPW1K/BSII[b]
Pathway IV				
A+A	0.00	0.00		
(RIV)	(0.00)	(0.00)	(0.00)	(0.00)
TSIV	50.51	74.67		
	(59.63)	(77.28)	(57.33)	(46.47)
P6+P7+P8	28.83	24.21		
(PIV)	(18.15)	(16.60)	(25.43)	(22.70)
Pathway IV´				
A+A	0.00	0.00		
(RIV´)	(0.00)	(0.00)	(0.00)	(0.00)
TSIV´	54.17	81.89		
	(63.43)	(87.36)	(46.85)	(45.31)
P7+P8+P9	37.44	40.39		
(PIV´)	(23.47)	(26.49)	(31.67)	(28.58)
Pathway V				
A+A	0.00	0.00		
(RV)	(0.00)	(0.00)	(0.00)	(0.00)
TSV	11.14	16.66		
	(20.27)	(22.13)	(24.10)	(24.16)
A+D	28.23	24.72		
(PV)	(15.48)	(13.44)	(14.85)	(14.91)
Pathway V´				
A+A	0.00	0.00		
(RV´)	(0.00)	(0.00)	(0.00)	(0.00)
TSV´	19.96	23.49		
	(28.22)	(28.53)	(33.19)	(32.84)
B+D	32.61	24.72		
(PV´)	(24.08)	(21.68)	(23.97)	(21.86)

a. B3LYP zero-point energy (ZPE) and thermal corrections included.
b. MPW1K zero-point energy (ZPE) and thermal corrections included.
c. Species in parenthesis are reactant wells or product wells including the hydrogen bond effect.

As shown in Table 7.5, the activation barrier of Pathway V is about 20 kcal/mol

above *trans*-hydroxylamine at the B3LYP level, which is significantly lower than that of

the unimolecular reaction in Pathway III. However, the barrier above ammonia oxide is

only about 4 kcal/mol. This low barrier for the reverse reaction may contribute to the

difficulty of detecting ammonia oxide by experimental methods, because it can easily

isomerize into the more stable hydroxylamine.
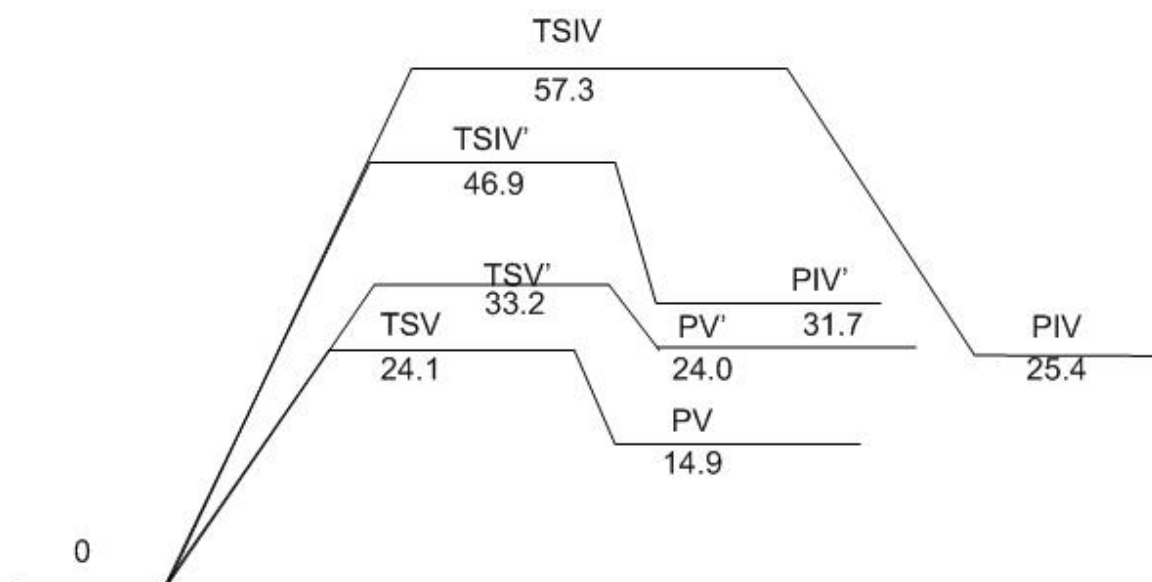
Figure 7.5. Bimolecular decomposition pathways of HA. Energetics were calculated at
the CCSD(T)/BSII//B3LYP/BSI level.

7.3.3.6. Solvent Effects

It is important to consider solvent effects on the hydroxylamine decomposition

pathways, because hydroxylamine is manufactured and used in aqueous solutions. From

above gas phase reaction pathway analysis, it shows that Pathway V is the most likely to

occur because of the lowest activation barrier of about 24 kcal/mol, as shown in Figure 7.5. This bimolecular reaction involves two hydrogen shifts and produces ammonia oxide, which is less stable than hydroxylamine. Pathways IV and IV′ are also important, because they produce radicals OH and NHOH/NH_2O. These radicals can react with HA to propagate the radical chain reactions. Therefore, solvent effects are considered for pathways IV, IV′ and V to determine the favorable decomposition pathway in solution.

Hydroxylamine and water clusters were used to simulate the solvation effects. All the structures in Pathway V were fully optimized at the MPW1K/BSII level, and the energetics are shown in Table 7.6. The inclusion of solvent molecules reduces the activation barriers, and water (14.17 kcal/mol) can stabilize the transition state better than HA (20.48 kcal/mol). With two water molecules (17.18 kcal/mol) included, the activation barrier is higher than with one (14.17 kcal/mol) or three (12.14 kcal/mol) water molecules, because the reactant well consisting of two water and two HA molecules poses a symmetric structure and is stabilized significantly. The endothermic heat of reaction decreases with an increasing number of water molecules. With three water molecules as solvent, the reaction becomes slightly exothermic (-1 kcal/mol).

Table 7.6. Solvent effects on the energetics (in kcal/mol at 298 K) for species involved in pathway V at MPW1K/BSII level of theory.

Species	No solvent	NH_2OH	H_2O	$2H_2O$	$3H_2O$
RV	0.00	0.00	0.00	0.00	0.00
TSV	24.16	20.48	14.17	17.18	12.14
PV	14.91	11.94	7.90	6.76	-1.00

The findings show that the solvent effect of water is evident in the small clusters containing only a few water molecules. Continuum models describing solute-solvent interactions were also used to study the decomposition pathway. Single point energy calculations were conducted using the CPCM polarizable conductor calculation model with Klamt's radii and an iterative solution (COSMO) [62, 63] at the MPW1K/BSII level, based on the optimized structure at the same level of theory. The free energy of activation at 298 K including the thermal correction for TSV is 16.81 kcal/mol using the COSMO method, which is very close to the result of 16.10 kcal/mol using a cluster containing three water molecules. Therefore, the solvent effect of a small water cluster converges quickly to that of bulk water.

The solvent effects on Pathways IV and IV′ were also studied to see if these pathways become favorable in solutions. For Pathway IV′, the gas phase free energy of activation at 298 K at the CCSD(T)/BSII level of theory including thermal corrections at the B3LYP/BSI level is 47.8 kcal/mol, and the gas phase free energy of reaction at 298 K is 34.0 kcal/mol. The COSMO model was used to simulate solvent effects at the CCSD(T)/BSII//B3LYP/BSI level, and the free energy of activation and the free energy of reaction at 298 K (including thermal correction effects) decrease to 39.8 and 10.8 kcal/mol, respectively. For Pathway IV, the free energy of activation and the free energy of reaction at 298 K (including thermal correction effects) are 100.17 and 1.09 kcal/mol, respectively, at the CCSD(T)/BSII//B3LYP/BSI level using the COSMO model. Therefore, these pathways are unlikely significant at room temperature because of high activation energies.

7.3.3.7. Water Catalyzed Reaction

In the previous section, solvent effects of water were discussed, and Pathway V was determined the most likely to occur in aqueous solutions. In Pathway V, water molecules lower the activation energy due to solvent effects. In this section, water catalyzed isomerization of HA is studied, and water molecules participate the reaction with HA via a hydrogen transfer processes. The structures of the transition state, reactant well, and product well are shown in Figure 7.6, and the energetics are presented in Table 7.7. Frequency analysis resulted in one imaginary frequency at $1325i$ cm^{-1}, and the corresponding normal mode is consistent with two hydrogen atoms transferring between HA and water. The activation barrier (25.95 kcal/mol) is slightly higher than Pathway V (24.16 kcal/mol) at the level of CCSD(T)/BSII//MPW1K/BSII. The COSMO model was used to simulate solvent effects at the CCSD(T)/BSII//B3LYP/BSI level, and the free energy of activation and the free energy of reaction at 298 K (including thermal correction effects) are 29.40 and 8.74 kcal/mol, respectively. Compared with gas phase values (27.62 kcal/mol and 19.80 kcal/mol, respectively), the activation barrier above HA increases slightly and the barrier above ammonia oxide increases significantly in aqueous solution. Therefore, for low concentrations of HA in aqueous solution, the isomerization can be catalyzed by water with a free energy of activation of 29.4 kcal/mol, which agrees with the activation energy (29 $\pm$ 4 kcal/mol) of the overall decomposition of 50 wt% HA in water [8]. The isomerization is most likely the limiting step of HA decomposition. At high concentrations of HA, the activation barrier is much lower (approximately 12 kcal/mol), which makes HA highly reactive.

Table 7.7. Energetics (in kcal/mol at 298 K) for the water catalyzed decomposition pathway at various levels of theory.

Relative E(298K)	B3LYP/BSI[a]	MPW1K/BSII[b]	CCSD(T)/BSII //B3LYP/BSI[a]	CCSD(T)/BSII //MPW1K/BSII[b]
A+H_2O	0.00	0.00		
(RVI)	(0.00)	(0.00)	(0.00)	(0.00)
TSVI	11.28	16.49		
	(21.31)	(22.74)	(25.80)	(25.95)
D+ H_2O	28.23	24.72		
(PVI)	(19.64)	(17.42)	(19.08)	(18.33)

    a. B3LYP zero-point energy (ZPE) and thermal corrections included.
    b. MPW1K zero-point energy (ZPE) and thermal corrections included.
    c. Species in parenthesis are reactant wells or product wells including the hydrogen bond effect.
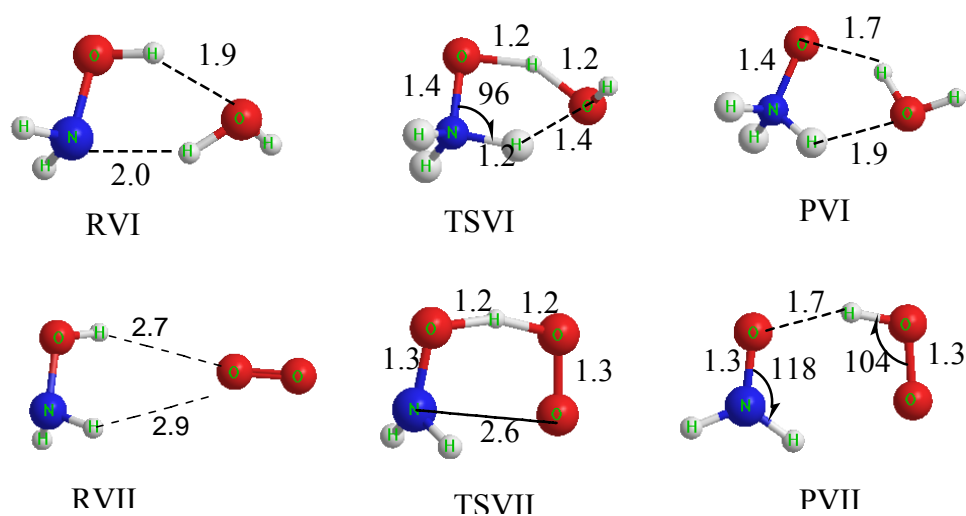
Figure 7.6. Molecular structures of hydroxylamine, transition states, and products involved in the water catalyzed decomposition pathway.

7.3.3.8. Oxidization by Molecular Oxygen

A transition state (TSVII in Figure 7.6) was located for the reaction between molecular oxygen and HA, and the normal mode of the only one imaginary frequency at 1887i cm^{-1} corresponds to the hydrogen transfer from HA to oxygen. The activation barrier and energy of reaction at 298K are 15.72 and 7.80 kcal/mol, respectively, at the level of MPW1K/BSII. This reaction has the lowest activation barrier in the gas phase among the studied pathways. One water molecule was included in the reaction to simulate solvent effects, and the activation barrier and energy of reaction at 298K decreased slightly to 15.44 and 6.98 kcal/mol, respectively. Therefore, the solvent effects of water on this pathway are not significant. This pathway is important because it produces two radicals, however, diffusion of oxygen from the gas phase into HA aqueous solution may also be a limiting factor. Some experimental tests are required to clarify the limiting step of the reaction.

7.4. Conclusions

Hydroxylamine decomposition pathways were investigated using density functional and ab initio methods. In this work, both unimolecular and bimolecular reactions were analyzed to locate the pathway with a low activation barrier. Simple bond dissociation and unimolecular hydrogen shift or elimination reactions require high activation energies.

Two bimolecular pathways were found to have lower activation barriers than unimolecular reactions. One hydrogen shift between two hydroxylamine molecules can

induce the dissociation of the N-O bond and produce two radicals. Two hydrogen shifts facilitate the isomerization of hydroxylamine into ammonia oxide. Accurate energetic calculations show that bimolecular isomerization steps have the lowest activation barrier of about 24 kcal/mol above the hydroxylamine bimolecular complex.

It was realized that all the reactions involved HA were undertaken in aqueous solutions. Although accurate gas phase decomposition pathway analysis can provide a good reference, solvent effects on the potential energy surface were investigated using cluster and continuum methods. Water solvent can stabilize the transition states and lower the activation barriers and the energies of reactions. The bimolecular isomerization step is the most favorable pathway and becomes slightly exothermic in solution with an energy barrier of 12 kcal/mol. Water was found to be a catalyst for the isomerization of HA to ammonia oxide. The theoretical study shows the potential of ammonia oxide formation in solutions and that ammonia oxide is less stable than hydroxylamine. The N-O bond dissociation enthalpy of NH_3O ($NH_3O \rightarrow NH_3 + {}^3O$) at 298 K is 35 kcal/mol at the G2 [121] level of theory. The decomposition of ammonia oxide will be studied further in the next chapter.

CHAPTER VIII

A THEORETICAL STUDY OF PROPAGATION AND TERMINATION STEPS

8.1. Introduction

Initial steps of hydroxylamine decomposition were discussed in Chapter VII. The most likely initiation step is the isomerization from hydroxylamine into ammonia oxide. The stability and geometry of ammonia oxide were studied using quantum mechanical methods [120, 122-127]. The N-O bond in ammonia oxide is less stable than hydroxylamine, as discussed in the previous chapter. The N-O bond dissociation energy in both gas phase and in aqueous solution will be discussed further in this chapter.

Knowledge of propagation and termination steps of radical reactions is important for mechanism generation. Runway reactions may involve thousands of propagation elementary steps. Identification of important kinetic steps, especially branching reactions, is need for designs of stabilizers and inhibitors. Previous work [3, 54, 58, 59, 128] has been conducted to generate mechanisms for hydrocarbons. The mechanisms were generated based on reaction types or reaction classes, which give the generic description of how molecules react. Reactions types involving hydrocarbons can be classified, for example, as dissociation, recombination, radical addition, beta-scission, H-abstraction, disproportionation, reverse disproportionation, H-shift, and ring-opening beta-scission [3].

Each reaction class represents the change of a set of atoms and bonds during the reaction. To generate an elementary reaction, the atoms and bonds of the reactant substructures of the reaction class must be matched with the reactant molecules. The products are then generated by changing the atom valences and bonds of the reactant molecule in the same way as in the reaction class. The products of each step can become the reactants of the next step. A complete mechanism consists of many such steps by iteratively applying a set of reaction classes to the reactants and the products.

8.2. Methods

A gas phase hydroxylamine decomposition network is generated using the method described in Chapter IV. The reaction class of hydroxylamine is different from that of hydrocarbons, and dissociation, recombination, H-abstraction, H-shift, N or O transfer, and ligand transfer reactions were considered. This set of reaction classes was applied to the reactants and the products of each step. The challenge associated with a mechanism generation method is that a combinatorial explosion of reactions may occur with an increasing number of intermediates. Some intermediates must be eliminated from the network, such as insignificant molecules that require high activation energies or unwanted molecules that do not react further.

The geometry of reactants, intermediates, and products were fully optimized, and frequency analysis was also conducted using Gaussian 03 [64] at the B3LYP/cc-pVDZ level. Evans-Polanyi's empirical rule was employed to estimate activation barriers from heats of reactions. The cutoff points of the activation barriers of initiation, propagation,

and termination steps were correlated with reaction temperatures based on empirical rules, as discussed in the section 3 of Chapter IV. The temperature range considered in this study is up to 250 °C, because the knowledge of reactions at this temperature range is important to control or prevent runaway reactions. Therefore, activation energies of propagation steps should be less than 36 kcal/mol, and there should be at least one intermediate cycle with activation energies less than 26 kcal/mol. Because hydroxylamine is unstable at room temperature, the activation barrier of an initiation reaction should be less than 40 kcal/mol to initiate the reaction.

8.3. Results and Discussions

8.3.1. N-O Bond Dissociation Energy of Ammonia Oxide

In the previous chapter, it was found out hydroxylamine molecule can isomerize into ammonia oxide with the assistance of another hydroxylamine or water molecule, and the activation energies in gas phase are 24.16 kcal/mol and 25.95 kcal/mol, respectively, at the CCSD(T)/BSII//MPW1K/BSII level. In aqueous solution, the activation energy of the bimolecular isomerization reduces to 12.14 kcal/mol at the level of MPW1K/BSII.

The N-O bond dissociation energy of ammonia oxide was calculated at different levels of theory and is represented in Table 8.1. MP2/BSIII theory provides a BDE of 36.97 kcal/mol, close to the result at the CBS-Q level (39.35 kcal/mol) level and the G2 level (34.99 kcal/mol), however CCSD/BSII underestimates the BDE (20.55 kcal/mol).

In aqueous solution, the N-O BDE of ammonia oxide decreases to -7.60 kcal/mol at the

MP2/BSIII level and -8.33 kcal/mol at the CCSD/BSII level.

Table 8.1. The calculated N-O bond dissociation enthalpy (BDE in kcal/mol) at various levels of theory. (H at 298K (H_{298}) = Σelectronic and thermal correction to enthalpy of products - Σelectronic and thermal correction to enthalpy of reactants.)

BDE	CCSD/BSII		MP2/BSIII		G2	CBS-Q
Phase	Gas	Aq.[a]	Gas	Aq.[a]	Gas	Gas
$(H_{298})_{N-O}$	20.55	-8.33	36.94	-7.06	34.99	39.35

a. The BDE in aqueous solution was calculated using the COSMO model, with gas phase thermal correction included.

In comparison, the N-O BDE of hydroxylamine is 69.06 kcal/mol in the gas

phase, and 5.83 kcal/mol in aqueous solution at the level of MP2/BSIII.   Therefore, the

N-O bond of ammonia oxide is easier to break than the N-O bond of hydroxylamine.

This is the most likely initiation step for hydroxylamine decomposition. The generated

NH_3 is a final product, and O (^{3}P) is a reactive intermediate.

8.3.2. Hydroxylamine Decomposition Network

Approximately 800 possible elementary reactions were generated using the

method described in this chapter. After initial screening and elimination based on

activation energies, about 80 important elementary reactions remained. The key

intermediates are labeled and the formation and destruction of the intermediates are

indicated by arrows. Two arrows come together when two species react, and the

products of the reaction are indicated by arrows leading away from the encounter. The reaction network is listed in Figure 8.1. Heats of reaction of the elementary steps are represented in Appendix C.

The initiation step is isomerization of hydroxylamine into ammonia oxide, following which ammonia oxide breaks into ammonia and oxygen atom. Then, by interacting among them and hydroxylamine, several intermediates are generated to produce the final products. The intermediates are formed and destroyed in a cyclic process, a key feature of initiation-propagation reactions. The process can always loop back to the original species by following the arrows. By going around the cycles many times, a considerable reaction rate can be obtained and a considerable amount of products can be generated. The digraph cannot only illustrate the generated mechanism but also help identify missing elementary steps. Most reaction mechanisms retain certain symmetry when expressed in graphs and catalytic cycles can be easily identified.

There are five branching reactions involved O, NH, O_2, HNO, and N_2H_2 in the order of increasing activation energies. The five branching reactions form catalytic cycles as illustrated by the loops (cycles 1, 2, 7, 3, and 4) in Fig. 8.1. The five catalytic cycles interact with each other intensively, as shown by the intervened arrows linking between them. The termination steps involve recombination of two radicals, forming final products, N_2, N_2O, NH_3, H_2O, and H_2.
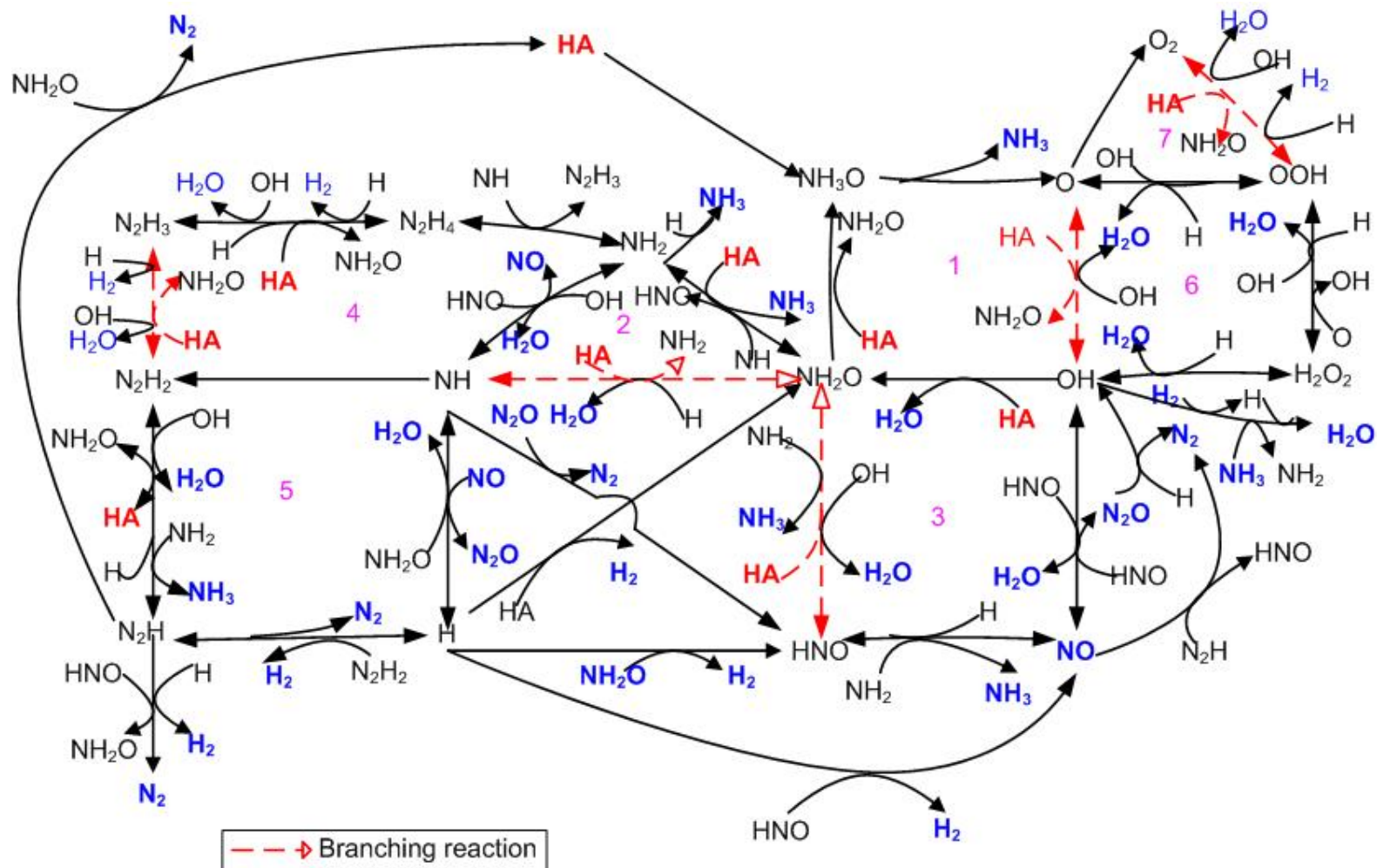
Figure 8.1. Digraph of reaction network for hydroxylamine decomposition in the gas phase.

8.3.3. Activation Energies

The activation energies are estimated using a linear free energy relationship based on different types of reactions employing the method discussed in Chapter IV. Transition states of some elementary reactions are calculated using Gaussian 03, and activation barriers are compared with estimated values from Evans-Polanyi's relationship. The preliminary results are presented in Appendix C at the level of B3LYP/BSI. The estimated activation energies are in reasonable agreement with the calculated values.

8.4. Conclusions and Recommendations

Using the proposed graph assisted mechanism generation method, a gas phase hydroxylamine decomposition network was generated. The predicted final products using this method are consistent with experimental results. This approach can potentially be applied to any chemical system under runaway conditions.

From the proposed mechanism, we can provide options to stabilize hydroxylamine. Because oxygen free radical is the important species that initiates the decomposition, oxygen free radical scavenger such as dimethylthiourea is expected to stabilize the hydroxylamine solution. In the literature, thioureas (EP-A-516933) were proposed as stabilizers for hydroxylamine.

All of the branching reactions involve the NH_2O radical. Therefore, a radical scavenger for NH_2O is expected to break down the catalytic cycles and control the runaway reaction.

CHAPTER IX

CONCLUSIONS AND RECOMMENDATIONS

9.1. Conclusions

Hydroxylamine system decomposition hazards and pathways were investigated using both calorimetric and theoretical methods. Presence of acid/base can initiate different pathways for hydroxylamine decomposition. Both base and acid contamination must be avoided for safe handling of hydroxylamine.

Hydroxylamine nitrate decomposition shows strong autocatalytic behavior. The APTAC was employed to detect autocatalytic decomposition. The proposed mechanism shows that the intermediate nitrous acid is the autocatalyst. In order to control the autocatalytic reaction, the concentration of nitrous acid must be controlled below a certain level.

A graph-assisted method was proposed to generate a hydroxylamine decomposition mechanism. Both Evans-Polanyi's relationship and quantum mechanical calculations were used to estimate activation barriers of elementary steps. Only kinetically important steps were considered in the decomposition pathway. The predicted final products using this method are consistent with experimental results. Based on the decomposition network, recommendations were provided to stabilize hydroxylamine

solution. This approach can potentially be applied to any chemical system under runaway conditions.

9.2. Recommendations

To validate the predicted mechanism, the predicted reactant conversions and product yields should be compared with experimental data. Calorimeters cannot provide concentration response but only temperature and pressure responses. It is more challenging to compare predicted temperature rise with calorimetric data because specific heat of the mixture and heat transfer to the environment must be incorporated into the model. Therefore, in-situ measurement by GC, MS, or FTIR can provide valuable information about the intermediates or gas products, which are needed to make predictions.

A detailed kinetic modeling approach was proposed as shown in Chapter III. This approach incorporates reaction network generation, rate constants estimation, and simulation of industrial conditions. However, generating a reaction network using this approach still relys on chemical intuition. The rate constants of elementary reactions can be calculated using GAUSSRATE that employs variational transition state theory and tunneling effects.

A computer program incorporating an automated mechanism generator, Gaussian, GAUSSRATE, and kinetics integration methods will make this reactive hazard prediction task easier and more applicable to industrial conditions.

REFERENCES

[1] U.S. Chemical Safety and Hazard Investigation Board, Hazard Investigation: Improving Reactive Hazard Management, (2001), http://www.csb.gov, accessed in May 2005.

[2] M. J. De Witt, D. J. Dooling, L. J. Broadbelt, Computer generation of reaction mechanisms using quantitative rate information: application to long-chain hydrocarbon pyrolysis, Ind. Eng. Chem. Res. 39 (2000) 2228-2237.

[3] D. M. Matheu, A. M. Dean, J. M. Grenda, J. William H. Green, Mechanism generation with integrated pressure dependence: a new model for methane pyrolysis, J. Phys. Chem. A 107 (2003) 8552-8565.

[4] A. Ratkiewicz, T. N. Truong, Application of chemical graph theory for automated mechanism generation, J. Chem. Inf. Comput. Sci. 43 (2003) 36-44.

[5] M. Reisch, Chemical plant blast kills five near Allentown, Chemical&Engineering News 77 (1999) 11.

[6] Chemical explosion in Japan kills four, Chemical&Engineering News 78 (2000) 15-16.

[7] L. O. Cisneros, W. J. Rogers, M. S. Mannan, Effect of air in the thermal decomposition of 50 mass% hydroxylamine/water, Journal of Hazardous Materials 95 (2002) 13-25.

[8] L. O. Cisneros, W. J. Rogers, M. S. Mannan, Adiabatic calorimetric decomposition studies of 50 wt.% hydroxylamine/water, Journal of Hazardous Materials 82 (2001) 13-24.

[9] L. O. Cisneros, X. Wu, W. J. Rogers, M. S. Mannan, J. Park, S. W. North, Decomposition products of 50 mass % hydroxylamine/water under runaway reaction conditions, Process Safety and Environmental Protection 81 (2003) 121-124.

[10] L. O. Cisneros, W. J. Rogers, M. S. Mannan, X. Li, H. Koseki, Effect of iron ion in the thermal decomposition of 50 mass % hydroxylamine/water solutions, Journal of Chemical and Engineering Data 48 (2003) 1164-1169.

[11] Y. Iwata, H. Koseki, Decomposition of hydroxylamine/water solution with added iron ion, Journal of Hazardous Materials 104 (2003) 39-49.

[12] U.S. Department of Energy, Technical Report on Hydroxylamine Nitrate, 1998, http://www.eh.doe.gov/chem_safety//Docs/hydroxlyamine.pdf, accessed in May 2005.

[13] C. A. V. Dijk, R. G. Priest, Thermal decomposition of hydroxylammonium nitrate at kilobar pressure, Combustion and Flame 57 (1984) 15-24.

[14] V. A. Rafeev, Y. I. Rubtsov, Kinetics and mechanism of thermal decomposition of hydroxylammonium nitrate, Russian Chemical Bulletin 42 (1993) 1811-1815.

[15] J. W. Schoppelrei, T. B. Brill, Spectroscopy of hydrothermal reactions. 7. Kinetics of aqueous $[NH_3OH]NO_3$ at 463-523 K and 27.5 MPa by infrared spectroscopy, J. Phys. Chem. A 101 (1997) 8593-8596.

[16] J. C. Oxley, K. R. Brower, Thermal decomposition of hydroxylamine nitrate, in: Proceedings of SPIE-The International Society for Optical Engineering 872 (1988) 63-70.

[17] A. Benuzzi, J. M. Zaldivar, Safety of Chemical Batch Reactors and Storage Tanks, Kluwer Academic Publishers, Boston 1991.

[18] T. Yoshida, Safety of Reactive Chemicals, Elsevier, New York 1987.

[19] D. J. Leggett, Thermochimica Acta 367-368 (2001) 351-365.

[20] R. J. Willson, Principles of Thermal Analysis and Calorimetry, Royal Society of Chemistry, Cambridge, UK 2002.

[21] Differential Scanning Calorimetry: An Introduction for Practitioners, Springer, Berlin, Germany 1995.

[22] Process and Reaction Hazard Analysis, HEL Group Co. Barnet, UK, http://www.helgroup.co.uk, accessed in May 2005.

[23] H. K. Fauske, 1993, U.S. Patent 5,229,074.

[24] S. Chippett, P. Ralbovsky, R. Granville, in: International Symposium on Runaway Reactions, Pressure Relief Design, and Effluent Handling, 1998, 81-108 American Institute of Chemical Engineers, New Orleans.

[25] R. Granville, D. Wallace, in: International Symposium on Runaway Reactions and Pressure Relief Design, 1995, American Institute of Chemical Engineers, New York.

[26] H. K. Fauske, J. C. Leung, New experimental technique for characterizing runaway reactions, Chemical Engineering Progress 81 (1985) 39-46.

[27] J. C. Leung, H. K. Fauske, H. G. Fisher, Thermal runaway reactions in a low thermal inertia apparatus, Thermochimica Acta 104 (1986) 13-29.

[28] Advanced Reactive System Screening Tool, Fauske & associates, Inc. http://www.ARSST.com, accessed in May 2005.

[29] L. Bretherick, in: International Symposium on Preventing Major Chemical Accidents, American Institute of Chemical Engineers, New York, (1987) 4.1-4.15.

[30] P. F. Nolan, J. A. Barton, Some lessons from thermal-runaway incidents, Journal of Hazardous Materials 14 (1987) 233-239.

[31] T. C. Ho, Y.S Duh, J.R. Chen, Case studies of incidents in runaway reactions and emergency relief, Process Safety Progress 17 (1998) 259-262.

[32] M. Wakakura, Y. Iiduka, Trends in chemical hazards in Japan, Journal of Loss Prevention in the Process Industries 12 (1999) 79-84.

[33] Center for Chemical Process Safety, Guidelines for chemical reactivity evaluation and application to process design, 1995.

[34] Center for Chemical Process Safety, Guidelines for safe storage and handling of reactive materials, 1995.

[35] G. Joseph, Recent reactive incidents and fundamental concepts that can help prevent them, Journal of Hazardous Materials 104 (2003) 65-73.

[36] Center for Chemical Process Safety, Essential Practices for Managing Chemical Reactivity Hazards, 2003.

[37] NOAA, Chemical Reactivity Worksheet, http://www.noaa.gov, accessed in May 2005.

[38] ChemOffice Ultra 2004, version 8.0 http://www.cambridgesoft.com/, accessed in May 2005.

[39] Converting chemical names into structures with Name=Struct http://www.cambridgesoft.com/products/pdf/whitepapers/NameStruct.pdf, accessed in May 2005.

[40] M. J. S. Dewar, E. Zoebisch, E.F. Healy, J.J.P. Stewar, , Development and use of quantum mechanical molecular models. 76. AM1: a new general purpose quantum mechanical molecular model, Journal of American Chemical Society 107 (1985) 3902-3909.

[41] M. J. S. Dewar, W. Thiel, Groud state of molecules. 38. The MNDO method. approximations and parameters, Journal of American Chemical Society 99 (1977) 4899-4907.

[42] R. C. Bingham, M.J.S. Dewar, D.H. Lo, Ground states of molecules. XXV. MINDO/3. Improved version of the MINDO semiempirical SCF-MO method, Journal of American Chemical Society 97 (1975) 1285-1293.

[43] J. J. P. Stewart, Optimization of parameters for semiempirical methods. I. Method, Journal of Computational Chemistry 10 (1989) 209-220.

[44] W. Thiel, Thermochemistry from semiempirical molecular orbital theory, in Computational Thermochemistry: Prediction and Estimation of Molecular Thermodynamics, American Chemical Society, (1998) 142-161.

[45] S. W. Benson, Thermochemical Kinetics (2nd ed.), Wiley, New York 1976.

[46] C.A. Davies, I. M. Kipnis, M.W. Chase, D.N. Treweek, The thermochemical and hazard data of chemicals. Estimation using the ASTM CHETAH program, ACS Symposium Series 274 (1985) 81-90.

[47] T. Grewer, D. J. Frurip, B. Keith Harrison, Prediction of thermal hazards of chemical reactions, Journal of Loss Prevention in the Process Industries 12 (1999) 391-398.

[48] S. R. Saraf, W. J. Rogers, M. S. Mannan, Prediction of reactive hazards based on molecular structure, Journal of Hazardous Materials 98 (2003) 15-29.

[49] P. Cardillo, M. Nebuloni, Theoretical and calorimetric evaluation of thermal stability of glycidol, Journal of Loss Prevention in the Process Industries 4 (1991) 242-245.

[50] P. Cardillo, M. Nebuloni, Reactivity limits of aluminium and halohydrocarbon mixtures: determination by the ASTM CHETAH program, Journal of Loss Prevention in the Process Industries 5 (1992) 81-88.

[51] E. S. Shanley, G. A. Melhem, A review of ASTM CHETAH 7.0 hazard evaluation criteria, Journal of Loss Prevention in the Process Industries 8 (1995) 261-264.

[52] E. S. Shanley, G. A. Melhem, A review and critique of ASTM CHETAH 4th edition, version 7.2, Journal of Loss Prevention in the Process Industries 13 (2000) 67-68.

[53] Screening Criteria Applied to the CSB Incident Database, in: Reactivity Management Roundtable, Iomosaic Coorporation, (2005), http://www.iomosaic.com, accessed in May 2005.

[54] H. J. Curran, P. Gaffuri, W. J. Pitz, C. K. Westbrook, A comprehensive modeling study of n-heptane oxidation, Combustion and Flame 114 (1998) 149-177.

[55] A. M. Dean, Detailed kinetic modeling of autocatalysis in methane pyrolysis, Journal of Physical Chemistry 94 (1990) 1432-1439.

[56] M. J. D. Witt, D. J. Dooling, L. J. Broadbelt, Computer generation of reaction mechanisms using quantitative rate information: application to long-chain hydrocarbon pyrolysis, Ind. Eng. Chem. Res. 39 (2000) 2228-2237.

[57] J.-L. Faulon, Stochastic generator of chemical structure. 3. reaction network generation, J. Chem. Inf. Comput. Sci. 41 (2001) 894-908.

[58] E. S. Blurock, Detailed mechanism generation. 1. generalized reactive properties as reaction class substructures., J. Chem. Inf. Comput. Sci. 44 (2003) 1336-1347.

[59] F. Kirchner, The chemical mechanism generation programme CHEMATA-Part 1: the programme and first applications, Atmospheric Environment 39 (2005) 1143-1159.

[60] F. O. Rice, K. K. Rice, The Aliphatic Free Radicals, The Johns Hopkins Press, Baltimore (1935).

[61] R. I. Masel, Chemical Kinetics and Catalysis, John Wiley&Sons, Inc., New York 2001.

[62] V. Barone, M. Cossi, Quantum calculation of molecular energies and energy gradients in solution by a conductor solvent model, Journal of Physical Chemistry A 102 (1998) 1995-2001.

[63] M. Cossi, N. Rega, G. Scalmani, V. Barone, Energies, structures, and electronic properties of molecules in solution with the C-PCM solvation model, Journal of Computational Chemistry 24 (2003) 669-681.

[64] M. J. Frisch, G. W. Trucks, H. B. Schlegel, G. E. Scuseria, M. A. Robb, J. R. Cheeseman, J. A. Montgomery, Jr., T. Vreven,

K. N. Kudin, J. C. Burant, J. M. Millam, S. S. Iyengar, J. Tomasi,
V. Barone, B. Mennucci, M. Cossi, G. Scalmani, N. Rega,
G. A. Petersson, H. Nakatsuji, M. Hada, M. Ehara, K. Toyota,
R. Fukuda, J. Hasegawa, M. Ishida, T. Nakajima, Y. Honda, O. Kitao,
H. Nakai, M. Klene, X. Li, J. E. Knox, H. P. Hratchian, J. B. Cross,
C. Adamo, J. Jaramillo, R. Gomperts, R. E. Stratmann, O. Yazyev,
A. J. Austin, R. Cammi, C. Pomelli, J. W. Ochterski, P. Y. Ayala,
K. Morokuma, G. A. Voth, P. Salvador, J. J. Dannenberg,
V. G. Zakrzewski, S. Dapprich, A. D. Daniels, M. C. Strain,
O. Farkas, D. K. Malick, A. D. Rabuck, K. Raghavachari,
J. B. Foresman, J. V. Ortiz, Q. Cui, A. G. Baboul, S. Clifford,
J. Cioslowski, B. B. Stefanov, G. Liu, A. Liashenko, P. Piskorz,
I. Komaromi, R. L. Martin, D. J. Fox, T. Keith, M. A. Al-Laham,
C. Y. Peng, A. Nanayakkara, M. Challacombe, P. M. W. Gill,
B. Johnson, W. Chen, M. W. Wong, C. Gonzalez, and J. A. Pople,
Gaussian 03, Revision B.04, Gaussian, Inc., Pittsburgh PA, 2003.

[65] J. C. Corchado, Y.-Y. Chuang, E. L. Coitino, D. G. Truhlar, Gaussrate, University of Minnesota, Minneapolis, MN, 2003.

[66] Jose C. Corchado, Yao-Yuan Chuang, Patton L. Fast, Jordi Villa, Wei-Ping Hu, Yi-Ping Liu, Gillian C. Lynch, Kiet A. Nguyen, Charles F. Jackels, Vasilios S. Melissas, Benjamin J. Lynch, Ivan Rossi, Elena L. Coitino, Antonio Fernandez Ramos, Jingzhi Pu, Titus V. Albu, R. Steckler, B.C. Garrett, A.D. Isaacson, and D.G. Truhlar, POLYRATE-version 9.1, University of Minnesota, Minneapolis, MN, 2002.

[67] J. L. Gustin, Influence of trace impurities on chemical reaction hazards, Journal of Loss Prevention in the Process Industries 15 (2002) 37-48.

[68] Hydroxylamine and its salts, Manufacturing Chemist and Aerosol News 35 (1964) 29-36.

[69] A. D. Becke, Density functional thermochemistry. III. The role of exact exchange, J. Chem. Phys. 98 (1993) 5648.

[70] J. P. Perdew, Density-functional approximation for the correlation energy of the inhomogeneous electron gas, Physical Review B33 (1986) 8822.

[71] T. H. Dunning, Jr., Gaussian basis sets for use in correlated molecular calculations. I. The atoms boron through neon and hydrogen, Journal of Chemical Physics 90 (1989) 1007-1023.

[72] M. J. Frisch, G. W. Trucks, H. B. Schlegel, G. E. Scuseria,
M. A. Robb, J. R. Cheeseman, V. G. Zakrzewski, J. A. Montgomery, Jr.,
R. E. Stratmann, J. C. Burant, S. Dapprich, J. M. Millam,
A. D. Daniels, K. N. Kudin, M. C. Strain, O. Farkas, J. Tomasi,
V. Barone, M. Cossi, R. Cammi, B. Mennucci, C. Pomelli, C. Adamo,
S. Clifford, J. Ochterski, G. A. Petersson, P. Y. Ayala, Q. Cui,
K. Morokuma, N. Rega, P. Salvador, J. J. Dannenberg, D. K. Malick,
A. D. Rabuck, K. Raghavachari, J. B. Foresman, J. Cioslowski,
J. V. Ortiz, A. G. Baboul, B. B. Stefanov, G. Liu, A. Liashenko,
P. Piskorz, I. Komaromi, R. Gomperts, R. L. Martin, D. J. Fox,
T. Keith, M. A. Al-Laham, C. Y. Peng, A. Nanayakkara, M. Challacombe,
P. M. W. Gill, B. Johnson, W. Chen, M. W. Wong, J. L. Andres,
C. Gonzalez, M. Head-Gordon, E. S. Replogle, and J. A. Pople,
Gaussian 98, Revision A.11.3, Gaussian, Inc., Pittsburgh PA, 2002.

[73] H. K. Fauske, in: International Symposium on Runaway Reactions, Pressure Relief
Design, and Effluent Handling, American Institute of Chemical Engineers, New
Orleans, (1998) 11-13.

[74] M. J. Creed, H. K. Fauske, An easy and inexpensive approach to the DIERS
methodology, Chem. Eng. Prog. 86 (1990) 45-49.

[75] D. I. Townsend, J. C. Tou, Thermal hazard evaluation by an accelerating rate
calorimeter, Thermochimica Acta 37 (1980) 1-30.

[76] Superchems, ioMosaic Corporation. http://ioxpress.com/sc, accessed May 2005.

[77] S. Lunak, J. Veprek-Siska, The catalytic effect of cations on the decomposition of
alkaline solutions of hydroxylamine, Collection of Czechoslovak Chemical
Communications 39 (1974) 391-395.

[78] K. A. Hofmann, F. Kroll, Thermal decomposition of hydroxylamine and hydrazine
salts, Ber. 57B (1924) 937-944.

[79] M. N. Hughes, H. G. Nicklin, Autoxidation of hydroxylamine in alkaline solutions,
Journal of the Chemical Society (A) 1 (1971) 164-168.

[80] E. Ebler, E. Schott, A study of hydroxylamine (I), Journal fuer Praktische Chemie
(Leipzig) 78 (1909) 289-342.

[81] E. L. Øiestad, E. Uggerud, The unimolecular chemistry of protonated
hydroxylamine, Int. J. Mass Spectrometry 185/186/187 (1999) 231-240.

[82] M. C. Lin, Y. He, C. F. Melius, Theoretical interpretation of the kinetics and mechanisms of the HNO + HNO and HNO + 2NO reactions with a unified model, Int. J. Chem. Kinet. 24 (1992) 489-516.

[83] K. Ruud, T. Helgaker, E. Uggerud, Mechanisms, energetics and dynamics of a key reaction sequence during the decomposition of nitromethane: HNO + HNO →N2O + H2O, J. Molecular Structure (Theochem) 393 (1997) 59-71.

[84] J. A. Miller, C. T. Bowman, Mechanism and modeling of nitrogen chemistry in combustion, Progress in Energy and Combustion Science 15 (1989) 287.

[85] A. Wilkinson, Compendium of Chemical Terminology, Blackwell Scientific Publications, Oxford, (1997).

[86] S. Chervin, G. T. Bodman, Phenomenon of autocatalysis in decomposition of energetic chemicals, Thermochimica Acta 392-393 (2002) 371-383.

[87] L. Bou-Diab, H. Fierz, Autocatalytic decomposition reactions, hazards and detection, Journal of Hazardous Materials 93 (2002) 137-146.

[88] Peña visits "most dangerous place on Earth" CNN (1997) http://www.cnn.com/EARTH/9708/27/hanford.pena/, accessed in May 2005.

[89] M. S. Mannan, W. J. Rogers, A. A. Aldeeb, in: Proceedings of HAZARDS XVI, (Institute of Chemical Engineers), November 6-8, 2001, 41-58, Manchester, United Kingdom.

[90] C. Wei, W. J. Rogers, M. S. Mannan, Application of screening tools in the prevention of reactive chemical incidents, Journal of Loss Prevention in the Process Industries 17 (2004) 261-269.

[91] L. A. Curtiss, K. Raghavachari, J. A. Pople, Gaussian-2 theory using reduced Møller--Plesset orders, The Journal of Chemical Physics 98 (1993) 1293-1298.

[92] J. W. Ochterski, Thermochemistry in Gaussian, http://gaussian.com/g_whitepap/thermo.htm (2000), accessed in May 2005.

[93] U.S. Chemical Safety and Hazard Investigation Board, The explosion at concept sciences: hazards of hydroxylamine, 2002, http://www.csb.gov, accessed in May 2005.

[94] C. Wei, S. R. Saraf, W. J. Rogers, M. S. Mannan, Thermal runaway reaction hazards and mechanisms of hydroxylamine with acid/base contaminants, Thermochimica Acta 421 (2004) 1-9.

[95] R. Nast, I. Foppl, The formation of hyponitrite by the disproportionation of hydroxylamine, Z. Anorg. U. Allgem. Chem. 263 (1950) 310-315.

[96] S. Lunak, J. Veprek-Siska, The catalytic effect of cations on the decomposition of alkaline solutions of hydroxylamine, Collection of Czechoslovak Chemical Communications 39 (1972) 391-395.

[97] H. Holzapfel, Decomposition of hydroxylamine in strongly alkaline aqueous solutions, Wissenschaftliche Zeitschrift - Karl-Marx-Universitaet Leipzig, Mathematisch-Naturwissenschaftliche Reihe 1959-1960 (1960) 17-25.

[98] M. N. Hughes, H. G. Nicklin, Oxidation of hydroxylamine by molecular oxygen in alkaline solutions, Chemistry and Industry 52 (1967) 2176.

[99] G. E. Alluisetti, A. E. Almaraz, V. T. Amorebieta, F. Doctorovich, J. A. Olabe, Metal-catalyzed anaerobic disproportionation of hydroxylamine. Role of diazene and nitroxyl intermediates in the formation of N_2, N_2O, NO^+, and NH_3, Journal of American Chemical Society 126 (2004) 13432-13442.

[100] G. Bengtsson, S. Fronaus, L. Bengtsson-Kloo, The kinetics and mechanism of oxidation of hydroxylamine by iron(III), J. Chem. Soc., Dalton Trans. (2002) 2548-2552.

[101] A. D. Becke, Density-functional thermochemistry. III. The role of exact exchange, Journal of Chemical Physics 98 (1993) 5648-5652.

[102] C. Lee, W. Yang, R. G. Parr, Development of the Colle-Salvetti correlation-energy formula into a functional of the electron density, Physical Review B 37 (1988) 785-789.

[103] B. J. Lynch, P. L. Fast, M. Harris, D. G. Truhlar, Adiabatic connection for kinetics, Journal of Physical Chemistry A 104 (2000) 4811-4815.

[104] W. J. Hehre, R. Ditchfield, J. A. Pople, Self-consistent molecular orbital methods. XII. Further extensions of Gaussian-type basis sets for use in molecular orbital studies of organic molecules, Journal of Chemical Physics 56 (1972) 2257-2261.

[105] T. Clark, J. Chandrasekhar, G. W. Spitznagel, Efficient diffuse function-augmented basis sets for anion calculations. III. The 3-21+G basis set for first-row elements, lithium to fluorine, Journal of Computational Chemistry 4 (1983) 294-301.

[106] M. J. Frisch, J. A. Pople, J. S. Binkley, Self-consistent molecular orbital methods. 25. supplementary functions for Gaussian basis sets, Journal of Chemical Physics 80 (1984) 3265-3269.

[107] Q. S. Li, X. D. Xu, S. Zhang, Predicting energies and geometries for reactions involved in atmosphere chemistry: a comparison study between hybrid DFT methods, Chemical Physics Letters 384 (2004) 20-24.

[108] M. L. Coote, Reliable theoretical procedures for the calculation of electronic-structure information in hydrogen abstraction reactions, Journal of Physical Chemistry A 108 (2004) 3865-3872.

[109] Y. Zhao, B. J. Lynch, D. G. Truhlar, Development and assessment of a new hybrid density functional model for thermochemical kinetics, Journal of Physical Chemistry A 108 (2004) 2715-1719.

[110] J. A. Pople, M. Head-Gordon, K. Raghavachari, Quadratic configuration interaction. A general technique for determining electron correlation energies, The Journal of Chemical Physics 87 (1987) 5968-5975.

[111] M. Head-Gordon, J. A. Pople, M. J. Frisch, MP2 energy evaluation by direct methods, Chemical Physics Letters 153 (1988) 503-506.

[112] G. A. Petersson, A. Bennett, T. G. Tensfeldt, M. A. Al-Laham, W. A. Shirley, A complete basis set model chemistry. I. The total energies of closed-shell atoms and hydrides of the first-row elements, J. Mantzaris, J. Chem. Phys. 89 (1988) 2193.

[113] C. Gonzalez, H. B. Schlegel, An improved algorithm for reaction path following, Journal of Chemical Physics 90 (1989) 2154-2161.

[114] C. Gonzalez, H. B. Schlegel, Reaction path following in mass-weighted internal coordinates, Journal of Physical Chemistry 94 (1990) 5523-5527.

[115] S. Tsunekawa, Microwave spectrum of hydroxylamine, Journal of Physical Society of Japan 33 (1972) 167-174.

[116] J. Tyrrell, W. Lewis-Bevan, D. Kristiansen, Equilibrium geometries, internal rotation potentials, and spectroscopic constants in NH_2OH, NH_2OF, $NHFOH$, and $NHFOF$, Journal of Physical Chemistry 97 (1993) 12768-12772.

[117] A. Chung-Phillips, K. A. Jebber, *Ab initio* studies of critical conformations in ethane, methylamine, methanol, hydrazine, hydroxylamine, and hydrogen peroxide, Journal of Chemical Physics 102 (1995) 7080-7087.

[118] P. Boulet, F. Gilardoni, J. Weber, H. Chermette, Y. Ellinger, Theoretical study of interstellar hydroxylamine chemistry: protonation and proton transfer mediated by H_3^+, Chemical Physics 244 (1999) 163-174.

[119] L. R. Mahoney, G. D. Mendenhall, K. U. Ingold, Calorimetric and equilibrium studies on some stable nitroxide and iminoxy radicals. Approximate O-H bond dissociation energies in hydroxylamines and oximes, Journal of American Chemical Society 95 (1973) 8610-8614.

[120] M. Brönstrup, D. Schröder, I. Kretzschmar, C. A. Schalley, H. Schwarz, Mass-spectrometric experiments together with electronic structure calculations support the existence of the elusive ammonia oxide molecule and its radical cation, Eur. J. Inorg. Chem. (1998) 1529-1538.

[121] L. A. Curtiss, K. Raghavachari, G. W. Trucks, J. A. Pople, Gaussian-2 theory for molecular energies of first- and second-row compounds, J. Chem. Phys. 94 (1991) 7221.

[122] Y. Han, D. Zhu, C. Zhao, Theoretical studies on ammonia oxide and its unimolecular reactions, Chinese Journal of Chemistry 5 (1990) 405-411.

[123] L. Radom, J. S. Binkley, J. A. Pople, The molecular structure of ammonia oxide (NH_3O). An ab initio study, Australian Journal of Chemistry 30 (1977) 699-703.

[124] B. T. Hart, Ammonia oxide. I. geometry and stability, Australian Journal of Chemistry 29 (1976) 231-239.

[125] B. T. Hart, Ammonia oxide. II. bonding and calculated properties, Australian Journal of Chemistry 29 (1976) 241-248.

[126] J. F. Olsen, J. M. Howell, A comparative ab-initio molecular orbital study of ammonia oxide and trifluoramine oxide, Journal of Fluorine Chemistry 10 (1977) 197-218.

[127] F. Grein, l. J. Lawlor, Ab initio studies on ammonia oxide (ONH_3) trifluoroamine oxide (ONF_3) and trifluoromethoxide anion OCF_3-, using polarization functions and configuration interaction methods, Theoretica Chimica Acta 63 (1983) 161-175.

[128] J. M. Grenda, I. P. Androulakis, A. M. Dean, J. William H. Green, Application of computational kinetic mechanism generation to model the autocatalytic pyrolysis of methane, Ind. Eng. Chem. Res. 42 (2003) 1000-1010.

APPENDIX A

OPTIMIZED STRUCTURES OF CHEMICALS INVOLVED IN

REACTOR INCIDENTS USING PM3
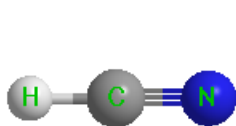
Hydrogen cyanide
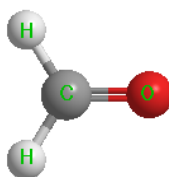
Formaldehyde
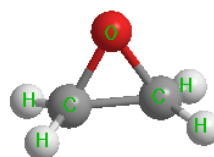
Ethylene Oxide
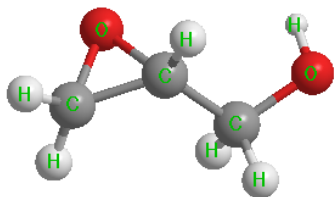
Glycidol
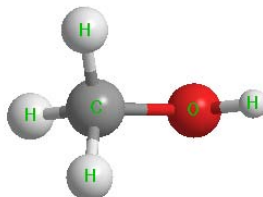
Methanol
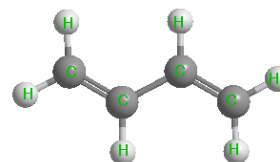
Butadiene
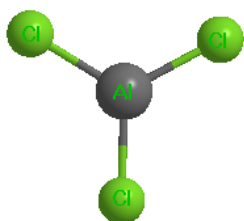
Aluminum Chloride
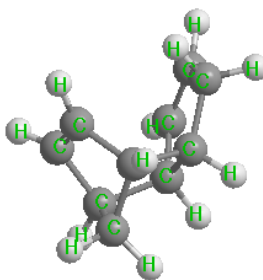
Dicyclopentadiene
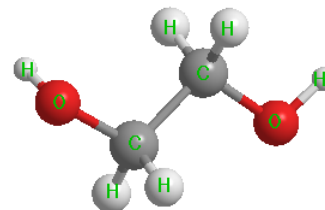
Ethylene glycol
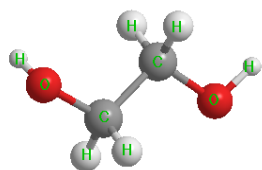
Maleic anhydride
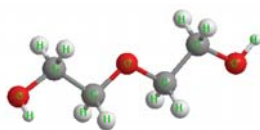
Diethylene glycol
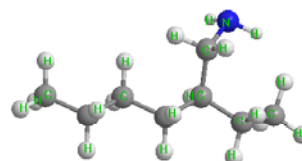
2-ethylhexylamine
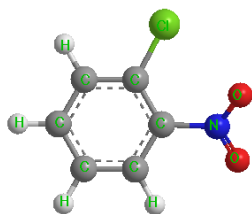
O-nitrochlorobenzene
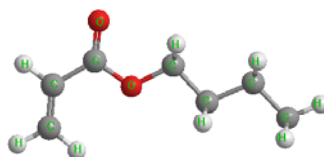
n-butyl acrylate
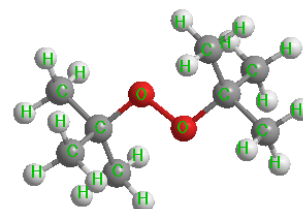
Di-tert butyl peroxide
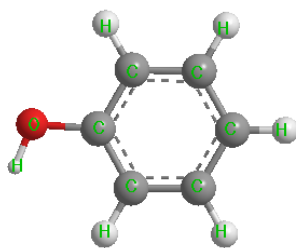
Phenol
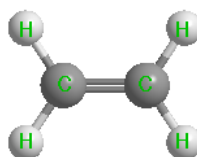
Ethylene
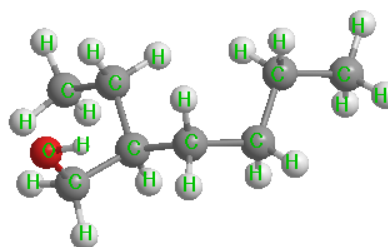
2-ethylhexanol
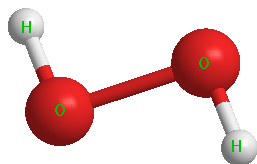
Hydrogen peroxide
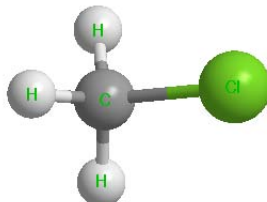
Methyl chloride
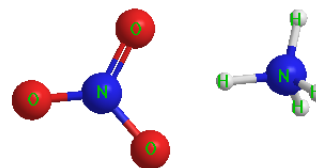
Ammonium nitrate
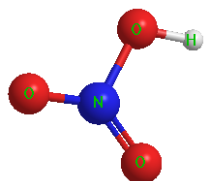
Nitric acid
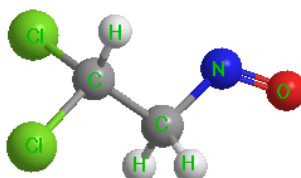
Dichloro-nitrosoethane
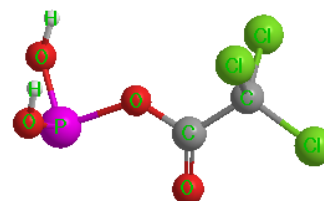
Chloralylphosphite
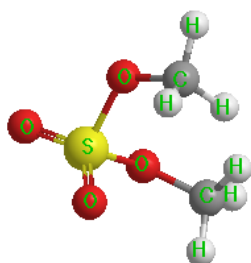
Dimethyl sulfate
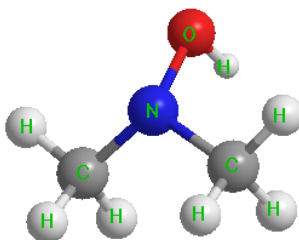
Dimethyl hydroxylamine
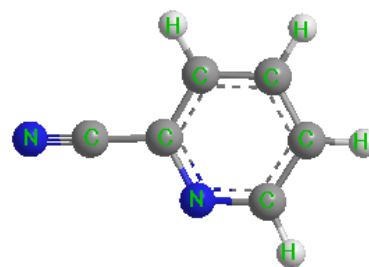
Cyanopyridine
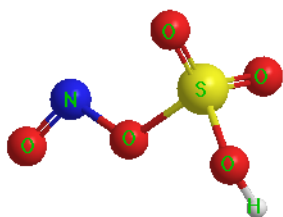
Nitrosylsulfuric acid
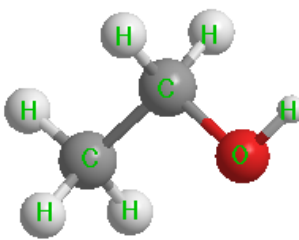
Alcohol
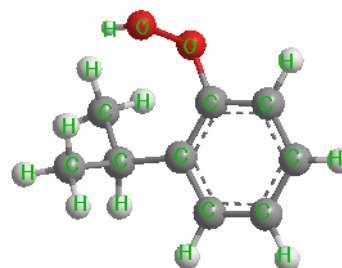
Cumene hydroperoxide
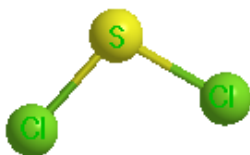
Sulfur dichloride
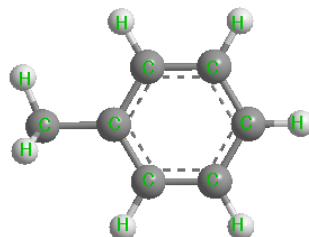
Toluene
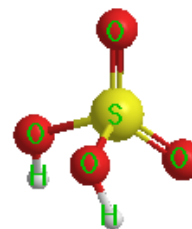
Sulfuric acid
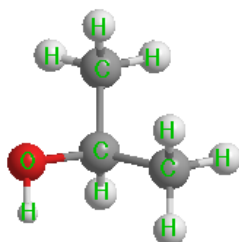
Isopropyl alcohol
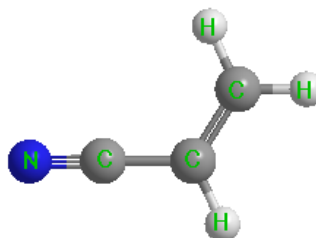
Acrylonitrile
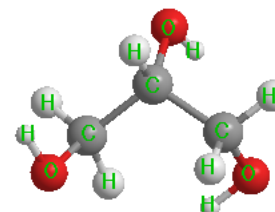
Glycerin
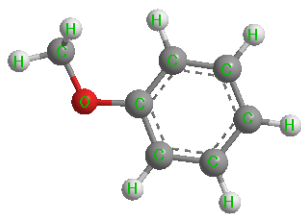
Anisol
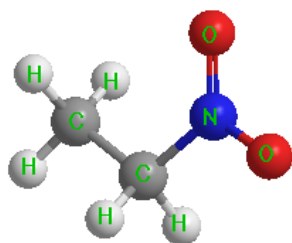
Nitro ethane
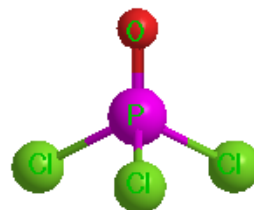
Phosphorous oxychloride
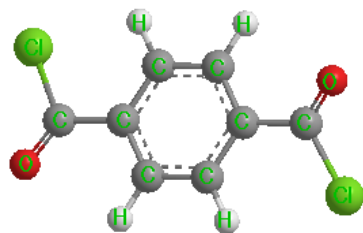
Terephthaloyl-dichloride

APPENDIX B

COMPARISON OF HEATS OF FORMATION DATA FROM

CHETAH, MOPAC WITH EXPERIMENTAL VALUES

Incident #	Chemical name	Δ_fH^0 (kcal/mol)					
		CHETAH	Experimental	AM1	MINDO/3	MNDO	PM3
2	Hydrogen cyanide	31.2	32.3	30.99	34.56	35.3	33.07
2,40,70,94	Formaldehyde	-29.95	-27.7	-31.51	-25.55	-32.9	-34.1
7,163,167	Ethylene oxide	-12.58	-12.58 or -22.88(liquid)	-8.99	-26.44	-15.57	-8.17
9	Glycidol	-84.48	-71.3(liquid)	-61.75	-81.67	-66.69	-56.74
9,132	Methanol	-48.08	-48 or -56.7(liquid)	-57.05	-50.6	-57.38	-51.9
25,74	Butadiene	26.33	26 or 21.6(liquid)	29.87	31.87	28.9	30.99
32	Aluminum chloride	-139.7	-139.72 or -161.28(liquid)	-140.31	*na*	-140.36	-122.09
33	Dicyclopentadiene	46.6	na	50.29	*80.78*	52.1	42.19
33	Ethylene glycol	-93.05	-94.26 or -109.9(liquid)	-109	-105.69	-105.88	-96.75
33,62	Maleic anhydride	-119.66[a]	-122.43(solid)	-76.44	-112.17	-88.55	-90.15
33, 163	Diethylene glycol	-131.36[a]	-150.22(liquid)	-157.24	-153.75	-149.45	-131.92
36	2-ethylhexylamine	-43.58[a]	na	-52.19	-39.36	-33.99	-44.66
36,132	O-nitrochlorobenzene	15.64[a]	-7.87(solid)	23.7	*180.52*	31.93	12.28
39	n-butyl acrylate	-94.98[a]	-89.7 or -101(liquid)	-89.49	-102.21	-83.37	-82.9
39	Di-tert butyl peroxide	-82.68[a]	-82 or -91.01(liquid)	-50.37	-54.58	-38.45	-61.63
40,70,94	Phenol	-23.03	-23.03 or -39.44(solid)	-21.95	-29.17	-26.76	-21.75
52	Ethylene	12.55	12.52	16.45	19.22	15.38	16.61
63,161	2-ethylhexanol	-87.76[a]	-103.46(liquid)	-98.27	-88.35	-82.93	-87.31
63	Hydrogen peroxide	-32.53	-32.53	-35.26	-29.11	-38.27	-40.8
66, 106	Methyl chloride	-20.55	-20	-18.97	-14.85	-22.52	-14.69
68	Ammonium nitrate	-70.3	-87.47(solid)[c]	-46.57	-35.26	-25.49	-48.46

Incident #	Chemical name	$\Delta_f H^0$ (kcal/mol)					
		CHETAH	Experimental	AM1	MINDO/3	MNDO	PM3
82	Dichloro-nitrosoethane	-20[b]	na	-18.9	*128.45*	-19.44	-4.51
90	Chloralylphosphite	-244.7[a]	na	-249.03	*-150.32*	-258.6	-265.55
91	Dimethyl sulfate	-157.1[b]	-164.2 or -175.73(liquid)	-174.84	*-217.33*	*-5.58*	-172.16
91	Dimethylhydroxylamine	-16.535[b]	na	-11.98	*-2.12*	-13.32	-13.3
92	Cyanopyridine	65.9[a]	67.09 or 50.2(solid)	67.86	47.25	61.12	67.69
99	Nitrosylsulfuric acid	-134.04[b]	na	-164.37	-194.72	*8.85*	-141.22
106	Alcohol	-56.12	-56.23or -66.2(liquid)	-62.7	-64.27	-63.03	-56.89
106	Cumene hydroperoxide	-19.4 [b]	-18.8 or -35.5(liquid)	-7.89	-15.68	-9.05	-16.69
129	Sulfur dichloride	-5.2	-4.2 or -11.9(liquid)	-26.26	-4.34	-23.86	-10.95
129	Toluene	11.95	11.95 or 2.87(liquid)	14.5	22.33	13.69	14.03
137,139,161	Sulfuric acid	-177	-175.7	-184.82	-213.11	*-3.75*	-186.90
137	Isopropyl alcohol	-65.15	-65.19 or -75.77(liquid)	-68.09	-69.26	-65.47	-63.99
137,157	Acrylonitrile	42.0[a]	42.95 or 33.5(liquid)	44.92	*na*	*na*	50.12
139	Glycerin	-137.04	-138.1 or -160(liquid)	-160.1	-154.14	-151.96	-141.42
139	Anisol	-17.3	-16.24 or -27.43(liquid)	-14.65	-19.16	-17.77	-14.64
142	Nitro ethane	-24.2	-34.4(liquid)	-16.88	-20.41	-2.15	-20.92
163	Phosphorous oxychloride	-133.5	-133.8	-117.98	*na*	*-86.97*	-140.2
164	Terephthaloyl-dichloride	-84[a]	-81(solid)	-51.3	*38.15*	-65.99	-57.7

Note: Values in italic show large deviation from experimental results; na = not available; a: using built-in Benson Groups; b: using estimated missing Benson Groups; c: J. Chem. Thermo. 11(8), (1979), p811.

APPENDIX C

ELEMENTARY STEPS OF HYDROXYALMINE

DECOMPOSITION NETWORK

Scheme	ΔH^0(kcal/mol)	Ea(kcal/mol)	
		Estimated	Calculated
$HA \rightarrow NH_2+OH$	62	63	62
$HA \rightarrow NH_2O+H$	69	70	60
$HA \rightarrow NHOH+H$	78	79	78
$NH_2OH \rightarrow NH(triplet) + H_2O$	31	32	63
$NH_2OH \rightarrow NH_2OH(cis)$	4	15	6
$NH_2OH(cis) \rightarrow HNO + H_2$	28	32	63
$NH_2OH \rightarrow NH_3O$	28	32	50
$NH_3O \rightarrow NH_3 + O(triplet)$	29	30	29
$2NH_2OH \rightarrow NH_3 + \bullet HNOH + \bullet OH$	29	33	50
$2NH_2OH \rightarrow NH_2OH(cis) + NH_3O$	33	35	28
$2NH_2OH \rightarrow NH_2OH + NH_3O$	28	32	20
$O(triplet) + NH_2OH \rightarrow \bullet OH + NH_2O\bullet$	-28	4	15
$NH_2+ HA \rightarrow NH_2O + NH_3$	-33	2	2
$NH_2+ HA \rightarrow NHOH + NH_3$	-24	5	
$OH + HA \rightarrow H_2O + NH2O$	-41	0	0
$OH + HA \rightarrow H_2O + NHOH$	-33	2	
$H+HA \rightarrow NH_2+H_2O$	-49	21	
$H+HA \rightarrow NH_3+OH$	-40	25	
$H+HA \rightarrow H_2+NH_2O$	-33	2	4
$H+NH_2O \rightarrow HNO+H_2$	-37	1	
$NH_2O+H \rightarrow NH_2+OH$	-7	10	
$NH_2+OH \rightarrow NH+H_2O$	-21	6	
$NHOH+H \rightarrow NH+H2O$	-37	27	
$NH+HA \rightarrow NH_2+NH_2O$	-21	6	4
$NH+NH_2O \rightarrow NH_2+HNO$	-25	5	
$NH+HNO \rightarrow NH_2+NO$	-46	0	
$NH+NO \rightarrow N_2O+H$	-36	1	

Scheme	ΔH^0(kcal/mol)	Ea(kcal/mol)	
		Estimated	Calculated
NH+NH→NHN+H	-60	0	
NHN→N$_2$+H	-1	0	
NH+NH→NHNH	-118	0	
NHN+H→N$_2$+H$_2$	-102	0	
NHN+OH→N$_2$+H$_2$O	-111	0	
NHN+NH$_2$→N$_2$+NH$_3$	-102	0	
NHN+HA→NHNH+NH$_2$O	11	20	
NHN+NH$_2$O→N$_2$+HA	-70	0	
NHN+NH$_2$O→NHNH+HNO	7	17	
NHN+HNO→N$_2$+NH$_2$O	-66	0	
NHN+HNO→N$_2$+NHOH	-57	0	
NHN+NHN→NHNH+N$_2$	-59	0	
NHNH+OH→NHN+H$_2$O	-52	0	
NHNH+H→NHN+H$_2$	-44	0	
NHNH+NH$_2$→NHN+NH$_3$	-44	0	
OH + NH$_2$O → HNO + H$_2$O	-46	0	0
OH+NHOH→HNO+H$_2$O	-54	0	
NH$_2$+NH$_2$O→HNO+NH$_3$	-37	1	
NH$_2$+NHOH→HNO+NH$_3$	-45	0	
HNO+NH$_2$OH→2NH$_2$O	4	15	18
HNO + NH$_2$OH → NHOH +NH$_2$O	13	21	
HNO + NH$_2$OH→ 2NHOH	21	27	
HNO+NH$_2$→NH$_3$+NO	-58	0	0
HNO+OH→NO+H$_2$O	-66	0	0
HNO+H→NO+H$_2$	-58	0	
NO + NH2OH → HNO + NH2O	25	30	
HNO+HNO → NH$_2$O +NO	-21	6	
NO+HNO→OH+N$_2$O	-18	7	
N$_2$O+H→N$_2$+OH	-52	0	
NH$_2$O+NH$_2$O→N$_2$+2H$_2$O	-117	N/a	
HNO+HNO→N$_2$O+H$_2$O	-84	N/a	
NH$_2$+H→NH$_3$	-102	0	
OH+H→H$_2$O	-111	0	
NO+H→HNO	-44	0	
NH$_3$+OH→ H$_2$O + NH$_2$	-9	9	
H$_2$ + OH → H$_2$O + H	-9	9	

Scheme	ΔH^0(kcal/mol)	Ea(kcal/mol)	
		Estimated	Calculated
$NHN+NO\rightarrow N_2+HNO$	-45	0	
$N_2O+NH\rightarrow N_2+HNO$	-69	0	
$O+O\rightarrow O_2$	-83	0	
$O_2+HA\rightarrow OOH+NH_2O$	-15	8	
$O+OOH\rightarrow OH+O_2$	-14	8	
$H+OOH\rightarrow H_2+O_2$	-18	7	
$H+OOH\rightarrow H_2O+O$	-41	24	
$H+OOH\rightarrow H_2O_2$	-78	0	
$O+OH\rightarrow OOH$	-69	0	
$OH+OH\rightarrow H_2O+O$	-13	8	
$OH+H_2O_2\rightarrow OOH+H_2O$	-33	2	
$H+H_2O_2\rightarrow H_2O+OH$	-61	15	
$H+H_2O_2\rightarrow OOH+H_2$	-24	5	
$O+H_2O_2\rightarrow OOH+OH$	-20	6	
$NH_2+NH_2\rightarrow N_2H_4$	-61	0	
$N_2H_4+NH\rightarrow NH_2+N_2H_3$	-16	7	
$N_2H_4+H\rightarrow N_2H_3+H_2$	-28	4	
$N_2H_4+OH\rightarrow N_2H_3+H_2O$	-37	1	
$N_2H_3+HA\rightarrow N_2H_4+NH_2O$	-5	11	
$N_2H_3+H\rightarrow N_2H_4$	-74	0	
$N_2H_3+H\rightarrow N_2H_2+H_2$	-54	0	
$N_2H_3+OH\rightarrow N_2H_2+H_2O$	-62	0	
$N_2H_3+NH_2\rightarrow N_2H_2+NH_3$	-53	0	
$N_2H_2+HA\rightarrow N_2H_3+NH_2O$	21	27	37
$N_2H_2+H\rightarrow N_2H_3$	-48	0	

VITA

Chunyang Wei was born in P. R. China in 1974. She received her B.E. with honors in chemical equipment and machinery from Dalian University of Technology in 1996. Then, she worked three years at the Research Institute of Beijing Yanshan Petrochemical Group Co., Ltd. She received her M.S. in chemical engineering from the University of Tulsa in 2001. Since then, she has been working at Texas A&M University for her PhD in chemical engineering. Her permanent address is

12-1-603 Shuangyushu North

Haidian District

Beijing, China 100086.